

The Gas Phase Association Reactions of Mixed-Metal Acetylacetonate Complexes

by

Daryl G. Mains Jr.

Submitted in Partial Fulfillment of the Requirements

For the Degree of

Master of Science

In the

Chemistry

Program

YOUNGSTOWN STATE UNIVERSITY

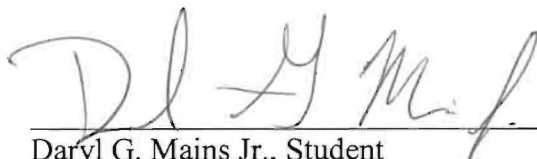
August 3, 2007

The Gas Phase Association Reactions of Mixed-Metal Acetylacetonate Complexes

Daryl G. Mains Jr.

I hereby release this thesis to the public. I understand that this thesis will be made available from the OhioLINK ETD Center and the Maag Library Circulation Desk for public access. I also authorize the University or other individuals to make copies of this thesis as needed for scholarly research.

Signature:



Daryl G. Mains Jr., Student

Date

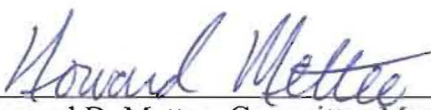
Approvals:



Dr. Brian D. Leskiw, Thesis Advisor

8-2-07

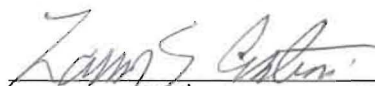
Date



Dr. Howard D. Mettee, Committee Member

8/2/07

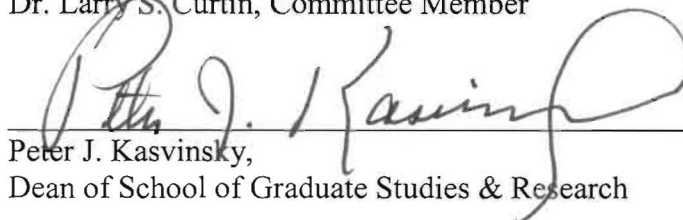
Date



Dr. Larry S. Curtin, Committee Member

8/2/07

Date



Peter J. Kasvinsky,
Dean of School of Graduate Studies & Research

8/2/07

Date

Abstract

The gas phase association reactions of mixed-metal acetylacetonate (acac) and hexafluoroacetylacetonate (hfac) complexes were analyzed using a high resolution double focusing mass spectrometer under low source pressure conditions. The unimolecular dissociation reactions of a collection of metal acetylacetonate complexes were investigated. When ensuing association reactions of co-subliming mixtures $\text{Al}(\text{hfac})_3$, $\text{Al}(\text{acac})_3$, $\text{Ni}(\text{acac})_2$, and $\text{Ni}(\text{hfac})_2$ were mixed with various complexes, many of the observed mixed-metal association products detected have the arrangement $\text{MM}'\text{L}_n\text{L}'_m$ where M is Li, Al, V, Cr, Mn, Co, Fe, Ni, Cu, Zn, Ga, Cd, or Rh, M' is Al or Ni, L is acetylacetonate (acac), L' is hexafluoroacetylacetonate (hfac), and $(n + m)$ is 2-5. Manganese tris(hexafluoroacetylacetonate) was successfully synthesized and matched with the crystal structure reported in the literature. The crystal structure of aluminum tris(hexafluoroacetylacetonate), $\text{Al}(\text{hfac})_3$, is presented for the first time.

Acknowledgements

I want to thank God, the Creator of Heaven and Earth, who through His love has given me life, a strong mind, and the desire to work hard, and it is through Him that my confidence to even come to graduate school first came. I was content sitting and watching television for a bulk of my time trying to run away from responsibility and recognition until God opened my eyes to the joy and disappointment of applying myself, especially in chemistry.

With the novelty of finding joy in something new, I was unsure whether this was a phase in my life that would quickly pass or be something lasting. For this reason, I thank the Chemistry Department, where I have developed more confidence and endurance for what should end up being a life filled with chemistry. I thank the professors who through their examples I have gotten a deeper look at the diversity of chemistry and styles at which to examine it.

With special regards, I would like to thank my advisor, Dr. Brian Leskiw. Dr. Leskiw took on the personal challenge of making me a better chemist, and pushed me into a world that was completely unknown to me. As we developed my research goals, I gained the confidence to take on new subjects and the knowledge of how to go about doing it. I thank him for his calming presence, his listening ear, and his advice, not to mention his drive to excel which I have learned much about in this short two year period.

I would also like to thank my fellow graduate students who through their camaraderie made it easier to come into school each day, especially I would like to thank Ryan Conway, Calvin Austin, Jordan Lerach, John Milo, and the rest of the group that went to Cincinnati. I owe a huge debt of gratitude to the department support staff

especially instrument specialist, Ray Hoff, with his countless stories and knowledge about the High-Res, I was able to gain confidence and understanding of the complex instrument and Dr. Mattais Zeller, who without his love for crystallography, my crystal structures would probably not have been solved.

I wish to thank my committee members, Dr. Larry Curtin and Dr. Howard Mettee, for their suggestions and their time spent in reviewing this thesis. Both the Chemistry Department and the Cushwa family, I acknowledge because without their financial support I could not devote my time to studying chemistry. Finally I would like to thank my family for their love, support and the little extras they provided for me while I took on this endeavor.

Table of Contents

Title Page	i
Signature Page	ii
Abstract	iii
Acknowledgements	iv
Table of Contents	vi
List of Equations	viii
List of Tables	ix
List of Schemes	x
List of Figures	xii
List of Abbreviations	xiv
Chapter 1 – Mass Spectrometry.	1-8
1.1 Introduction	1
1.2 Double Focusing Mass Spectrometry	2
1.3 Experimental Section and Typical Data Analysis	6
Chapter 2 – Dissociation Pathways of Metal Acetylacetonates	9-31
2.1 Introduction	9
2.1 Acetylacetone	10
2.2 Hexafluoroacetylacetone	12
2.3 Metal Acetylacetonates	15
2.4 Metal Hexafluoroacetylacetonates	24
2.5 Synthesis and Characterization	27
2.5.1 Mn(hfac) ₃	27
2.5.2 Al(hfac) ₃	29

2.6 Conclusions	31	
Chapter 3 – Exchange Reactions and Mixed-Metal Complexes.	32-60	
3.1 Exchange and Association Reactions of Metal Acetylacetonates and Derivatives	32	
3.2 Experimental Design	35	
3.3 Results and Discussion	36	
3.3.1 Al(hfac) ₃ series	37	
3.3.2 Al(acac) ₃ series	38	
3.3.2.1 Ni(hfac) ₂ mixed with Al(acac) ₃		
3.3.2.2 Co(hfac) ₂ mixed with Al(acac) ₃		
3.3.2.3 Fe(hfac) ₂ mixed with Al(acac) ₃		
3.3.2.4 Mn(hfac) ₂ mixed with Al(acac) ₃		
3.3.2.5 Mn(hfac) ₃ mixed with Al(acac) ₃		
3.3.3 Ni(acac) ₂	46	
3.3.3.1 Cu(hfac) ₂ mixed with Ni(acac) ₂		
3.3.3.1 Mn(hfac) ₂ mixed with Ni(acac) ₂		
3.3.3.1 Mn(hfac) ₃ mixed with Ni(acac) ₂		
3.3.4 Ni(hfac) ₂	52	
3.3.4.1 Cu(acac) ₂ mixed with Ni(hfac) ₂		
3.3.4.1 Mn(acac) ₂ mixed with Ni(hfac) ₂		
3.3.4.1 Mn(acac) ₃ mixed with Ni(hfac) ₂		
3.3.4.1 Mn(hfac) ₂ mixed with Ni(hfac) ₂		
3.3.4.1 Mn(hfac) ₃ mixed with Ni(hfac) ₂		
3.4 Conclusions	60	
References	62	
Appendix of Pertinent Spectra		65-80
A.1	65	
A.2	72	

List of Equations

EQUATIONS	PAGE
1.1 $mv = Brz$	2
1.2 $mv^2 = ER_E Z$	2
1.3 $m/z = B^2 r^2 / ER_E$	2
1.4 $R = m / \Delta m$	4

List of Tables

TABLES	PAGE
1.1 Complexes mixed with the two aluminum and two nickel complexes to test their ability to form mixed-metals. Isotopic abundances were used to verify the identity of the mixed-metal complex ion.	7
1.2 The coordination number, common oxidation state, some complexes in the series, and possible coordination environment are listed for metals relevant to this study.	17
A.1 Crystal data and structure refinement of Mn(hfac) ₃ .	65
A.2 Atomic coordinates [$\times 10^4$] and equivalent isotropic displacement parameters [$\text{\AA}^2 \times 10^3$] for Mn(hfac) ₃ . U(eq) is defined as one third of the trace of the orthogonalized U _{ij} tensor.	66
A.3 Bond lengths [\AA] and angles [deg] for Mn(hfac) ₃ .	67
A.4 Anisotropic displacement parameters [$\text{\AA}^2 \times 10^3$] for Mn(hfac) ₃ . The anisotropic displacement factor exponent takes the form: $-2 \pi^2 [(h a^*)^2 U_{11} + \dots + 2 h k a^* b^* U_{12}]$	69
A.5 Hydrogen coordinates ($\times 10^4$) and isotropic displacement parameters ($\text{\AA}^2 \times 10^3$) for Mn(hfac) ₃ .	70
A.6. Torsion angles [deg] for Mn(hfac) ₃ .	70
A.7 Crystal data and structure refinement for Al(hfac) ₃ .	73
A.8. Atomic coordinates [$\times 10^4$] and equivalent isotropic displacement parameters [$\text{\AA}^2 \times 10^3$] for Al(hfac) ₃ . U(eq) is defined as one third of the trace of the orthogonalized U _{ij} tensor.	75
A.9 Bond lengths [\AA] and angles [deg] for Al(hfac) ₃ .	76
A.10 Anisotropic displacement parameters [$\text{\AA}^2 \times 10^3$] for Al(hfac) ₃ . The anisotropic displacement factor exponent takes the form: $-2 \pi^2 [(h a^*)^2 U_{11} + \dots + 2 h k a^* b^* U_{12}]$	78
A.11 Hydrogen coordinates ($\times 10^4$) and isotropic displacement parameters ($\text{\AA}^2 \times 10^3$) for Al(hfac) ₃ .	79
A.12. Torsion angles [deg] for Al(hfac) ₃ .	80

Table of Schemes

SCHEME	PAGE	
2.1	Dissociation to products of acetylacetone as observed in mass spectrometry.	12
2.2a	The predominant species in the dissociation of H(hfac) with two ions, B _{hf} and C _{hf} , leading to the formation of D _{hf} .	13
2.2b	Further dissociation products of H(hfac) starting from C _{hf} with the final pathway not detected by the departmental instrument.	13
2.3a	The initial major dissociation from A _{ma} is the loss of an odd-electron fragment which is followed by even-electron fragments where B _{ma} is the most abundant ion in for the second group. (M = Cr, Mn, Fe, Co, and Al and L = acac)	19
2.3b	The dissociation pathway followed when the metal does not reduce in oxidation state. The dissociation of Al(acac) ₃ is illustrated in Figure 2.6. (M = Al, Cr, Mn, Fe, and Co and L = acac)	19
2.3c	Dissociation pathway of metal tris(acetylacetonate) when the metals do reduce. (M = Cr, Mn, Fe, Co, and Al and L = acac)	20
2.4a	The dissociation pathway of M(acac) ₃ , where M = Ti or V and L is acetylacetonate, showing the loss of an odd-electron species to maintain the preferred even-electron species.	21
2.4b	The dissociation pathway of M(acac) ₃ , where M = Ti or V and L is acetylacetonate, when an increase in oxidation state occurs to form an even-electron ion which then dissociates further.	21
2.5a	The initial dissociation of CuL ₂ where L is acetylacetonate can occur by three different pathways with the N _{ma} changing oxidation state.	23
2.5b	Copper is reduced from 2+, J _{ma} , to 1+, P _{ma} , which stabilizes the loss of a methyl radical to form Q _{ma} .	23
2.5c	The reduced copper only losses even-electron fragments to form R _{ma} and Q _{ma} where R _{ma} is mass degenerate with J _{ma} and P _{ma} .	23
2.6a	The two fragmentation pathways possible for M(III)(hfac) ₃ where C _{mf} maintains the oxidation state and D _{mf} reduces in oxidation state. (L' = hfac)	24

2.6b	The dissociation pattern for metal complexes of oxidation state 3+ that does not reduce in oxidation state. ($L' = \text{hfac}$)	
2.6c	The dissociation pathways for metals that readily reduce in oxidation state. ($M = \text{Cr, Fe, Co}$ with $L' = \text{hfac}$)	25
2.7	Synthesis reaction for $\text{Mn}(\text{hfac})_3$ where the arrows indicate coordination.	27
3.1	General scheme for exchange reactions and association reactions.	32
3.2	A general example of an exchange reaction where two different pathways lead to the formation of $[\text{ML}'\text{L}]^+$ ion where $M = \text{Ni, Fe, Co, and Mn}$, $L = \text{acac}$, and $L' = \text{hfac}$.	38
3.3	The possible association reactions between $\text{M}(\text{hfac})_2$ and $\text{Al}(\text{acac})_3$ where M is Co , and Mn , L is acac , and L' is hfac .	39
3.4	Two possible pathways leading to mixed-metal product, N_{Alac} , where one is association and the other dissociation. ($M = \text{Ni, Fe, Co, and Mn}$, $L = \text{acac}$, and $L' = \text{hfac}$.)	40
3.5	Two possible pathways leading to cluster ions in the gas phase where L' is hfac .	44
3.6	Three possible pathways that $\text{Mn}(\text{III})$ can reduce to $\text{Mn}(\text{II})$ where L' is hfac .	46
3.7	Two possible pathways to form the mixed-metal complex, C_{Niac} . ($L = \text{acac}$, $L' = \text{hfac}$)	47
3.8	Proposed association reactions to form the three mixed-metal ions where L is acac and L' is hfac .	49
3.9	General ligand exchange reaction between $\text{M}(\text{acac})_n$ ($n = 1-3$) and $\text{Ni}(\text{acac})_2$ where i and j are from 0 to 3.	52
3.10	Possible reaction pathways to form the mixed-metal ion C_{Nihf} where L is acac and L' is hfac . The upper pathway describes the association reaction, and the lower pathway describes dissociation from a previous association product.	54
3.11	Two possible reactions yielding ion E_{Nihf} where the upper pathway describes the association reaction necessary, and the lower pathway describes the dissociation of a larger association product.	58

Table of Figures

FIGURE		PAGE
1.1	Schematic of a reverse geometry double focusing mass spectrometer where the bold lines demonstrate the trajectory of the ions and the focusing effect of the double sector.	2
1.2	The mass spectrum of $\text{Cd}(\text{acac})_2$ where the isotope pattern is clearly seen with the principle isotope (^{114}Cd) being the most abundant peak. The mass of 198 amu accounts for the mass of two acac ligands which have a mass of 99 amu each.	8
2.1	Tautomerism of acetylacetone where the keto form is on the left and the two resonant enol forms are on the right.	10
2.2	Mass spectrum of the dissociation of $\text{H}(\text{acac})$ with major fragment ions labeled where ions E_{ha} and F_{ha} were not observed on the departmental MS.	11
2.3	1,1,1-5,5,5-hexafluoroacetylacetone (hfac), a derivative of acetylacetone.	13
2.4	Mass spectrum of the dissociation of $\text{H}(\text{acac})$ with fragment ions labeled with minus signs indicating a loss of that particular fragment.	15
2.5	Diagram of manganese tris(acetylacetonate) where the enolate form of acetylacetonate dominates and arrows indicate coordination.	16
2.6	Mass spectrum of the dissociation of $\text{Al}(\text{acac})_3$ which does not reduce to a lower oxidation state.	18
2.7	Mass spectrum of the dissociation of $\text{Cu}(\text{acac})_2$ where L is acetylacetonate, and fragment J_{ma} has two other mass degenerate forms labeled P_{ma} and R_{ma} .	22
2.8	Mass spectrum of synthesized $\text{Mn}(\text{hfac})_3$ with major dissociation peaks indicative of a metal center that reduces from a 3+ to a 2+ oxidation state. ($L' = \text{hfac}$)	26
2.9	The crystal structure of Manganese tris(hexafluoroacetylacetonate).	27
2.10	Mass spectrum of synthesized $\text{Mn}(\text{hfac})_3$ with doubly charged ions at m/z 165.5, 234.5 and 303.5 where $[\text{Mn}(\text{L}-\text{CF}_3)]$ signifies that the ligand lost a methyl group and L is hfac.	28
2.11	The crystal structure of aluminum tris(acetylacetonate).	30

3.1	The mass spectrum of Mn(hfac) ₂ mixed with Al(hfac) ₃ .	.	.	37
3.2	The mass spectrum of Ni(hfac) ₂ mixed with Al(acac) ₃ .	.	.	41
3.3	The mass spectrum of Co(hfac) ₂ mixed with Al(acac) ₃ .	.	.	42
3.4	The mass spectrum of Fe(hfac) ₂ mixed with Al(acac) ₃ .	.	.	43
3.5	The mass spectrum of Mn(hfac) ₂ mixed with Al(acac) ₃ .	.	.	44
3.6	The mass spectrum of Mn(hfac) ₃ mixed with Al(acac) ₃ .	.	.	45
3.7	The mass spectrum of Cu(hfac) ₂ mixed with Ni(acac) ₂ .	.	.	48
3.8	The mass spectrum of Cu(hfac) ₂ mixed with Ni(acac) ₂ in the upper mass range.	.	.	48
3.9	The mass spectrum of Mn(hfac) ₂ mixed with Ni(acac) ₂ .	.	.	50
3.10	The mass spectrum of Mn(hfac) ₂ mixed with Ni(acac) ₂ in the upper mass range.	.	.	50
3.11	The mass spectrum of Mn(hfac) ₃ mixed with Ni(acac) ₂ .	.	.	51
3.12	The mass spectrum of Cu(acac) ₂ mixed with Ni(hfac) ₂ .	.	.	53
3.13	The mass spectrum of Mn(acac) ₂ mixed with Ni(hfac) ₂ .	.	.	55
3.14	The mass spectrum of Mn(acac) ₂ mixed with Ni(hfac) ₂ in the upper mass range.	.	.	55
3.15	The mass spectrum of Mn(acac) ₃ mixed with Ni(hfac) ₂ .	.	.	56
3.16	The mass spectrum of Mn(acac) ₃ mixed with Ni(hfac) ₂ in the upper mass range.	.	.	57
3.17	The mass spectrum of Mn(hfac) ₂ mixed with Ni(hfac) ₂ .	.	.	58
3.18	The mass spectrum of Mn(hfac) ₃ mixed with Ni(hfac) ₂ .	.	.	59
3.19	The mass spectrum of Mn(hfac) ₃ mixed with Ni(hfac) ₂ in the upper mass range.	.	.	60
A.1	The crystal structure of manganese tris(acetylacetonate).	.	.	64
A.2	The crystal structure of aluminum tris(hexafluoroacetylacetonate).	.	.	72

List of Abbreviations

Δm	mass difference between a calibrant and the sample
μA	microampere
(g)	gas phase
(s)	solid phase
acac	acetylacetonate anion
amu	atomic mass unit
B	magnetic field strength
bzac	benzoylacetylacetonate
DI	direct insertion
eV	electron volts
E	electric field strength
EI	electron impact ionization
FFR	field free region
H(acac)	acetylacetone
H(hfac)	hexafluoroacetylacetone
hfac	hexafluoroacetylacetonate anion
KER	kinetic energy release
L	acetylacetonate ligand
L'	hexafluoroacetylacetonate ligand
L*	acetylacetone, hexafluoroacetylacetone or a mixture of both ligands
(L-CH ₃)	a methyl group was lost from acetylacetate ligand
M	metal

m	mass of the ion
m	coordination number
m/z	mass to charge ratio
M(acac)	metal acetylacetonates
M(hfac)	metal hexafluoroacetylacetonates
MIKES.	mass-analyzed ion kinetic energy spectroscopy
MS	mass spectrometry
n	oxidation state
PFK	perfluorokerosenes
R	resolution
$R_E(r)$	radius of the Curve
RA	relative abundance
RF	radio frequency
RL_3	rare-earth chelates
V	voltage
v	velocity
z	charge of the ion

Chapter 1: Introduction

1.1 Introduction

Mass Spectrometry (MS) is an analytical approach used to identify the molecular mass of various samples. While there exists a variety of different types of mass spectrometers, each design can be separated into three parts where the details of each part differ and better suit certain applications. In many cases mass spectrometers behave as a mass filter separating the newly formed ions by their mass to charge ratio (m/z). The mass to charge ratio for a collection of ions is displayed in a mass spectrum where the relative abundance of each detected ion is presented as a function of m/z . The most abundant peak is considered to be 100% and all other peak percentages are relative to this peak.

Applications of mass spectrometry include characterizing synthesized samples, determining the composition of an unknown sample, and detecting trace amounts of substances in an analytical sample. Forensic studies use MS to characterize unknown substances at crime scenes. Wineries employ MS to detect traces of aromatic compounds to ensure a great tasting wine. Environmental studies have used MS to identify the speciation of metals such as Cr and V in soil and plant samples.¹ Lui utilized MS to simultaneously quantify the amount of venlafaxine and three metabolites in human blood.²

Mass spectrometry has also been employed to determine the kinetic rate of isothermal desorption,³ and to investigate the newly formed clusters in gas phase reactions. In the work presented herein, a high resolution double focusing mass spectrometer was utilized to investigate the formation of various mixed-metal complexes in gas phase reactions.

1.2 Double Focusing Mass Spectrometry

Double focusing mass spectrometry was designed to achieve better resolution than single field instruments by focusing an ion of a particular m/z using a magnetic sector and an electric sector. These two sectors separate ions according to two different principles: momentum and kinetic energy, respectively. The trajectory of an ion through a magnetic sector may be described mathematically by Equation 1.1, where mv is the momentum of an ion, B is the magnetic field strength, and r is the constant radius of the deflected ion, so that only ions of a particular m/z will possess the appropriate trajectory and reach the detector.⁴

$$mv = Brz \quad \text{Equation 1.1}$$

An electric sector deflects ions according to their kinetic energy and can be described by Equation 1.2, where E is the electric field, and R_E is the radius of deflection by the electric field.⁴

$$mv^2 = ER_Ez \quad \text{Equation 1.2}$$

During a double focusing scan, the two fields (B and E) are scanned together to allow ions of some mass to charge ratio (m/z) through the two constant radii, r and R_E of the sectors. Equation 1.3 describes mathematically how a particular magnetic and electric field can allow only ions of one particular m/z is detected.⁴

$$m/z = B^2r^2/ER_E \quad \text{Equation 1.3}$$

A schematic of the double focusing MS, used in the present studies, is illustrated in Figure 1.1 where the trajectory of the ions is such that they are focused by the two separate sectors. Double focusing the ions ensures that the ions have the same velocity, making the m/z ratio dependent only on the radii of the two sectors and the strength of the two fields. Since slightly varied velocities cause peak broadening, this instrument configuration greatly increases the possible resolution.⁴

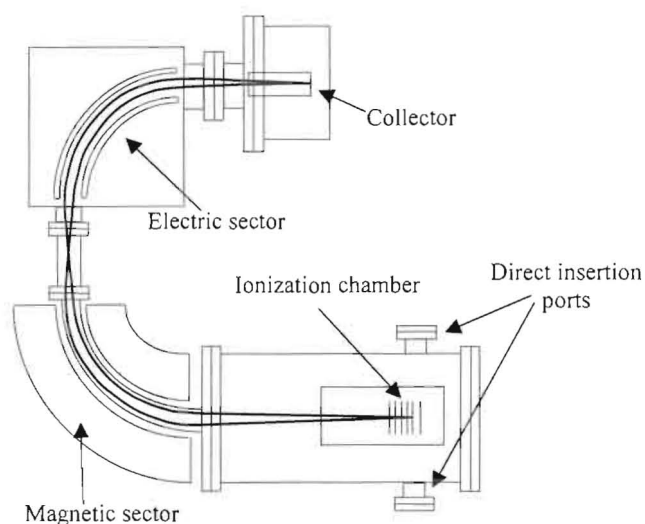


Figure 1.1: Schematic of a reverse geometry double focusing mass spectrometer where the bold lines demonstrate the trajectory of the ions and the focusing effect of double sector.

The utility of mass spectrometry is often limited by its' resolving capabilities, or in other words, how well neighboring peaks can be separated. Resolution (R) can be quantified in MS using Equation 1.4, and is measured as the mass of sample ion divided by the mass difference between the known mass of a calibration ion and the mass of a

sample ion (upper mass minus lower mass). One definition of resolution considers peaks to be resolved when only 10% (5% of each peak) of the peaks overlap.⁴

$$R = m/\Delta m \quad \text{Equation 1.4}$$

Magnetic sectors, unlike quadrupole MS, maintain the same resolution throughout the calibrated mass range where low resolution tends to run from 800-2000 and high resolution occurs from 2,500 and greater. Resolution depends greatly on the distribution of accelerating voltages through electronic lenses in the ionization chamber where slight variations in voltages cause peak broadening. The electronic lenses must be monitored and adjusted occasionally to ensure the appropriate resolution.

Double focusing instruments provide improved resolution, yet there are different orientations and arrangements possible. A Mattauch-Herzog double focusing mass spectrometer has an electric sector followed by a magnetic sector that disperses the ions simultaneously into different radii. The Nier-Johnson design is similar in that an electric sector is followed by the magnetic sector with the added ability to change the magnetic field and scan over masses at constant radii. Instead of the ions being analyzed by the electric sector first, the sector order can be switched where the magnetic sector analyzes the ion first. This general arrangement is regularly referred to as reverse geometry. The reversed geometry design allows for new experiments and is the orientation and arrangement that the following mass spectrometry studies were performed.⁴

With a reverse geometry Nier-Johnson mass spectrometer, a variety of experiments can be performed. High intensity scans with resolution, $R = 800-2,000$, are

easily performed for maximizing the intensity of small peaks. High resolution scans where $R = 2,500-70,000$ may be performed to distinguish the exact mass of a substance for characterization. Metastable ion scans can also be performed where the molecular (original) ions dissociate as they flow through the mass spectrometer, so you can detect their dissociation. To enhance the dissociation or induce a separate reaction, a collision cell may be placed in between the two sectors of a double focusing MS in a field free region (FFR). The collision cell is filled with a gas to promote collisions which tend to enhance the breakdown of the ion of interest. This type of experiment is called metastable analysis, and when you observe a metastable ion it indicates that that dissociation pathway exists. Since the electric sector is the second sector of the reverse geometry Nier-Johnson MS, the kinetic energy released (KER) by the ion can be detected. Mass-analyzed ion kinetic energy spectroscopy (MIKES) uses the magnetic sector to filter the ions to one specific mass to charge ratio, the ion dissociates in the field free region, and then the electric sector scans its field in terms of the kinetic energy (Equation 1.2).⁵

Direct insertion is a preferred ionization technique for the MS analysis of solid samples. The direct insertion (DI) probe introduces solid samples into the ionization chamber of a mass spectrometer where the sample of interest is placed in a crucible and heated. Figure 1.1 illustrates the possible ports where the DI probe can be added where the subliming samples are introduced at the center of the acceleration region. Once the appropriate amount of sample is added, the loaded sample holder is inserted into the mass spectrometer with the appropriate seals tightened to maintain a high vacuum in the MS. The shaft of the DI probe is utilized to transfer the sample from atmospheric pressure to the low source pressure region of the ionization chamber. Once the sample is near to the

ionization chamber, the probe may be resistively heated to facilitate the sublimation of the solid. The ionization chamber itself is maintained at elevated temperatures to avoid the deposition of the solid onto the chambers walls.

Electron impact (EI) ionization bombards an electron into the sample with enough energy to remove an electron from the sample. The electron deficient sample is accelerated by a voltage gradient used by electric lenses. The accelerated ions are analyzed through the magnetic and electric sectors as previously described, and collected by an electron multiplier.⁴

1.3 Experimental Section and Typical Data Analysis

Using the departmental high resolution reverse geometry double focusing mass spectrometer, Finnigan MAT 8430, the gas phase reactions of various metal-bound acetylacetonates were investigated. To maximize gas phase collisions, without charge transfer reactions occurring, the solid samples of two metal acetylacetonates were mixed inside of the crucible at low source pressure conditions. The mixtures showing a possible reaction were then separated by evaporating a methanol solution of one complex on the outside of the crucible and the other complex was deposited into the cup of the crucible to ensure that a gas phase reaction occurred. In both cases, a direct insertion probe introduced the samples into the ionization chamber.

High intensity scans on the order of 2 decades per second were utilized to detect any mixed-metal complexes below m/z 800. As heating occurs, these complexes sublime, and are available for collisions in the ionization chamber. Electron impact ionization (70 eV) ionizes the complexes, where further collisions may occur with other neutral gas phase complexes resulting in large single metal or mixed-metal complexes. Four series

consisting of mixing the complexes listed in Table 1.1 with Al(hfac)₃, Al(acac)₃, Ni(acac)₂, or Ni(hfac)₂ examined the ability of the four complexes to form mixed-metal complexes were determined.

Table 1.1: Complexes mixed with the two aluminum and two nickel complexes to test their ability to form mixed-metals. Isotopic abundances were used to verify the identity of the mixed-metal complex ion.

Complexes in Series	Metal	Principle Isotope (natural abundance)	Other Isotopes (natural abundance)
Li(acac)	Li	7 (92.6%)	6 (7.4%)
Al(acac) ₃ Al(hfac) ₃	Al	27 (100.0%)	
V(acac) ₃	V	51 (99.8%)	50 (0.2%)
Cr(acac) ₃	Cr	52 (83.8%)	50 (3.3%), 53 (9.5%), 54 (2.4%)
Mn(acac) ₂ Mn(acac) ₃ Mn(hfac) ₂ Mn(hfac) ₃	Mn	55 (100.0%)	
Fe(acac) ₃ Fe(hfac) ₂	Fe	56 (91.7%)	54 (5.8%), 57 (2.2%), 58 (.3%)
Co(acac) ₂ Co(acac) ₃ Co(hfac) ₂	Co	59 (100.0%)	
Ni(acac) ₂ Ni(acac) ₂	Ni	58 (68.3%)	60 (26.1%), 61 (1.1%), 62 (3.6%), 64 (0.9%)
Cu(acac) ₂ Cu(hfac) ₂	Cu	63 (69.2%)	65 (30.8%)
Zn(acac) ₂	Zn	64 (48.6%)	66 (27.9%), 67 (4.1%), 68 (18.8), 70 (0.6%)
Ga(acac) ₃	Ga	69 (60.1%)	71 (39.9%)
Rh(acac) ₃	Rh	103 (100.0%)	
Cd(acac) ₂	Cd	114 (28.7%)	106 (1.2%), 110 (12.5%), 111 (12.8), 112 (24.1%), 113 (12.2%), 116 (7.5%)

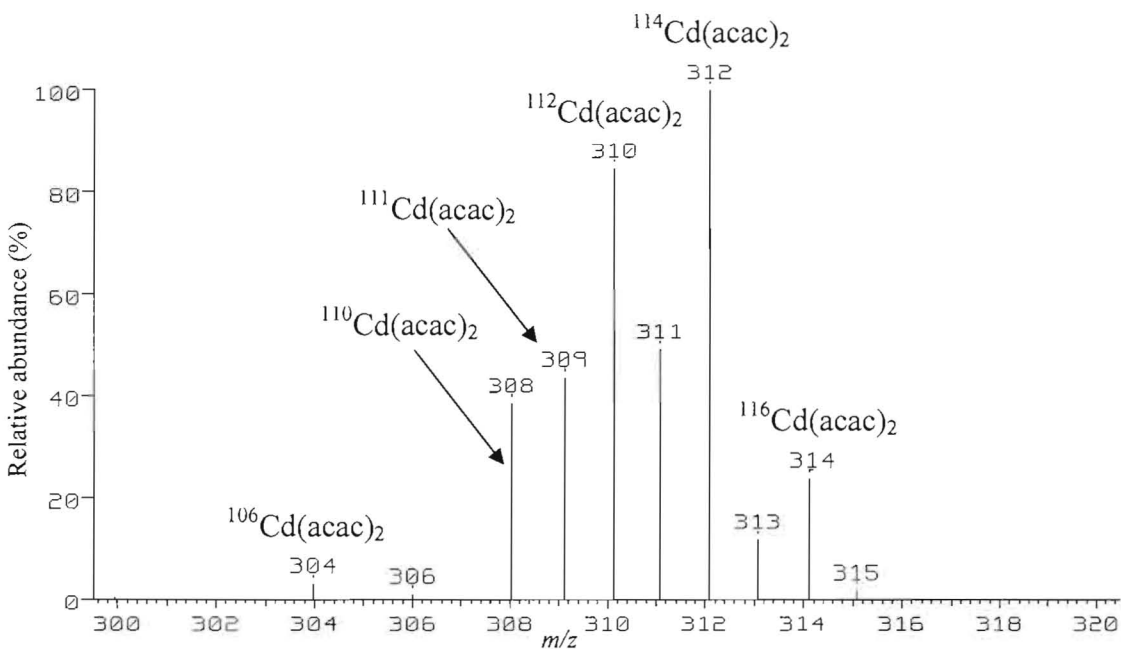


Figure 1.2: The mass spectrum of $\text{Cd}(\text{acac})_2$ where the isotope pattern is clearly seen with the principle isotope (^{114}Cd) being the most abundant peak. The mass of 198 accounts for the mass of two acac ligands which have a mass of 99 amu each.

The spectra of the mixed complexes were analyzed by subtracting out of the individual mass spectra of each component. Each complex was first examined by mass spectrometry, and the observed dissociation reactions were compared to those reported in the literature. Common peaks between the two complexes of related size were subtracted to retain only the peaks that occur from a reaction between the two mixed complexes. The remaining peaks were then identified by using the predicted isotope pattern of the complex and the general dissociation schemes of the complexes as a guide.

Chapter 2: Dissociation and Crystal Structures of Metal Acetylacetonates

2.1 Introduction

Metal acetylacetonates, $M(\text{acac})$, are coordinating compounds with volatility and solubility in organic solvents. $M(\text{acac})$ s are used as catalysts in a number of reactions, but of more interest to the present study, is its use as precursors in thin film layer formation. Different ways to deposit thin films using various metal acetylacetonates as precursors are continually being discovered where Duta et. al.⁶ studied the morphology of a dense and nanoporous thin film by forming the thin film with $\text{Ti}(\text{acac})_3$. Yan and coworkers⁷ developed a process for self-assembly of high quality rare-earth oxide nanocrystals by using rare-earth acetylacetonates as precursors.

As technology increases, the importance of precision and accuracy also increases where advanced knowledge on a broad array of reactions is necessary, especially the minor species formed in gas phase reactions. The gas phase association reactions of metal acetylacetonates have the potential of greatly affecting the properties of the nanocrystal being formed. It is necessary to identify and characterize the reactions formed from two metal acetylacetonates as to minimize imperfections in nanostructures or be utilized to selectively dope thin films. The low pressure gas phase association reaction experiments described here use a double focusing mass spectrometer to examine the reactivity of 4 particular metal complexes, $\text{Al}(\text{hfac})_3$, $\text{Al}(\text{acac})_3$, $\text{Ni}(\text{acac})_2$, or $\text{Ni}(\text{hfac})_2$.

The gas phase unimolecular dissociation of acetylacetone ($\text{H}(\text{acac})$), hexafluoroacetylacetonate ($\text{H}(\text{hfac})$), metal acetylacetonates and metal hexafluoroacetylacetonates ($\text{M}(\text{hfac})$) investigated using the departmental high resolution

double focusing mass spectrometer were compared to similar studies reported in literature in order to properly characterize the association reactions.

2.2 Acetylacetonate (H(acac))

Acetylacetonate, 2,4-pentadione, an organic compound often used in separating out trace amounts of metals from various types of samples,⁸ coordinates extremely well to metals given its enhanced stability from the keto, enol tautomerism.⁹ The enol form (84%)⁹ is much more abundant than the keto form, and displays aromatic behavior.¹⁰

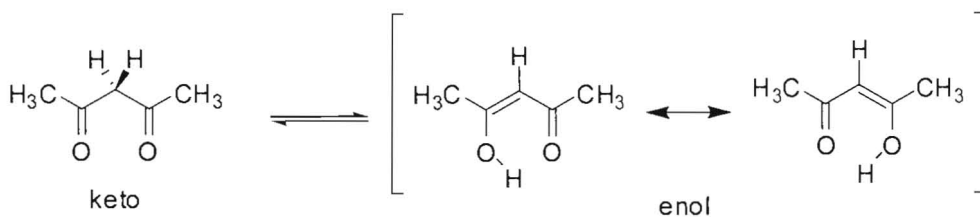


Figure 2.1: Tautomerism of acetylacetone where the keto form is on the left and the two resonant enol forms are on the right.¹⁰

The dissociation of acetylacetone has been observed using mass spectrometry where fragment ions from several pathways were detected. The fragment ions observed in the mass spectrum are illustrated in Figure 2.2 with Scheme 2.1 describing the most dominate dissociation pathways. The pathways leading to the observed ions have been confirmed through metastable analysis and isotopic labeling where deuterated water will readily exchange deuterium with the two lone hydrogens on acetylacetone distinguishing which hydrogens are in the fragment ion.¹⁰ For example, in the dissociation pathway leading to fragment ion F_{ha} , the hydrogens lost in the neutral fragment, CH_2CO , are from the methyl group and not from the two lone hydrogens.

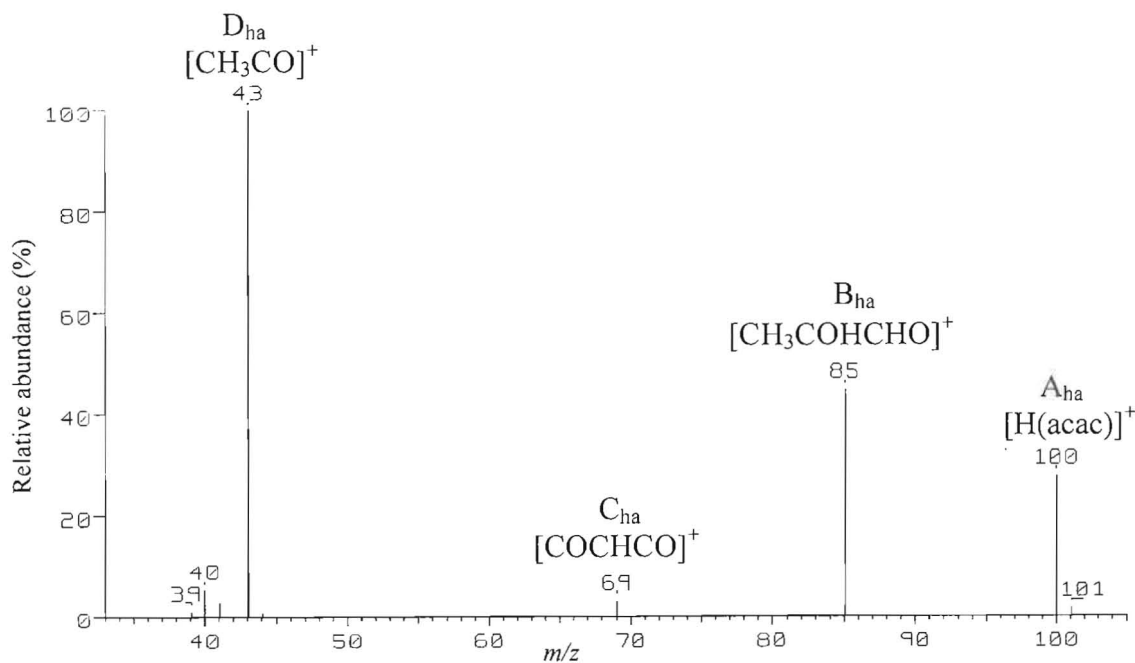
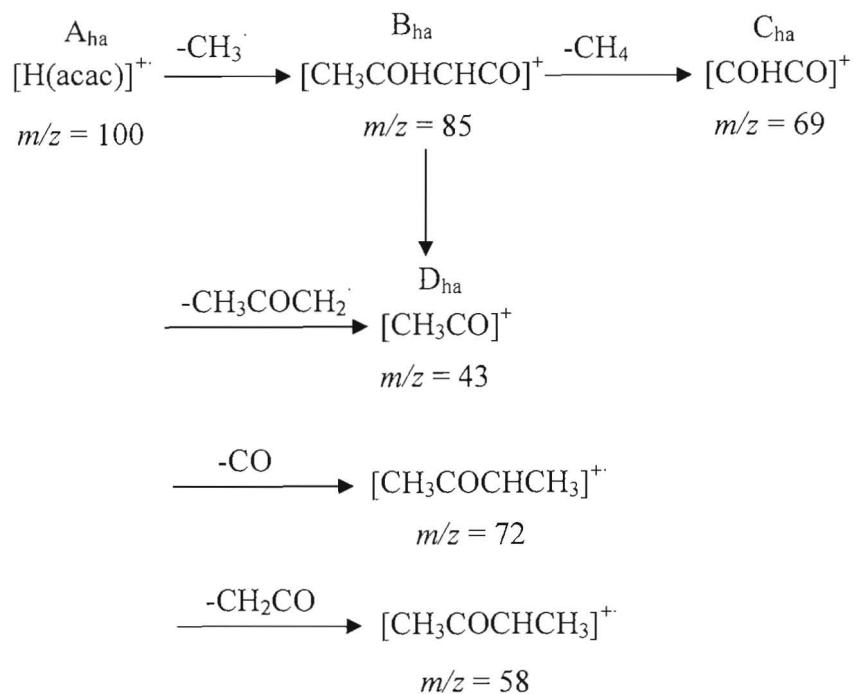


Figure 2.2: Mass spectrum of the dissociation of H(acac) with major fragment ions labeled where ions E_{ha} and F_{ha} were not observed on the departmental MS.

As demonstrated in the dissociation Scheme 2.1, acetylacetone (A_{ha}) dissociates like most organic molecules where odd-electron ions tend to lose odd-electron fragments to afford the more stable even-electron species. The preferred loss of a methyl radical (CH₃) from H(acac) (*m/z* 100) illustrates the relative stability of even-electron species with a relatively large peak at *m/z* 85 peak (B_{ha}). The newly formed fragment may in turn lose an even-electron methane group (16 amu) producing the fragment ion at *m/z* 69 (C_{ha}). The loss of ketene, CH₂CO, from the fragment ion B_{ha} to form fragment ion D_{ha} was confirmed through metastable analysis.¹⁰ Acetylacetone (A_{ha}), the molecular ion, may also lose a CH₃COCH₂ radical to form the same ion at *m/z* 43 (D_{ha}). Acetylacetone, though a minor pathway, has also been observed to lose a carbonyl (28 amu) to form fragment ion E_{ha} or lose a ketene (42 amu) to form fragment ion F_{ha}.¹⁰



Scheme 2.1: Dissociation to products of acetylacetone as observed in mass spectrometry.¹⁰

2.3 Hexafluoroacetylacetonate (H(hfac))

Acetylacetone can be easily manipulated to form many different derivative compounds with the oxygen, for example, being substituted with sulfur or nitrogen,^{11,12} the γ -hydrogen being exchanged with many electrophilic substituent groups,¹³ or the methyl groups being exchanged with either alkyl, phenyl, or fluorinated alkyl groups.¹⁴ The fluorinated compounds are the preferred derivative in mass spectrometric studies as they enhance the compounds volatility, stabilize the enol form of the compound,¹⁵ and aid greatly in clarifying the mass spectra where a loss of fluorine (19 amu) is much easier to distinguish than the loss of hydrogen (1 amu).

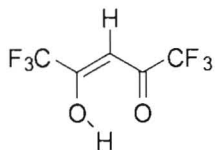
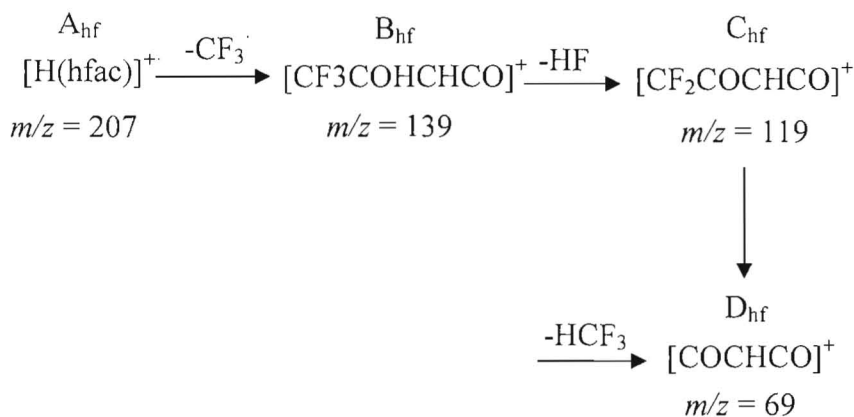
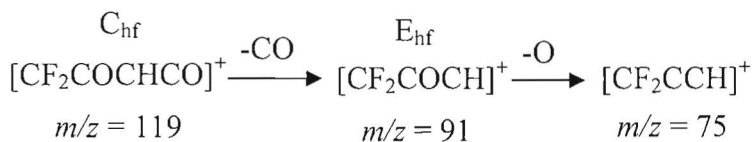


Figure 2.3: 1,1,1-5,5,5-hexafluoroacetylacetone (hfac), a derivative of acetylacetone.¹⁵

The fragmentation of many of the fluorinated derivatives have been studied using mass spectrometry with the specific derivative 1,1,1-5,5,5-hexafluoro-2,4,-pentadione being used extensively in these studies and hereafter abbreviated H(hfac). Rubesch et. al.¹⁵ show that the dissociation pattern of H(acac) changes due to the fluorine substitution.



Scheme 2.2a: The predominant species in the dissociation of H(hfac) with two ions, B_{hf} and C_{hf}, leading to the formation of D_{hf}.¹⁵



Scheme 2.2b: Further dissociation products of H(hfac) starting from C_{hf} with the final pathway not detected by the departmental instrument.¹⁵

As illustrated in Scheme 2.2a, the major dissociation pathway of H(hfac) (A_{hf}) is the loss of a fluorinated methyl radical (CF_3) to form fragment ion B_{hf} . This fragmentation is analogous to the dissociation of H(acac), as presented in Scheme 2.1, where a methyl radical leaves. After the initial odd-electron fragment is lost, even-electron fragmentations dominate. Another fragment lost analogous to H(acac) dissociation is the loss of HCF_3 from the fragment ion B_{hf} to form an ion with m/z 69 (F_{hf}). The loss of HF (20 amu) from ion B_{hf} to form ion C_{hf} is a major dissociation channel for H(hfac) with no correlation to the fragmentation of H(acac). The loss of HF results from fluorine migrating to a lone hydrogen in the compound and is confirmed.¹⁵

As presented in Scheme 2.2b, a carbonyl could be lost from ion C_{hf} to form m/z 91 (D_{hf}) unlike the H(acac) species where it is lost from the molecular ion. A peak at m/z 97, analogous to the dominant loss channel in the H(acac) spectrum, m/z 43, was not observed suggesting that CF_3CO is not a favored fragment in this derivative due to the preferential loss of HF.¹⁵

The gas phase dissociation of $Cu(hfac)_2$ is illustrated in Figure 2.4 where the dissociation of H(hfac) is also observed. The most abundant peak in the spectrum corresponds to the loss of a fluorinated methyl radical, CF_3 , from hexafluoroacetylacetonate and is labeled as $[Cu(hfac-CF_3)]^+$. The natural abundance isotope pattern for copper, as presented in Table 1.1, is clearly observed in the mass spectrum.

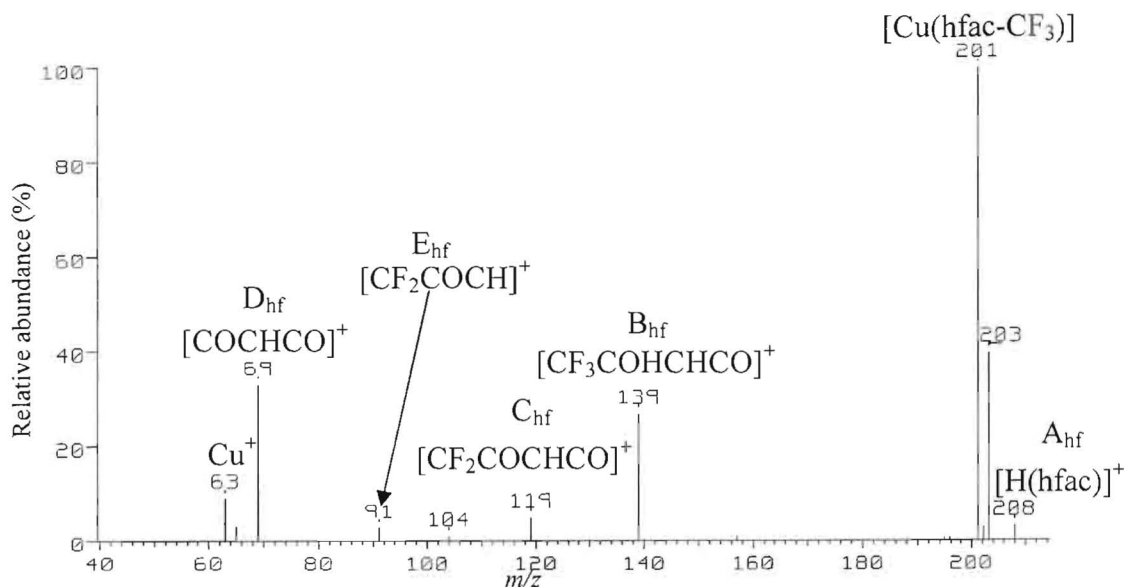


Figure 2.4: Mass spectrum of the dissociation of H(acac) with fragment ions labeled with minus signs indicating a loss of that particular fragment.

2.4 Metal Acetylacetonates (M(acac))

The metal coordination of acetylacetonate greatly increases the complexity of the mass spectra where nearly every metal and metalloid in the periodic table has been coordinated with a derivative of acetylacetonate.⁹ The predominant structure of these complexes is similar to that of the manganese complex shown in Figure 2.5. Coordination with acetylacetonate helps the metal act like a covalent compound with properties such as increased volatility and solubility in organic solvents.⁹ The most abundant form of coordination is bidentate through oxygen where the bidentate ligand forms an enolate with a single negative charge. Other forms exist including bonding by one oxygen (unidentate), bidentate coordination through the keto form of the ligand, and bonding through double bonds or to a carbon.⁹

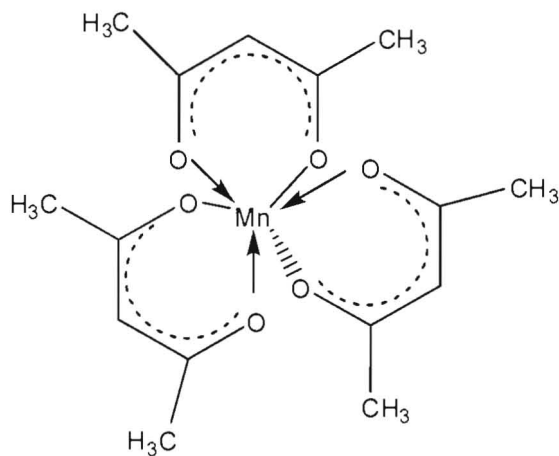


Figure 2.5: Diagram of manganese tris(acetylacetonate) where the enolate form of acetylacetonate dominates and arrows indicate coordination.

The enolate chelation by the metal occurs most readily for metal acetylacetonates where the coordination number (m) and oxidation state (n) of the metal complex determines the number of acetylacetonate ligands that chelate to the metal. Table 2.1 contains a list of coordination numbers and oxidation states for the metals used in this study with a list of possible environments for the starting oxidation state of the complexes. Depending on the oxidation state of the metal, three different types of environments exist. For example, if the coordination number is equal to twice the oxidation state ($m=2n$), then a neutral complex, like Mn(III)(acac)₃ will form as illustrated in Figure 2.5. When the coordination number is larger than twice the oxidation state ($m>2n$), the complex acts like a Lewis acid forming adducts, oligomers, or polymers like [Zn(acac)₂(NH₃)₂] and [Ni(acac)₂]₃. The third configuration is when the coordination number is less than twice the coordination ($m<2n$), where a complex ion of the form [Si(acac)]⁺ may result.⁹

Table 2.1: The coordination number, common oxidation state, some complexes in the series, and possible coordination environment are listed for metals relevant to this study.

Metal	Coordination Number (m)	Common Oxidation States (n)	Complexes in Series	Environment ⁹
Li	4	+1	Li(acac)	$m > 2n$
Al	6	+3	Al(acac) ₃	$M = 2n$
V	6, 4	+4, +3, +2	V(acac) ₃	$M = 2n$
Cr	6, 4	+3, +2	Cr(acac) ₃	$M = 2n$
Mn	6, 4	+4, +3, +2	Mn(acac) ₂ , Mn(acac) ₃	$m > 2n$, $m = 2n$ $M = 2n$
Fe	6, 4	+3, +2	Fe(acac) ₃ , Fe(hfac) ₂	$m = 2n$ $m > 2n$, $m = 2n$
Co	6, 4	+3, +2	Co(acac) ₂ , Co(acac) ₃	$m > 2n$, $m = 2n$ $M = 2n$
Ni	6, 4	+3, +2	Ni(acac) ₂	$m > 2n$, $m = 2n$
Cu	6, 4	+2, +1	Cu(acac) ₂	$m > 2n$, $m = 2n$
Zn	6, 4	+2	Zn(acac) ₂	$m > 2n$, $m = 2n$
Ga	6	+3	Ga(acac) ₃	$M = 2n$
Rh	6	+4, +3, +2	Rh(acac) ₃	$M = 2n$
Cd	6, 4	+2	Cd(acac) ₂	$m > 2n$, $m = 2n$

MacDonald and Shannon¹⁶ completed the first detailed MS study on metal acetylacetonates. They investigated a series of metal acetylacetonates and metal benzoylacetylacetonate (bzac) complexes to determine the general dissociation pathway and structure of these complexes. The ability of the metal to retain its oxidation state was found to greatly influence the appearance and intensity, i.e. stability, of the fragmented ions. This interpretation is again based on the fact that even-electron species tend to fragment even-electron neutral compounds, and odd-electron species tend to lose odd-electron fragment as described in Scheme 2.3a, b, and c. As illustrated in Figure 2.6 below, fragment ion B_{ma} subsequently can lose even-electron fragments CH₂CO or CH₃COCCOCH₃ to form C_{ma} or D_{ma} as illustrated by the resulting product ion observed in Figure 2.6 were L represents an acetylacetonate ligand. With this trend in mind, a

preferential even-electron metal acetylacetonate ion could form from an odd-electron ion by either losing an odd-electron fragment or having the metal donate an electron to the ligand to form an even-electron ion.¹⁶

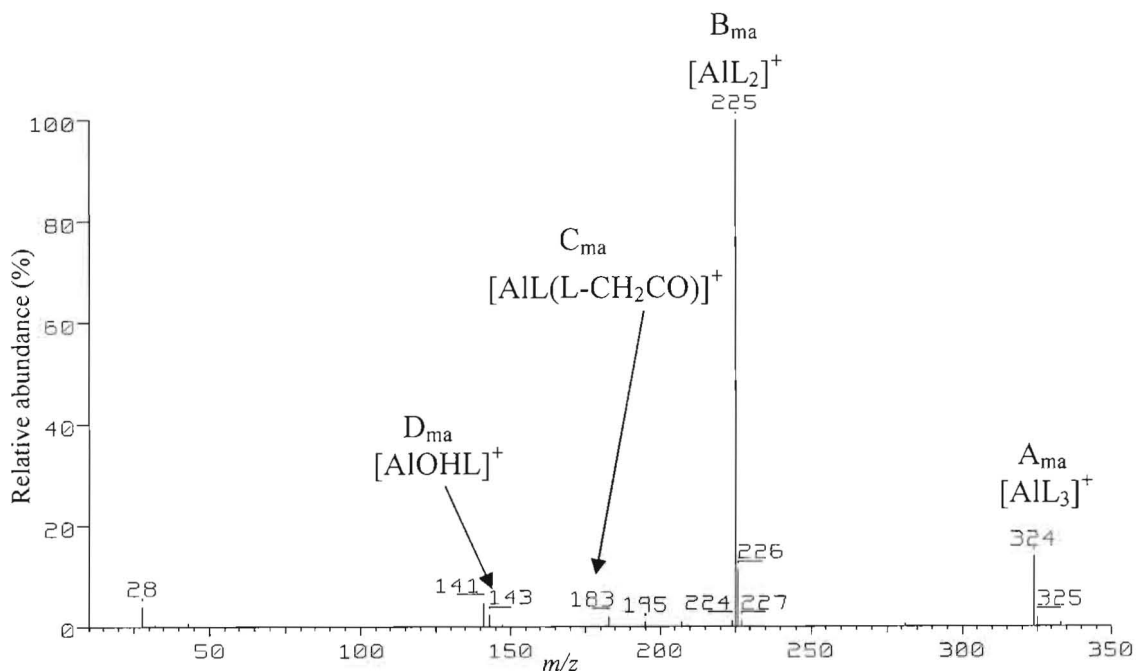
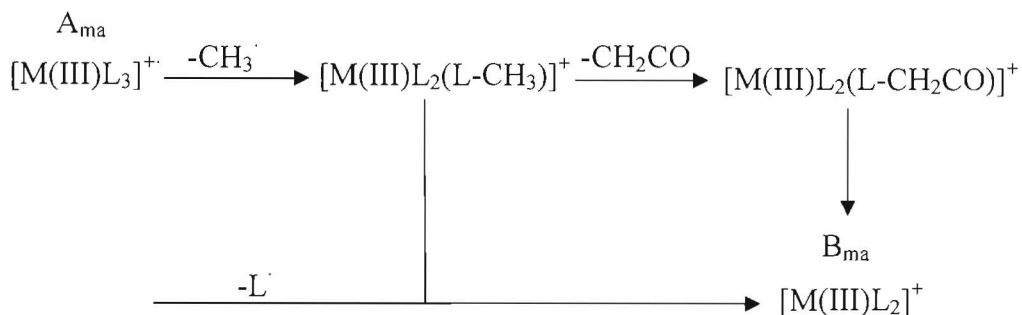


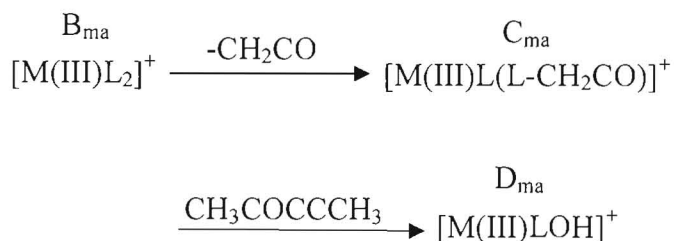
Figure 2.6: Mass spectrum of the dissociation of Al(acac)₃ which does not reduce to a lower oxidation state.

Bancroft, et. al.¹⁷ investigated how metals of oxidation state 3+ (Ti, V, Cr, Mn, Fe, Co, and Al), chelated to acetylacetonates, can be split into two groups depending on the observed dissociation patterns of these complexes using mass spectrometry. The first group of 3+ species consists of titanium and vanadium which more readily observed form an oxy or hydroxyl species with oxygen only bonded to the metal, while the second group consisting of aluminum, chromium, manganese, iron, and cobalt does not have many dissociation products with oxy or hydroxy groups. The dissociation pathways of the second group illustrated in Scheme 2.3a, b and c, shows that it can be further separated by the metals that readily reduce (Cr, Mn, Fe, and Co) and those that do not (Al). The

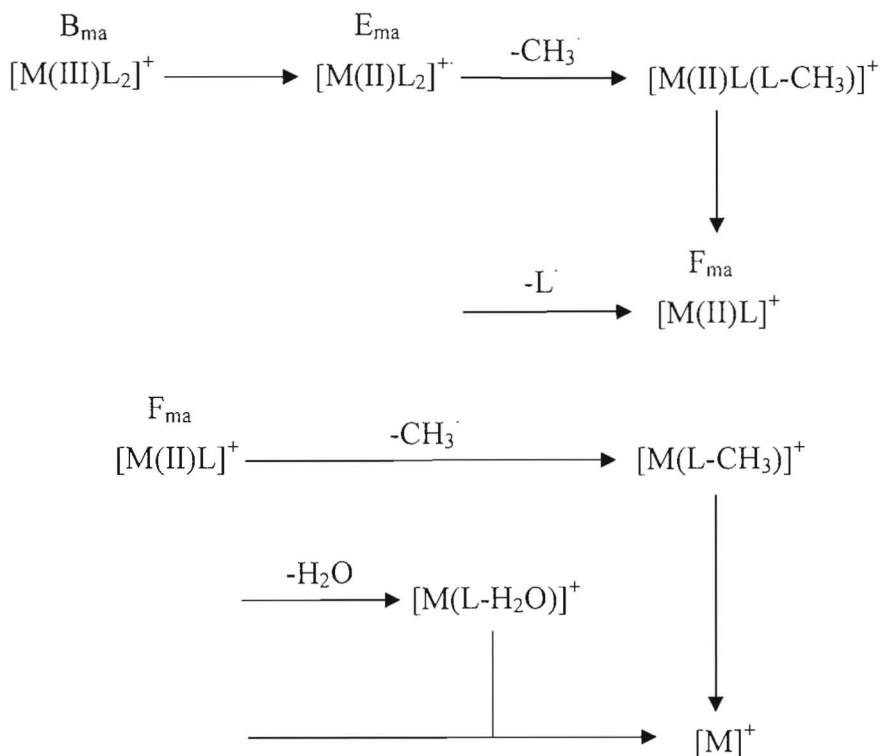
reduction of the oxidation state is best observed by the relative intensity of the $[M(\text{acac})]^+$ peak where chromium (23%) does not reduce as readily as cobalt (29%), and aluminum, which does not readily reduced barely detects the $[M(\text{acac})]^+$, F_{ma} , peak as observed in Figure 2.6. Scheme 2.3a, b, and c presents the general scheme for all metal acetylacetonates and preserves the odd-/even-electron tendencies if changes in oxidation state are considered.¹⁷



Scheme 2.3a: The initial major dissociation from A_{ma} is the loss of an odd-electron fragment which is followed by even-electron fragments where B_{ma} is the most abundant ion in for the second group.¹⁷ (M = Cr, Mn, Fe, Co, and Al and L = acac)



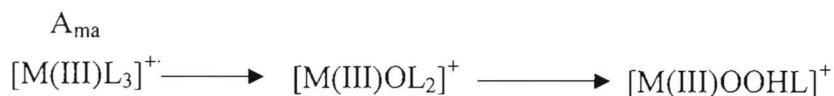
Scheme 2.3b: The dissociation pathway followed when the metal does not reduce in oxidation state. The dissociation of $\text{Al}(\text{acac})_3$ is illustrated in Figure 2.6.¹⁷ (M = Al, Cr, Mn, Fe, and Co and L = acac)



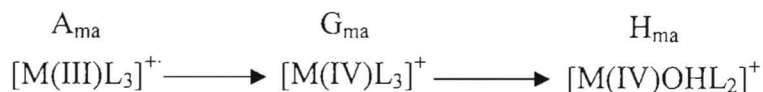
Scheme 2.3c: Dissociation pathway of metal tris(acetylacetonate) when the metals do reduce.¹⁷ (M = Cr, Mn, Fe, Co, and Al and L = acac)

The two groups of metals (V and Ti versus Al, Cr, Mn, Fe, and Co) can be distinguished depending on the presence and intensity of fragment ions observed as shown in Scheme 2.4. Vanadium and titanium complexes exhibit a significant increase of fragment ions shown in Scheme 2.4 compared to the complexes in the other group. Vanadium and titanium tris(acetylacetonate) both tend to oxidize rapidly in the presence of air, and although necessary precautions were made to maintain the purity of the $\text{M}(\text{acac})_3$, the presence of a stable oxidized ion was still observed in the mass spectra. It was suggested that the metals of the first group, V and Ti, may change their oxidation state as they dissociate, however instead of making an odd-electron ion, they increase their oxidation state with the additional electron making the odd-electron ion an even-

electron fragment. The increase in oxidation state is suggested because the starting odd-electron ion predominately loses an even-electron which is normally an unfavored process.¹⁷



Scheme 2.4a: The dissociation pathway of $M(\text{acac})_3$, where $M = \text{Ti}$ or V and L is acetylacetonate, showing the loss of an odd-electron species to maintain the preferred even-electron species.¹⁷



Scheme 2.4b: The dissociation pathway of $M(\text{acac})_3$, where $M = \text{Ti}$ or V and L is acetylacetonate, when an increase in oxidation state occurs to form an even-electron ion which then dissociates further.¹⁷

Reichert and Westmore¹⁸ examined the dissociation pattern of various metal bis(acetylacetonate) complexes with metal centers Mn , Fe , Co , Ni , Cu , and Zn . The metal bis(acetylacetonate) complexes show significant to high relative abundances of the molecular ion, $[M(\text{acac})_2]^+$. The loss of a full ligand is the most abundant peak in the mass spectra for Mn , Fe , Co , Ni , and Zn . These species were observed to dissociate similar to the previously described metal tris(acetylacetonate) complexes with some minor differences in relative intensities and the absence of the third ligand as illustrated in Figure 2.7 where the highest mass is the molecular ion, $[Cu(\text{acac})_2]^+$.¹⁸

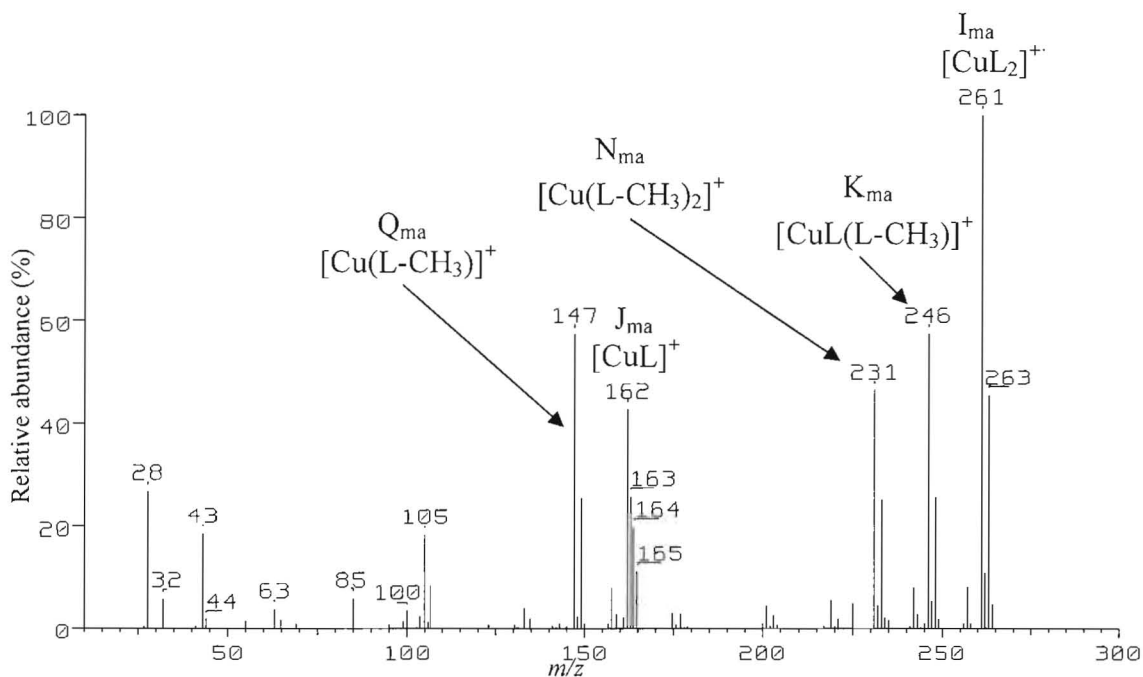
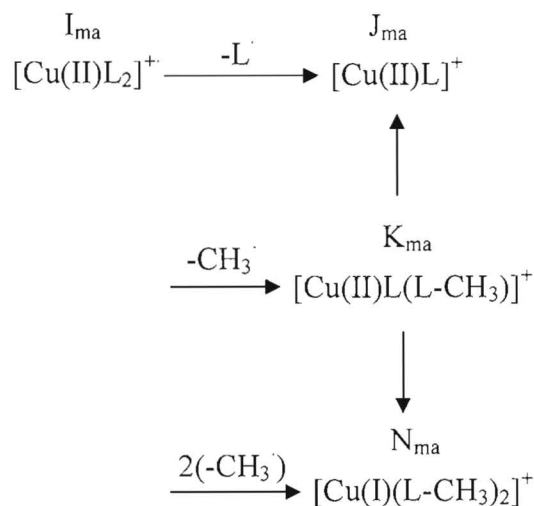


Figure 2.7: Mass spectrum of the dissociation of $\text{Cu}(\text{acac})_2$ where L is acetylacetonate, and fragment J_{ma} has two other mass degenerate forms labeled P_{ma} and R_{ma} .

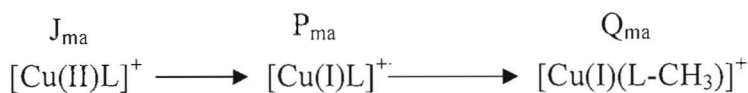
Copper varies from the other metal bis(acetylacetonate) complexes because it has a stable oxidation state of 1+. The reduction of Cu(II) to Cu(I) supports additional fragmentation pathways shown in Scheme 2.5 illustrating three converging pathways to the formation of fragment ion Q_{ma} . The increase in relative abundance is shown in Figure 2.7 for Q_{ma} .¹⁸

As described in Scheme 2.5a, b, and c, the dissociation mechanism begins with the molecular ion, I_{ma} , losing a radical which creates an even-electron species, J_{ma} or K_{ma} . The even-electron copper fragment ion J_{ma} can reduce oxidation states to 1+ to form P_{ma} as illustrated in Scheme 2.5b. Fragment ion P_{ma} can lose a methyl radical to form ion Q_{ma} . The other even-electron copper fragment ion, K_{ma} , can either lose an even-electron fragment to form J_{ma} or the copper can be reduced allowing another odd-electron radical

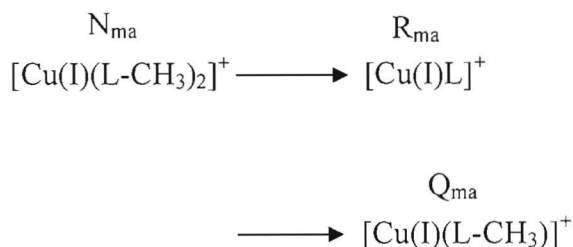
to be lost forming N_{ma} . The subsequent dissociation of N_{ma} leads to R_{ma} and Q_{ma} where R_{ma} is mass degenerate with J_{ma} and P_{ma} .



Scheme 2.5a: The initial dissociation of CuL_2 where L is acetylacetonate can occur by three different pathways with the N_{ma} changing oxidation state.¹⁸



Scheme 2.5b: Copper is reduced from 2+, J_{ma} , to 1+, P_{ma} , which stabilizes the loss of a methyl radical to form Q_{ma} .¹⁸



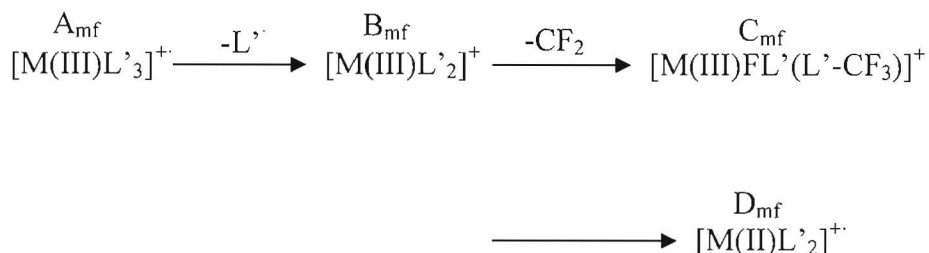
Scheme 2.5c: The reduced copper only loses even-electron fragments to form R_{ma} and Q_{ma} where R_{ma} is mass degenerate with J_{ma} and P_{ma} .¹⁸

A third pathway, confirmed through metastable analysis, exists where the molecular ion, I_{ma} , loses two methyl radicals in succession to get to fragment ion N_{ma} .

The increased intensity due to the increased pathways to Q_{ma} , $[\text{Cu}(\text{L}-\text{CH}_3)]^+$, represents convincing evidence that the oxidation state changes throughout the dissociation of a metal acetylacetonate complex.¹⁸

2.5 Metal Hexafluoroacetylacetonates ($\text{M}(\text{hfac})_n$)

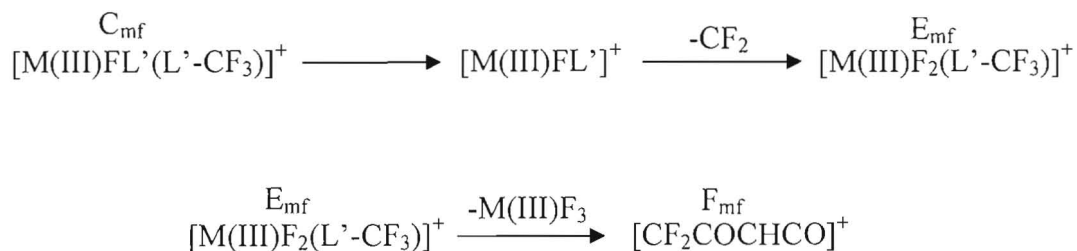
The fluorinated metal acetylacetonate complexes have a higher volatility and have a slightly higher ionization potential, yet the dissociation pathways are similar to the non-fluorinated metal acetylacetonate complexes. Clobes et. al.¹⁹ studied the mass spectra of partially fluorinated acetylacetonate complexes of Al(III), Cr(III), Fe(III), and Co(III). Various metal 1,1,1,-5,5,5-hexafluoro-2,4-pentadionate (hfac) complexes were reported with the general scheme of their dissociation illustrated in Scheme 2.6. The metal centers ability to change oxidation state determines what fragments are favored.¹⁹



Scheme 2.6a: The two fragmentation pathways possible for $\text{M}(\text{III})(\text{hfac})_3$ where C_{mf} maintains the oxidation state and D_{mf} reduces in oxidation state.¹⁹ ($\text{L}' = \text{hfac}$)

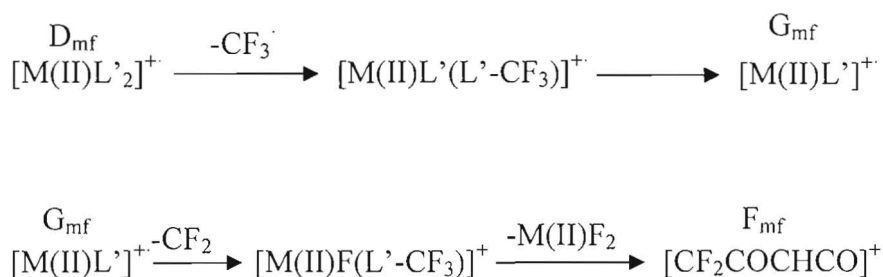
The dissociation of the metal tris(hexafluoroacetylacetonate) starts with the loss of an odd-electron ligand as described in Scheme 2.6a. The subsequent dissociations differ depending on whether they reduce in oxidation state. If, like Al, the metal does not reduce, a rearrangement occurs where fluorine migrates to the metal and a net loss of CF_2 is observed. Fragment ion C_{mf} illustrates the arrangement with fluorine before the ligand signifying a metal to fluorine bond, and a loss of CF_3 from the ligand for a net loss of

CF₂. Successive losses from C_{mf} are presented in Scheme 2.6b. Scheme 2.6c presents the dissociation pattern of D_{mf} when the metal in ion B_{mf} removes an electron from the ligand and reduces in oxidation state forming the odd-electron ion D_{mf}.¹⁹



Scheme 2.6b: The dissociation pattern for metal complexes of oxidation state 3+ that does not reduce in oxidation state.¹⁹ (L' = hfac)

The predominant dissociation path for Al and other metals that do not readily reduce in oxidation state is followed in Scheme 2.6b. The strong metal to fluorine bond remains intact while C_{mf} loses an even-electron fragment. The following reaction is a rearrangement to form another metal to fluorine bond labeled E_{mf} where the ligand loses a fluorinated methyl group and the metal gains fluorine. Fragment ion E_{mf} can rearrange again to form a neutral metal fluoride and ion F_{mf} at *m/z* 119.¹⁹



Scheme 2.6c: The dissociation pathways for metals that readily reduce in oxidation state.¹⁹ (M = Cr, Fe, Co with L' = hfac)

Metal centers that can remove an electron from the ligand allow consecutive losses of odd-electrons. The first odd-electron lost was the full ligand demonstrated in Scheme 2.6a, and the second is the loss of a fluorinated methyl radical occurring after the metal reduces. The rest of the ligand is then lost to form fragment ion G_{mf} . Since the metals are at their lowest common oxidation state, fragment ion G_{mf} rearranges to have fluorine migrate to the metal with a net loss of CF_2 . The final loss is of the neutral metal (II) fluoride leaving the fragment ion F_{mf} . This leads to the conclusion that fluorine migration is indicative of a metal's resistance to reduce in oxidation state.¹⁹

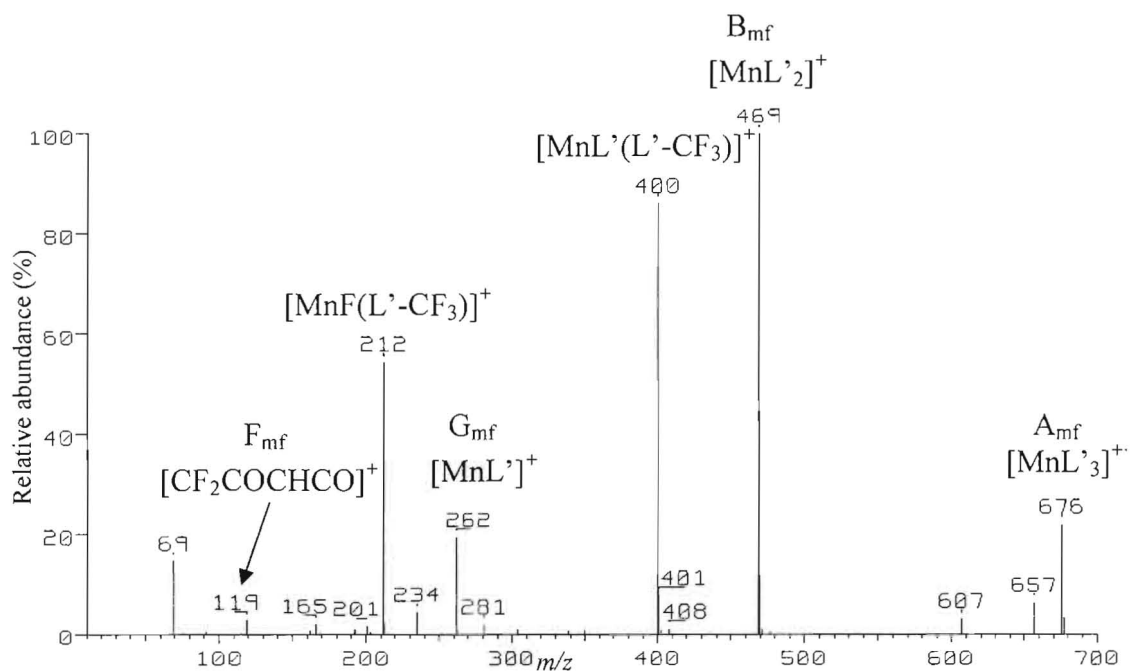


Figure 2.9: Mass spectrum of synthesized $Mn(hfac)_3$ with major dissociation peaks indicative of a metal center that reduces from a 3+ to a 2+ oxidation state. (L = hfac)

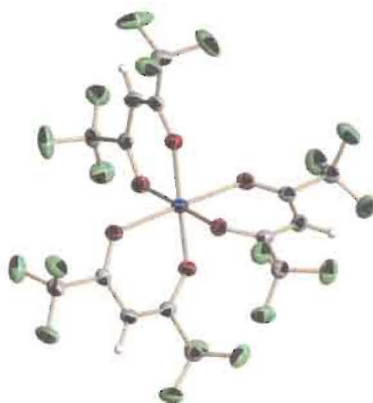
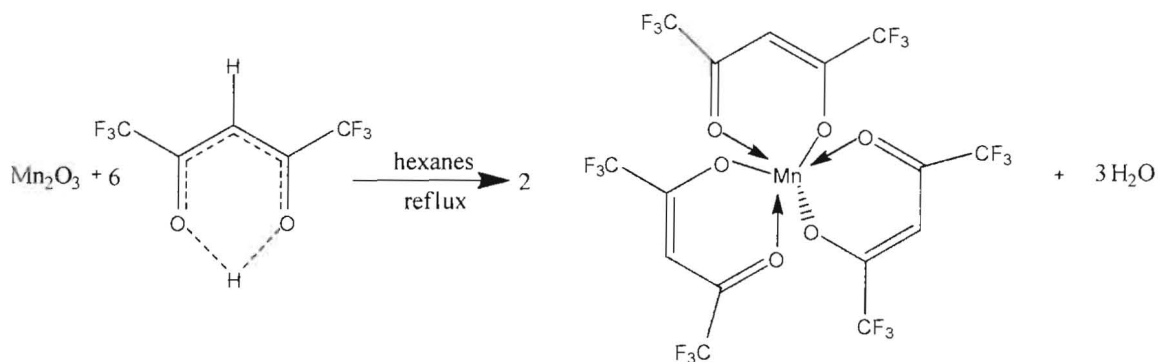


Figure 2.8: The crystal structure of manganese tris(hexafluoroacetylacetonate).

Morris and Koob²⁰ tested the fluorine migration of metal hexafluoroacetylacetonate complexes to fit into hard/soft acid/base theory (HSAB) assuming the metal is acidic and the fluoride behaves as a base. A series of metal center complexes were studied including Co(II), Fe(III), Cr(III), Al(III), Zn(II), Ni(II), Mn(II), and Cu(I). Competition between the formation of HF and metal fluorides make the hardness of the metal important as to which pathway is favored.²⁰ All the metal complexes, except Cu(hfac), show the loss of a neutral metal fluoride fragment with Al(III)(hfac)₃ showing the unique loss of AlF₂(hfac).

2.5 Synthesis and Characterization

2.5.1 Mn(hfac)₃



Scheme 2.7: Synthesis reaction for Mn(hfac)₃ where the arrows indicate coordination.

The synthesis of $\text{Mn}(\text{hfac})_3$ was performed by reacting 0.5856 g (3.71 mmol) of Mn_2O_3 with 1.7 mL (12.1 mmol) (3.3 eq) of $\text{H}(\text{hfac})$ to yield 0.1808 g (6.7% yield) of pure $\text{Mn}(\text{hfac})_3$ crystals. The reactant slurry refluxed for 24 hours under nitrogen with 10 mL of hexanes as the solvent. The resulting product was cooled to -78°C and the liquid decanted. The solid was dried by vacuum, and was purified by sublimation twice.²¹ The resulting black crystals were characterized by mass spectrometry and X-ray single crystallography. MS: m/z (%) 676 (22.2%), 657 (6.5%), 607(3.2%), 469 (100.0%), 400 (86.2%), 281 (2.2%), 262 (19.6%), 234.5 (4.5%), 212 (54.6%), 193 (1.1%), 165.5 (2.2%), 119 (3.0%), 69 (14.8%) The crystal structure of $\text{Mn}(\text{hfac})_3$ agrees with literature²². The monoclinic structure is in space group $\text{P}2_1/\text{n}$ with very similar unit cell dimensions. The appendix contains additional supporting information about the crystal structure.

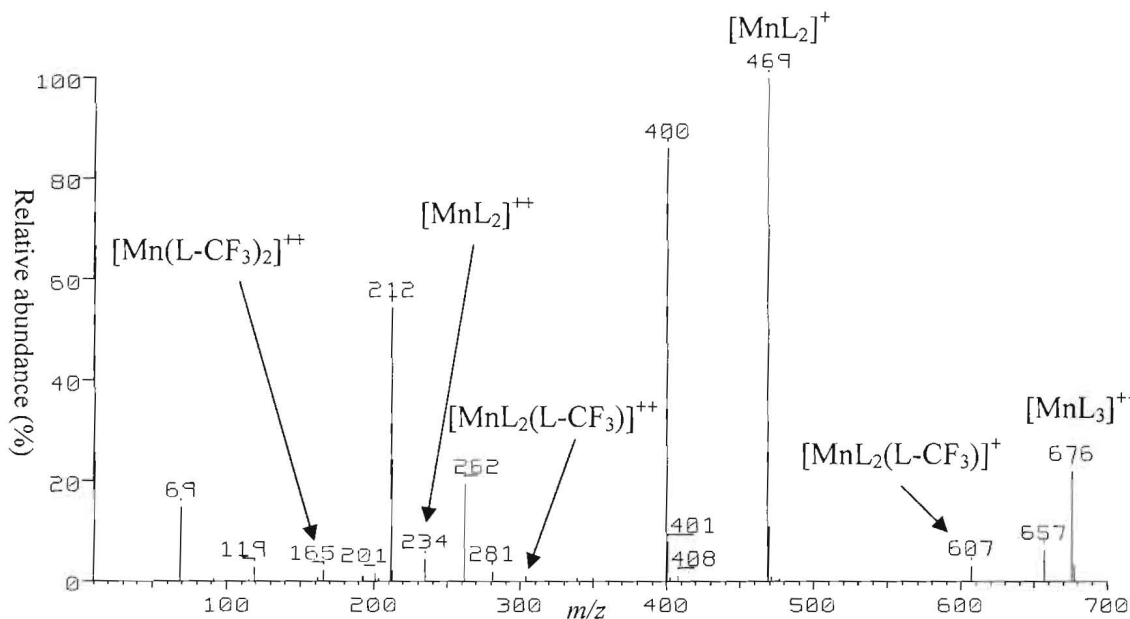


Figure 2.10: Mass spectrum of synthesized $\text{Mn}(\text{hfac})_3$ with doubly charged ions at m/z 165.5, 234.5 and 303.5 where $\text{Mn}(\text{L}-\text{CF}_3)$ signifies that the ligand lost a fluorinated methyl group and L is hfac.

The fragmentation pattern of $\text{Mn}(\text{hfac})_3$ follows that of the pattern outlined for metal tris(hexafluoroacetylacetonate)s, as shown in Scheme 2.6 where the appearance of the $[\text{MnF}(\text{hfac}-\text{CF}_3)]^+$, and absence of $[\text{MnF}_2(\text{hfac}-\text{CF}_3)]^+$ ion demonstrates that manganese reduces its oxidation state during dissociation. A neutral MnF_2 could be lost from the relatively abundant $[\text{MnF}(\text{hfac}-\text{CF}_3)]^+$ ion yielding $[\text{CF}_2\text{COCHCO}]^+$ (m/z 119). Two unique aspects of the $\text{Mn}(\text{hfac})_3$ dissociation is the increased presence of the doubly charged ions and the loss of fluorine from the molecular ion. There are three doubly charged ions represented in the spectra: m/z (%) 303.5 (0.9%), 234.5 (4.5%), and 165.5 (2.2%). These m/z ratios correspond to $[\text{Mn}(\text{hfac})_2(\text{hfac}-\text{CF}_3)]^{++}$ (607/2), $[\text{Mn}(\text{hfac})_2]^{++}$ (469/2), and $[\text{Mn}(\text{hfac}-\text{CF}_3)_2]^{++}$ (331/2), respectfully. The doubly charged ions analogous to the 165.5 peak for $\text{Mn}(\text{hfac})_3$ were observed in the spectra of $\text{Al}(\text{acac})_3$ and $\text{Fe}(\text{acac})_3$.²³

$\text{Mn}(\text{hfac})_3$ was observed to decompose promptly in the course of recrystallization. During MS characterization of $\text{Mn}(\text{hfac})_3$, the observed ions changed from that characteristic of $\text{Mn}(\text{III})(\text{hfac})_3$ to ions characteristic of $\text{Mn}(\text{hfac})_2$ within a few minutes. The molecular ion, $[\text{Mn}(\text{hfac})_3]^+$, is initially at medium relative intensity, however as time increases, the relative intensity of the molecular ion decreases and the intensity of $[\text{Mn}_2(\text{hfac})_3]^+$ increases until the molecular ion is no longer observed. The $\text{Mn}_2(\text{hfac})_3$ ion is characteristic of $\text{Mn}(\text{II})(\text{hfac})_2$ reacting with itself and has a m/z of 731.²⁴ Initially, there is no peak observed at 731.

2.5.2 $Al(hfac)_3$

$Al(hfac)_3$ was purchased from Aldrich and recrystallization by slow evaporation of a concentrated sample (~10 mg) dissolved in diethyl ether (~1 mL) and gave colorless, needle-like crystals. The crystal structure of $Al(hfac)_3$ was solved for the first time, and was found to be merohedrally twinned with disorder and psuedosymmetry. The crystal structure was solved by the application of the correct twin matrix and restraints on the crystal. Further information on the crystal structure can be seen in section A.2 of the Appendix. The $Mn(hfac)_3$ and $Al(hfac)_3$ differ in the crystal system where $Mn(hfac)_3$ is monoclinic and $Al(hfac)_3$ is trigonal even though these two metals have very similar atomic radii and the same ligands coordinating them.

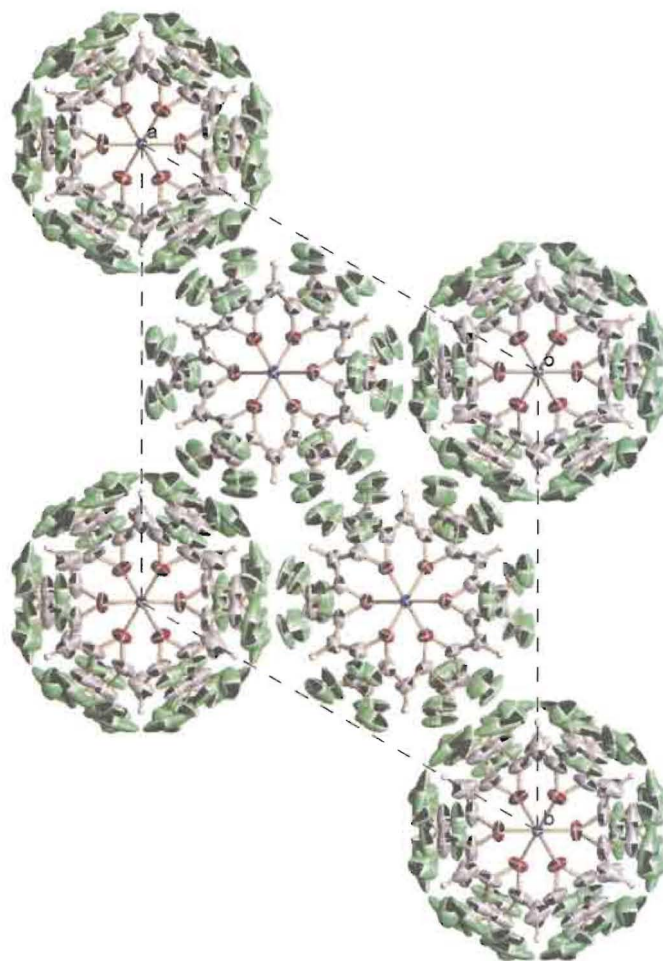


Figure 2.11: The crystal structure of aluminum tris(acetylacetonate).

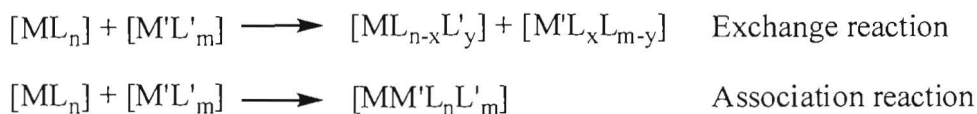
2.6 Conclusions

The observed dissociation reactions of the metal acetylacetonate and derivative complexes listed in Table 1.1 agree well with those reported in literature where the dominant loss channel followed the expected oxidation changes for the various metals. For metal hexafluoroacetylacetonates, the migration of fluorine to the metal demonstrates a metal conserving its oxidation state while a metal acetylacetonate maintaining its oxidation state is demonstrated by the absence of the $[M(\text{acac})]^+$ peak. Manganese tris(hexafluoroacetylacetonate) was successfully synthesized with mass spectra and crystal structure presented.

Chapter 3: Exchange Reactions and Mixed-Metal Complexes

3.1 Exchange and Association Reactions of Metal Acetylacetonates and Derivatives

The mass spectrometric studies presented in the previous chapter focus on the unimolecular dissociation of a series of metal acetylacetonates where only one complex was sublimed into the mass spectrometer.²⁰ The unimolecular dissociation of metal acetylacetonates is well documented where nearly every possible fragment ion is readily observed. If two different sample complexes are sublimed together, reactions may occur yielding a variety of different complexes. The formation and reactivity of new species is of particular interest. In the presence of different metal centers or ligands, exchange and association reactions have been observed to occur and are described in Scheme 3.1.¹⁶



Scheme 3.1: General scheme for exchange reactions and association reactions.²⁵

Exchange reactions with metal acetylacetonate complexes occur quite regularly, and are easily observed when two different types of ligands are mixed together. To find the peaks corresponding to the ligand exchange reaction, the individual spectra of each complex are subtracted from the mass spectrum of the mixture. MacDonald and Shannon¹⁶ were the first to demonstrate ligand exchange in a mass spectrometer by co-subliming $\text{Fe}(\text{acac})_3$ with $\text{Fe}(\text{bzac})_3$. Many of the observed peaks in the mass spectrum correspond to mixed ligand complex ions such as $\text{Fe}(\text{acac})(\text{bzac})_2$. These observations suggest that while in the gas phase the two complexes substitute ligands to form a new complex.¹⁶

One distinguishing feature of association reactions is the presence of species with larger m/z than the molecular ion due to the addition of the metal complex and additional ligands. In the $\text{Fe}(\text{acac})_3$ study, these larger masses are likely due to polynuclear species from either the sublimation of polymers from the solid or from an association reaction in the gas phase where two complexes collide to form a new larger complex. To demonstrate that the gas phase association reaction occurs, two complexes with different metals were sublimed from different origins which formed mixed-metal complexes. Three mixtures in their study formed mixed-metal complexes: $\text{Ca}(\text{acac})_2 + \text{Mg}(\text{acac})_2$, $\text{Sc}(\text{acac})_3 + \text{Fe}(\text{acac})_3$, $\text{Fe}(\text{acac})_3 + \text{Co}(\text{acac})_3$ giving ions of the order $\text{MM}'_2(\text{acac})_5$, $\text{MM}'(\text{acac})_5$, $\text{MM}'(\text{acac})_4$, and $\text{MM}'(\text{acac})_3$ which are all higher in mass than any single complex.¹⁶

Schildcrout²⁴ studied the association reaction of many metal acetylacetonates in a mass spectrometer under high pressure source conditions to gain a better understanding of whether polynuclear species form from sublimation from the solid, as the collision of neutrals, or as the collision of an ion with a neutral (ion/molecule reactions). Varying the conditions of the reactions, i.e. sample pressure, temperature, and repeller potential, polynuclear ions were observed to form from an association reaction between ions and neutral species, and not from gaseous polynuclear precursors.²⁴

Six different types of polynuclear ions were identified in Schildcrout's study²⁴ ranging from M_2L_n to M_3L_m where $n = 2-5$ and $m = 4,5$.²⁴ Under low source pressure conditions the resulting ion distribution, as observed in the mass spectrum, was dramatically different from the high pressure spectra in the relative abundance of the polynuclear ions in all cases except $\text{Al}(\text{hfac})_3$. Charge transfer from an ion to a neutral

fragment may responsible for the increase in the relative abundance of the neutral fragment according to the mass spectrum implying that the neutral has a lower ionization potential than the original ion. The ion/neutral reaction also does not appear to have a transition state with significant restructuring about the metal in a neutral complex.²⁴

Using the same instrument as in the pressure studies, Schildcrout²⁶ also investigated the gaseous ion chemistry of metal acetylacetonate derivatives with bulky substituents to distinguish steric effects in association reactions known as ion/molecule reactions. It was found that more bulky groups tended to hinder the association reaction, but enhance charge transfer. Reactivity trends were observed, and were shown to be dependent on the polarizability of the ligand. The metal's oxidation state determines which type of polynuclear ion is formed (M(II) forms M_2L_3 and M(III) forms M_2L_5). The complexity of the interactions, whether it was through charge transfer or an association reaction, confounded the data for Co(II), Zn(II), Al(III), and Cu(II) reactivity which made differentiating trends difficult, although one clear trend is that the planar complexes do not have the same steric hindrance, most likely due to more access to the metal.²⁶

Association and exchange reactions between alkali-metal derivatives of β -diketones with rare-earth chelates (RL_3) were reported by Majer and Perry.²⁵ Using trifluoro-, pentafluoro-, and heptafluoroacetylacetonate ligands, they reported many metal complexes containing two different metal atoms: NaMg, NaK, NaSr, NaBa, NaHo, NaSm, NaGa, CuCr, and CuHo having arrangements of $MM'LL'$, $MM'L_2$, $MM'L_3$, $MM'LL'_2$, $MM'L_2L'$, $MM'LL'_3$, $MM'L_4$, $MM'_2L_2L'_2$, $MM'_2LL'_3$, MM'_2L_4 , $MM'_2L_2L'_3$, $MM'_2LL'_4$, MM'_2L_5 , $MM'_2L_2L'_3$, MM'_2L_4L' which they attributed to occur during sublimation into the mass spectrometer.²⁵

3.2 Experimental Design

A mixture of two sample complexes analyzed in this study were sublimed under low source pressure conditions of about 10^{-5} to 10^{-7} torr from a direct insertion probe which was heated from 30°C to 200°C to optimize the gas phase mixing of the sample complexes. The Finnigan MAT 8430 double focusing mass spectrometer ionized and scanned the gas phase mixture to identify peaks originating from individual sample complexes and the peaks formed from the reaction between the two sample complexes. The mass spectra of the individual sample complexes were compared to the mass spectra of the mixed sample complexes to find variations between them. The variations were assumed to be mixed-metal complex or ligand exchange ions and were identified using m/z and isotope abundances. Four series of MS experiments were conducted to examine the reactivity of $\text{Al}(\text{hfac})_3$, $\text{Al}(\text{acac})_3$, $\text{Ni}(\text{acac})_2$, and $\text{Ni}(\text{hfac})_2$ with various metal acetylacetonates and metal hexafluoroacetylacetonates, where each metal acetylacetonate or metal hexafluoroacetylacetonate (listed in Table 1.1) were sublimed with $\text{Ni}(\text{acac})_2$, $\text{Ni}(\text{hfac})_2$, $\text{Al}(\text{acac})_3$, and $\text{Al}(\text{hfac})_3$.

The gas was ionized by electron impact (EI) ionization set at 70 eV with an electron current of 490 μA , and the masses were scanned from 10-800 amu. The ionization chamber temperature was maintained at 200°C to minimize deposition of the sample complex in the ionization chamber. The scan rate was set at 2 decades per second for low resolution studies (~ 1000). High boiling point perfluorokerosenes (PFKs) were used for mass calibrations, and pressures were measured inside the ion source or analyzer region leaving the exact pressure in the ionization chamber unknown.

3.3 Results and Discussion

Polynuclear ions, those complexes containing additional metals, were observed in a number of the individual mass spectra with the nickel and manganese bis(hexafluoroacetylacetonate) producing the most significant quantity of peaks with masses higher than the molecular ion. The most abundant polynuclear ion among these two was the $Mn_2(hfac)_3$ peak, which is indicative of the M(II) oxidation state. The mass spectra of each individual complex were in good agreement with what was reported in literature. The individual spectra were combined and compared to the mass spectra resulting from the mixture in each series. Many observed reactions were the result of the hexafluoroacetylacetonate ligand exchanges with the acetylacetonate ligand. The mixed-metal association reactions, however, are only observed in a few select mixtures since these are based more on the metal than the ligand. The general arrangements for these mixed-metal ions are $MM'L_nL'_{5-n}$, $MM'L_nL'_{4-n}$, $MM'L_nL'_{3-n}$, $MM'FLL'$, and $MM'LL'$ where L = acetylacetonate and L' = hexafluoroacetylacetonate. These general arrangements have been reported previously, but the specific mixed-metal ions are detected for the first time in this study.

3.3.1 *Al(hfac)₃ series*

Before $Al(hfac)_3$ was tested for its reactivity with the full series of complexes listed in Table 1.1, it was examined by itself. The $Al(hfac)_3$ spectra shows peaks at m/z 691 and 805 that are higher than the molecular mass of $Al(hfac)_3$ (m/z 648). While these peaks are evidence of some interesting chemistry, they do not conform to the expected polynuclear forms. The two peaks may take the form $[Al_2O(hfac)_3]^+$ and $[AlF(hfac)_3(hfac-CF_3)]^+$, where fluorine migration has a net loss CF_2 from the latter

complex. Since aluminum maintains its 3+ oxidation state, one of the ligands must be in the neutral keto form, instead of in the anionic enolate form. These conditions suggest that $\text{Al}(\text{hfac})_3$ does not associate like the other metal hexafluoroacetylacetonates in agreement with Schildcrout's high pressure studies.²⁴

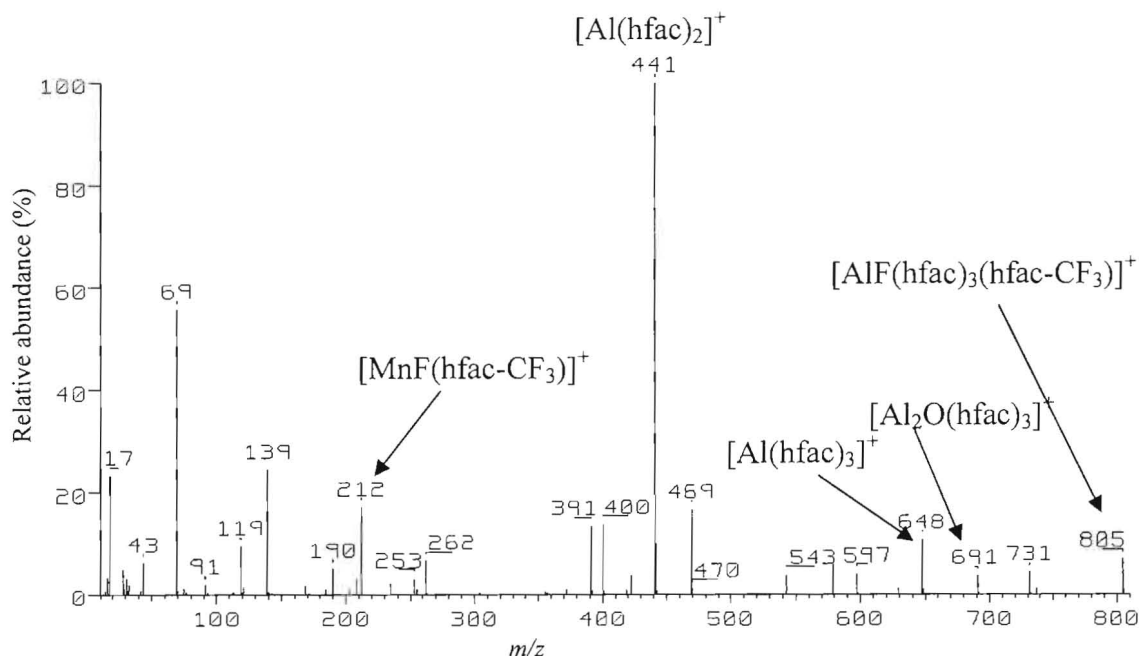
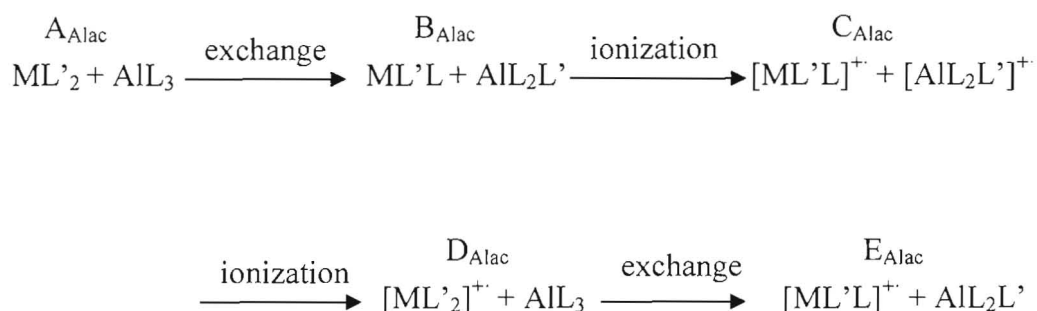


Figure 3.1: The mass spectrum of $\text{Mn}(\text{hfac})_2$ mixed with $\text{Al}(\text{hfac})_3$.

When the $\text{Al}(\text{hfac})_3$ was tested against the series of other metal containing complexes, no mixed-metal species were identified, however exchange reaction peaks were evident when $\text{Al}(\text{hfac})_3$ was reacted with the a metal acetylacetonate complexes. Figure 3.1 shows the combined spectra between $\text{Mn}(\text{hfac})_2$ and $\text{Al}(\text{hfac})_3$ where all the peaks in the mass spectrum can be identified pertaining to the individual mass spectra of either $\text{Mn}(\text{hfac})_2$ or $\text{Al}(\text{hfac})_3$.

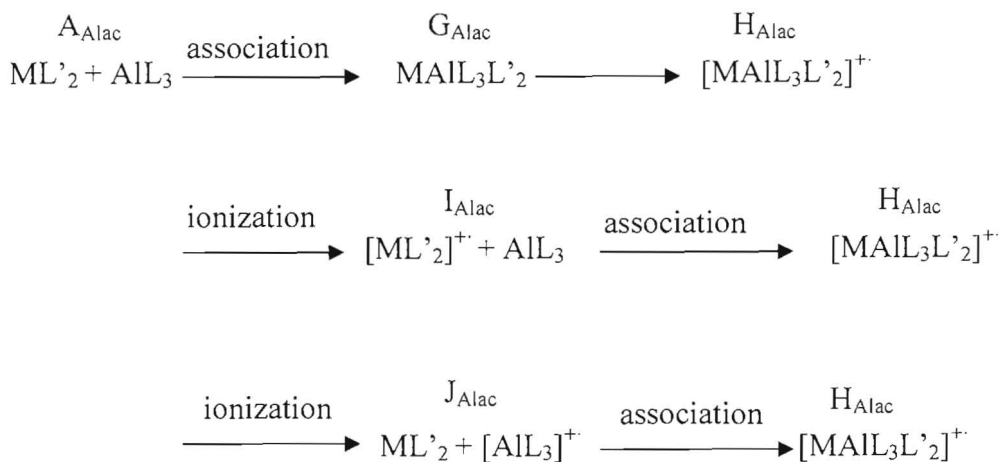
3.3.2 Al(acac)₃ series

The mass spectrum and dissociation channel of Al(acac)₃ were previously described in Scheme 2.3 and Figure 2.6. When Al(acac)₃ was sublimed with the following metal hexafluoroacetylacetonates, Ni(hfac)₂, Fe(hfac)₂, Co(hfac)₂, Mn(hfac)₂, and Mn(hfac)₃, a series of exchange and association reactions were observed. In Scheme 3.2, a general example of an exchange reaction is illustrated where A_{Alac} can either exchange to form B_{Alac} and ionize to form C_{Alac} or ionize to form D_{Alac} and then the ligand exchanges to form E_{Alac}.



Scheme 3.2: A general example of an exchange reaction where two different pathways lead to the formation of [ML'L]⁺ ion where M = Ni, Fe, Co, and Mn, L = acac, and L' = hfac.

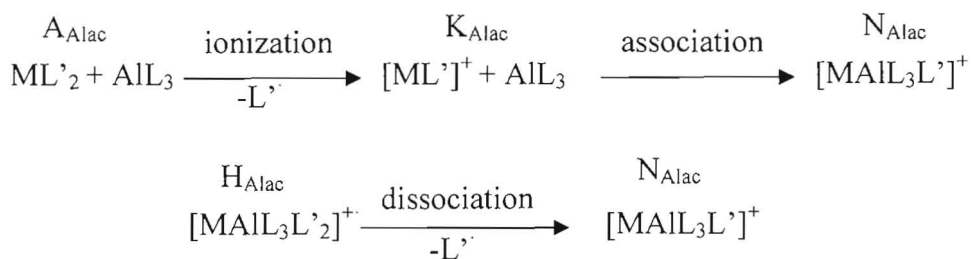
The observed association reactions yielded products of the form of MAl(acac)₃(hfac) (abbreviated as N_{Alac}) and MAl(acac)₃(hfac)₂ (abbreviated as H_{Alac}) which correspond to the two possible reactions presented in Scheme 3.3 and Scheme 3.4. In Scheme 3.3, the sublimed mixture yields the observed complex ion H_{Alac} by three different pathways. Complex G_{Alac} is the association product of the neutrals which then get ionized to form H_{Alac}. Mixtures I_{Alac} and J_{Alac} have one complex ionized, and then the association reaction takes place. The latter two cases are examples of ion/neutral reactions.



Scheme 3.3: The possible association reactions between $M(\text{hfac})_2$ and $Al(\text{acac})_3$ where M is Co, and Mn, L is acac, and L' is hfac.

Complex ion H_{Alac} has the general arrangement of two metals complexed to five ligands, which in previous studies²⁴ is indicative of metals in the 3+ oxidation state. The two mixtures that yielded this complex were a mixture of metals in the 3+ and 2+ oxidation states suggesting that the metal of 2+ oxidation state either forms an adduct with non-bonding electrons of oxygen or increases in oxidation state to 3+. Both are readily available for the specific 2+ metals.

The mixed-metal product N_{Alac} is the predominant mixed-metal ion observed in the $Al(\text{acac})_3$ reactivity series. The complex ion, $[MAIL_3L']^+$ can form in two different ways where either an association or a dissociation reaction occurs. For the association reaction to occur, the ML'_2 must first lose a ligand, most likely after ionization, and then associate with the $Al(\text{acac})_3$ neutral complex. The dissociation reaction would occur after the formation of complex ion H_{Alac} where H_{Alac} loses an hfac ligand to form N_{Alac} .



Scheme 3.4: Two possible pathways leading to mixed-metal product, N_{Alac} , where one is association and the other dissociation. (M = Ni, Fe, Co, and Mn, L = acac, and L' = hfac.)

3.3.2.1 Ni(hfac)₂ mixed with Al(acac)₃

The gas phase reaction of Ni(hfac)₂ with Al(acac)₃ is shown in Figure 3.2, where the characteristic peaks of the individual mass spectra and the resulting new species are easily recognized. The most abundant peak in the spectrum appears at m/z 225 corresponding to $[\text{Al}(\text{acac})_2]^+$, and is the loss of a ligand from the molecular ion Al(acac)₃. Peaks at m/z 403 and 472 are identified as $[\text{Ni}(\text{hfac})(\text{hfac}-\text{CF}_3)]^+$ and $[\text{Ni}(\text{hfac})_2]^+$, respectively where the exchange reaction product of $[\text{Al}(\text{acac})(\text{hfac})]^+$ is also observed at m/z 333. An association reaction forming $[\text{NiAl}(\text{acac})_3(\text{hfac})]^+$ at m/z 589 is also observed. The minor peak at m/z 589 is a new mixed-metal complex observed for this gas phase mixture. The natural isotopic abundance confirms the presence of this ion, validating this dissociation channel.

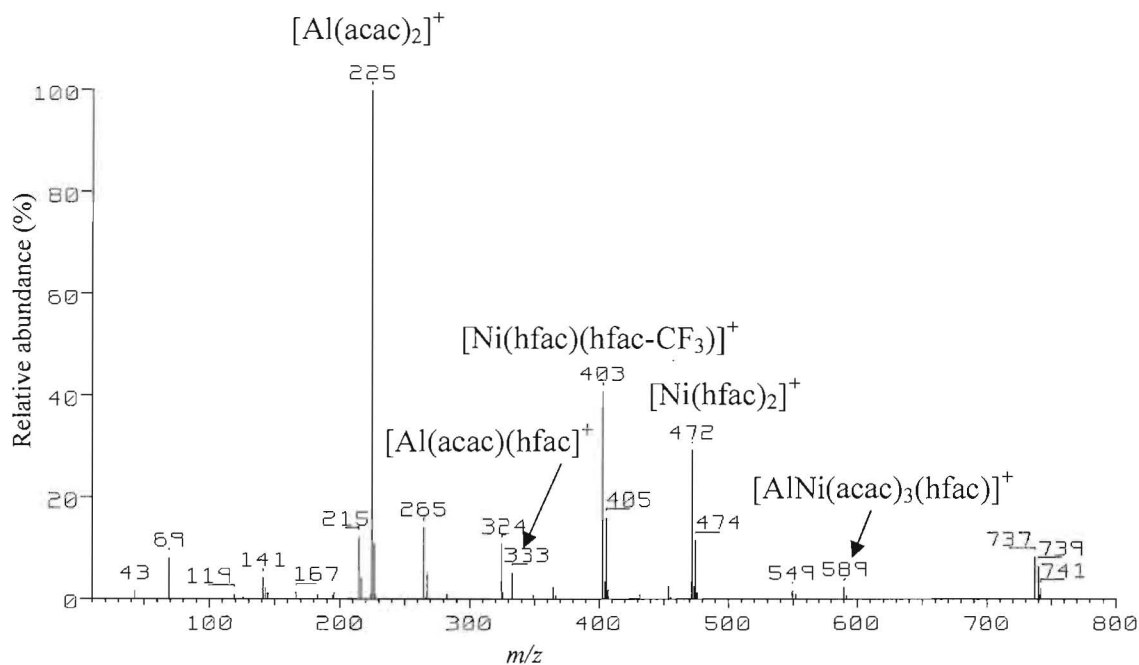


Figure 3.2: The mass spectrum of Ni(hfac)₂ mixed with Al(acac)₃.

3.3.2.2 Co(hfac)₂ mixed with Al(acac)₃

The reaction of Co(hfac)₂ with Al(acac)₃ is very similar to that of the Ni(hfac)₂ reaction with the previously described peaks of Al(acac)₃ dominating the spectra. Peaks at *m/z* 404 and 473 correspond to [Co(hfac)(hfac-CF₃)]⁺ and [Co(hfac)₂]⁺, respectively, which are analogous to those of the nickel complex shown earlier. The exchange reaction has occurred with evidence for the formation of five new products at *m/z* 145, 283, 333, 365, and 432 corresponding to [(acac)AlF]⁺, [(acac)AlF(hfac-CF₃)]⁺, [Al(acac)(hfac)]⁺, [Co(acac)(hfac)]⁺ and [Al(acac)₂(hfac)]⁺, respectively. The association reaction yielded two peaks [CoAl(acac)₃(hfac)]⁺ and [CoAl(acac)₃(hfac)₂]⁺ which have the same arrangement of ligands already noted in Scheme 3.3 and 3.4.

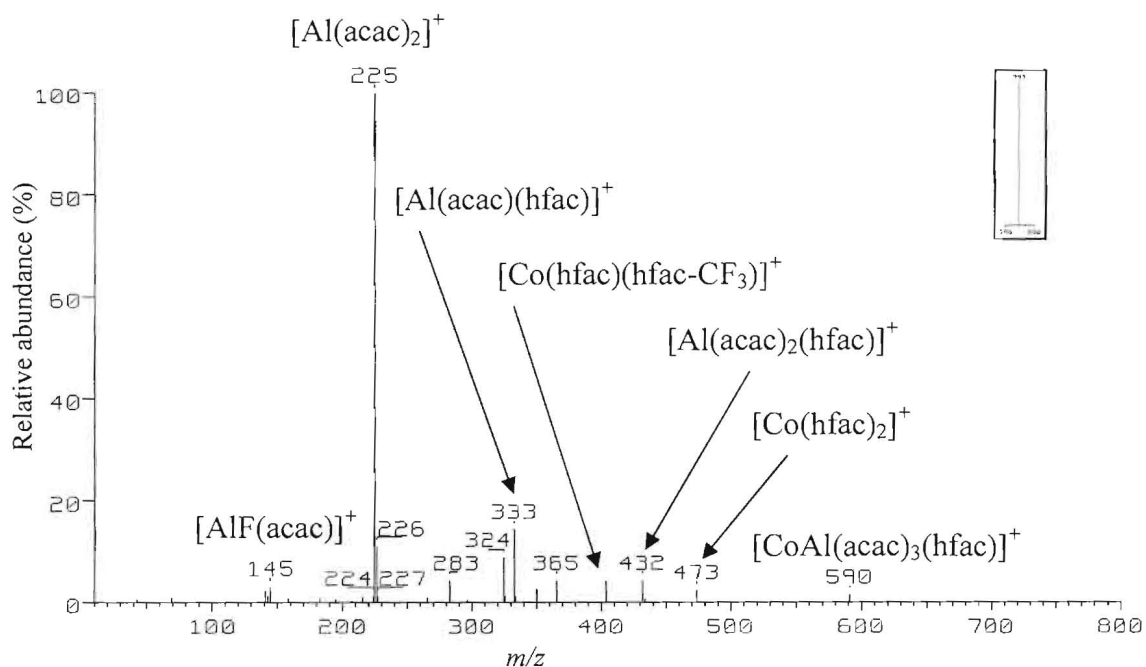


Figure 3.3: The mass spectrum of $\text{Co}(\text{hfac})_2$ mixed with $\text{Al}(\text{acac})_3$.

3.3.2.3 $\text{Fe}(\text{hfac})_2$ mixed with $\text{Al}(\text{acac})_3$

The gas phase reaction of $\text{Fe}(\text{hfac})_2$ with $\text{Al}(\text{acac})_3$ did not produce many new products by association as illustrated by the mass spectrum in Figure 3.4. The $[\text{Al}(\text{acac})_2]^+$ still dominates the spectra, but the molecular ion peak of $[\text{Fe}(\text{hfac})_2]^+$ at m/z 470 is barely perceptible. Instead the ion of m/z 254 grows in intensity and corresponds to $[\text{Fe}(\text{acac})_2]^+$. The individual complexes mass spectra are not easily discernable since the exchange reaction occurs to such an extent and greatly complicates the spectra. The peak at m/z 587 is some evidence that the association reaction occurs in the formation of $[\text{FeAl}(\text{acac})_3(\text{hfac})]^+$, and is the first observation of this complex.

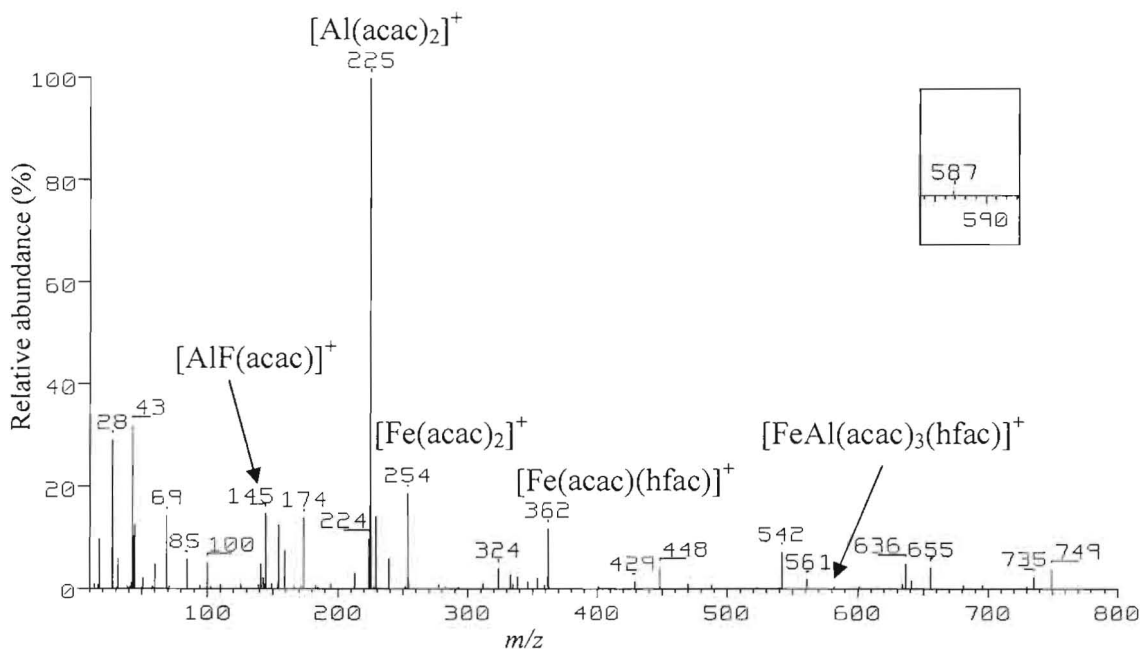
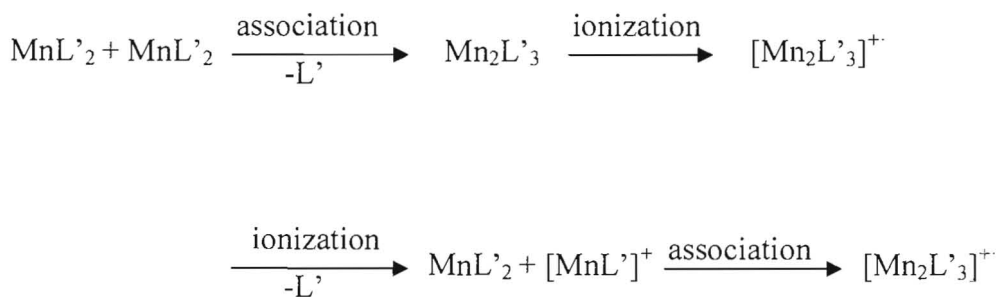


Figure 3.4: The mass spectrum of $\text{Fe}(\text{hfac})_2$ mixed with $\text{Al}(\text{acac})_3$.

3.3.2.4 $\text{Mn}(\text{hfac})_2$ mixed with $\text{Al}(\text{acac})_3$

The gas phase reaction of $\text{Mn}(\text{hfac})_2$ with $\text{Al}(\text{acac})_3$ resulted in the formation of two new mixed-metal ions. The peaks resulting from the individual complexes are quite evident, especially the abundant molecular ion of $\text{Mn}(\text{hfac})_2$ at m/z 469. The individual mass spectra of $\text{Mn}(\text{hfac})_2$ contains many cluster ions including peaks at m/z 355, 493, 543, and 731 relating to $[\text{Mn}_2\text{F}_2(\text{hfac})]^+$, $[\text{Mn}_2\text{F}_2(\text{hfac})(\text{hfac}-\text{CF}_3)]^+$, $[\text{Mn}_2\text{F}(\text{hfac})_2]^+$, and $[\text{Mn}_2(\text{hfac})_3]^+$, respectively. Examples of possible formation pathways are presented in Scheme 3.5 where the ion $[\text{Mn}_2(\text{hfac})_3]^+$ is formed. The $[\text{Al}(\text{acac})_2]^+$ peak at m/z 225 remains strong around 65% relative abundance with the exchange reaction products still evident at m/z 145 and 333.



Scheme 3.5: Two possible pathways leading to cluster ions in the gas phase where L' is hfac.

The relative intensity of $[\text{AlMn}(\text{acac})_3(\text{hfac})]^+$ is higher than in any other complex in the $\text{Al}(\text{acac})_3$ reaction series with a slight peak at $[\text{AlMn}(\text{acac})_3(\text{hfac})_2]^+$. The properties that aid cluster formation with $\text{Mn}(\text{hfac})_2$, as observed in the individual spectra, aid in the mixed-metal ions based on the increased intensity at m/z 586 compared to the other metal centers in the series. Two mixed-metal peaks are inferred from the data at m/z 793 and 586 where these peaks are $[\text{AlMn}(\text{acac})_3(\text{hfac})_2]^+$ and $[\text{AlMn}(\text{acac})_3(\text{hfac})]^+$, respectively.

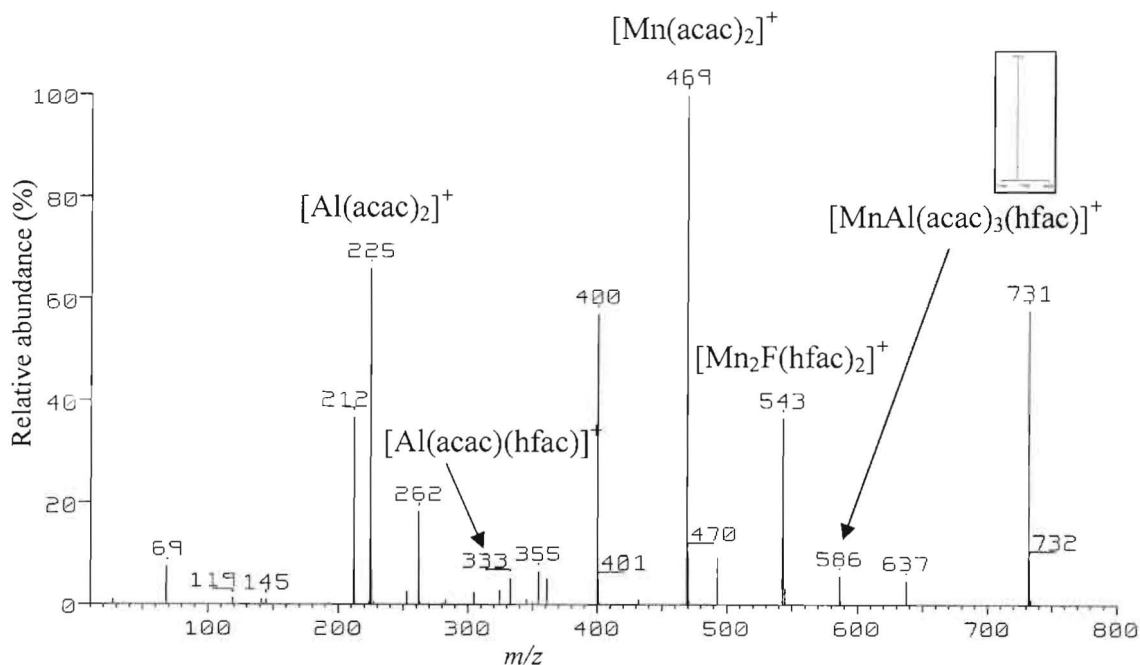


Figure 3.5: The mass spectrum of $\text{Mn}(\text{hfac})_2$ mixed with $\text{Al}(\text{acac})_3$.

3.3.3.5 $Mn(hfac)_3$ mixed with $Al(acac)_3$

The reaction of $Mn(hfac)_3$ with $Al(acac)_3$ has many similar features to the reaction of $Mn(hfac)_2$ with $Al(acac)_3$ as presented in section 3.3.2.4. The most abundant peak is $[Al(acac)_2]^+$, and the $[Mn(hfac)_2]^+$ ion has a relative abundance around 50%. The exchange reactions take place with peaks seen at m/z 145, 283, 333, 441, and 540 corresponding to complexes $[AlF(acac)]^+$, $[AlF(acac)_2]^+$, $[Al(acac)(hfac)]^+$, $[Al(hfac)_2]^+$, and $[Al(acac)(hfac)_2]^+$. The mixed-metal ion, $[MnAl(acac)_3(hfac)]^+$ is observed in Figure 3.6 at m/z 586.

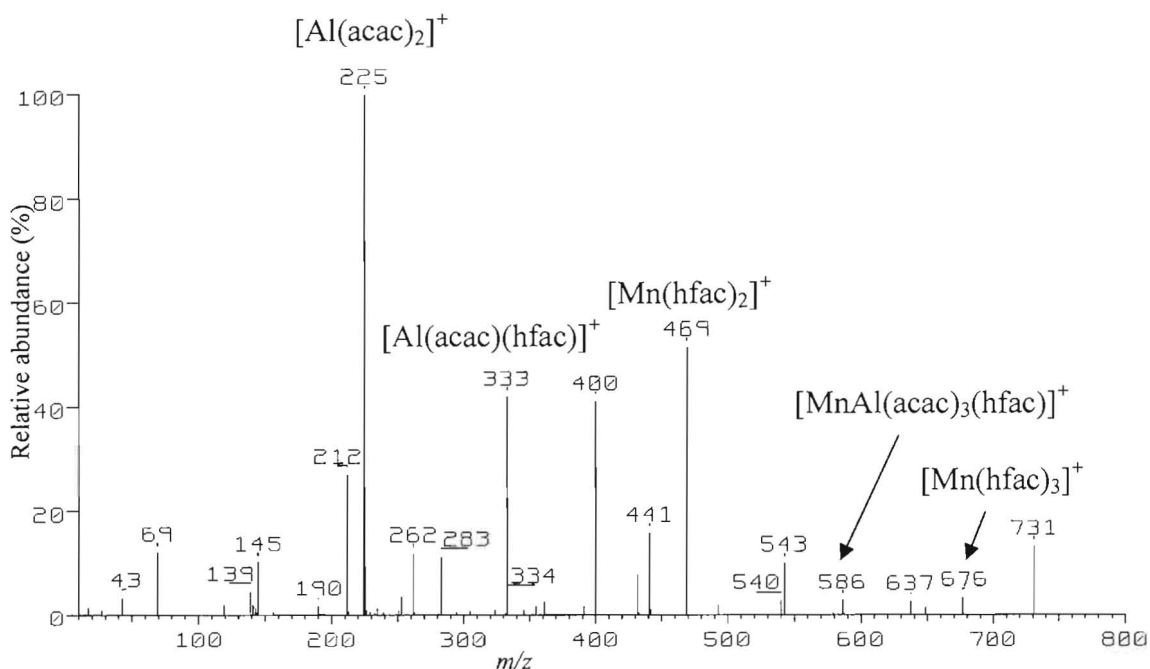
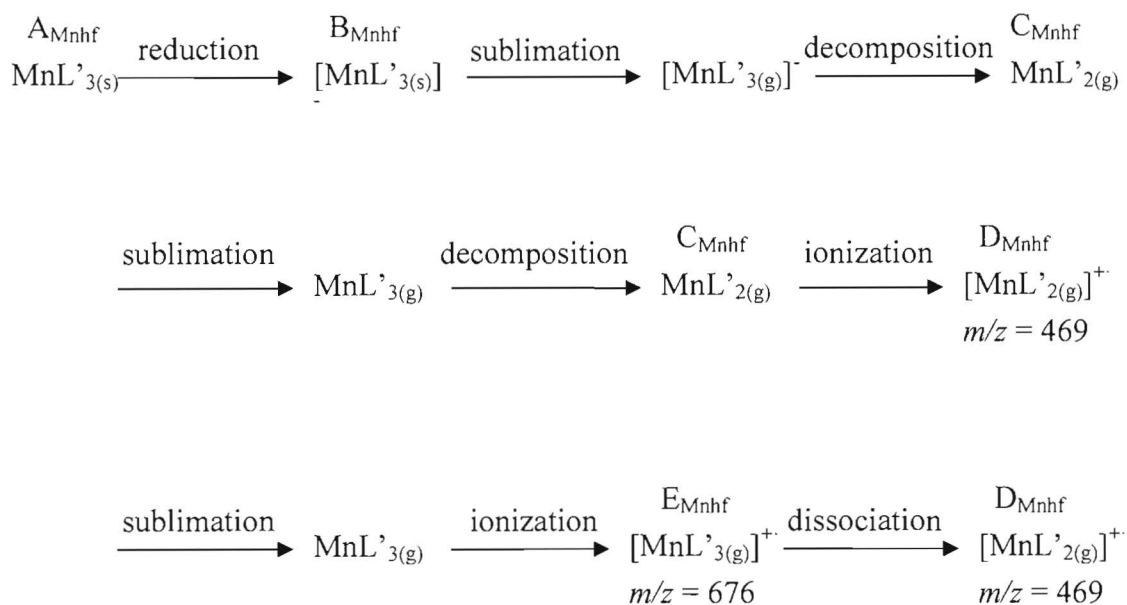


Figure 3.6: The mass spectrum of $Mn(hfac)_3$ mixed with $Al(acac)_3$.

These reactions are very similar to the mixture of $Mn(hfac)_2$ with $Al(acac)_3$. Since $Mn(hfac)_3$ has a change in fragmentation pattern during the course of a few short minutes it is uncertain how the mixed-metal forms. The mass spectrum of $Mn(hfac)_3$ initially has a peak at m/z 676 corresponding to E_{Mnhf} , the molecular ion illustrated in Scheme 3.6. As

time elapses, the $E_{Mn_{hfh}}$ ion dissipates and the intensity of the cluster ion $[Mn_2(hfac)_3]^+$ increases. The cluster ion $[Mn_2(hfac)_3]^+$ is formed from Mn(II) and not from Mn(III), suggesting that the metal has a preferred oxidation state of 2+. As illustrated in Figure 3.6, the peak corresponding to $[Mn_2(hfac)_3]^+$, 731, is more intense than that of the molecular ion $[Mn(hfac)_3]^+$ possibly indicating that the pathways leading to the decomposition product $C_{Mn_{hfh}}$ may be becoming more prominent than the pathway to ion $E_{Mn_{hfh}}$.



Scheme 3.6: Three possible pathways that Mn(III) can reduce to Mn(II) where L' is hfac.

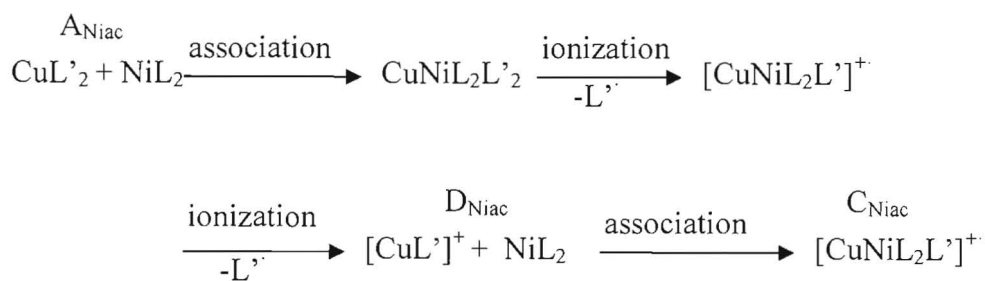
3.3.3 Ni(acac)₂ series

Nickel bis(hexafluoroacetylacetonate) was sublimed in the presence of different metal acetylacetonate complexes under low source pressure conditions. Exchange reactions were observed with Ni(acac)₂ for all metal hexafluoroacetylacetonate complexes, however only three complexes showed evidence of mixed-metal complexes: Cu(hfac)₂, Mn(hfac)₂, and Mn(hfac)₃. A number of different products were observed in

the association reactions with Ni(acac)₂ where the general form was MNi(acac)_n(hfac)_{3-n}. The oxidation states of both metals are assumed to be 2+ from the high pressure studies on metal acetylacetonates and derivatives.²⁴

3.3.3.1 Cu(hfac)₂ mixed with Ni(acac)₂

The gas phase reaction of Cu(hfac)₂ with Ni(acac)₂ are illustrated in Figures 3.7 and 3.8. The combined mass spectra of the individual species comprise much of the spectra with the most abundant peak being, the molecular ion [Ni(acac)₂]⁺, at *m/z* 256. Peaks at *m/z* 408 and 477 correspond to loss of a fluorinated methyl radical from the molecular ion, [Cu(hfac)(hfac-CF₃)]⁺, and the molecular ion of copper bis(hexafluoroacetylacetonate), [Cu(hfac)₂]⁺, respectively. Products of exchange reactions are observed by the peaks at *m/z* 147, 162, 349, 364, and 369 which are [Cu(acac-CH₃)]⁺, [Cu(acac)]⁺, [Ni(acac-CH₃)(hfac)]⁺, [Ni(acac)(hfac)]⁺, and [Cu(acac)(hfac)]⁺ ion, respectively. A very small mixed-metal ion peak occurs at *m/z* 526 with a major isotope peak at *m/z* 528, as observed in Figure 3.8 having never been reported previously. This peak corresponds to [CuNi(acac)₂(hfac)]⁺ being formed by two possible association pathways presented in Scheme 3.7. An analogous nickel polynuclear ion is seen at *m/z* 521 which helps to confirm the composition of the mixed-metal complex also seen in Figure 3.8.



Scheme 3.7: Two possible pathways to form the mixed-metal complex, C_{Niac} . ($L = acac$, $L' = hfac$)

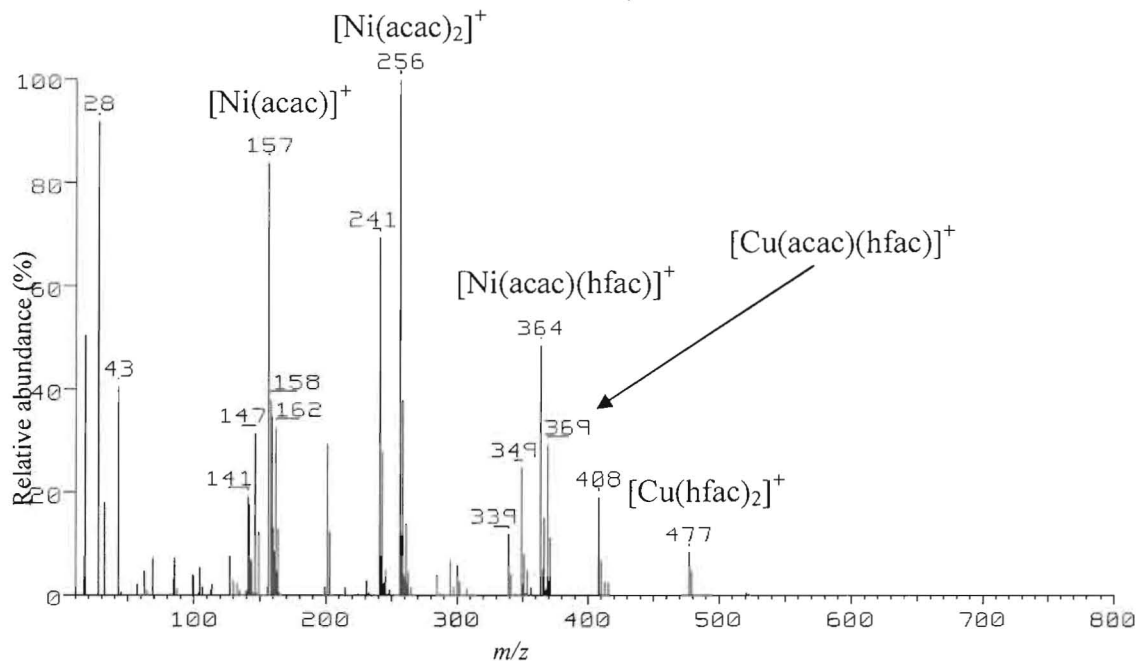


Figure 3.7: The mass spectrum of $Cu(hfac)_2$ mixed with $Ni(acac)_2$.

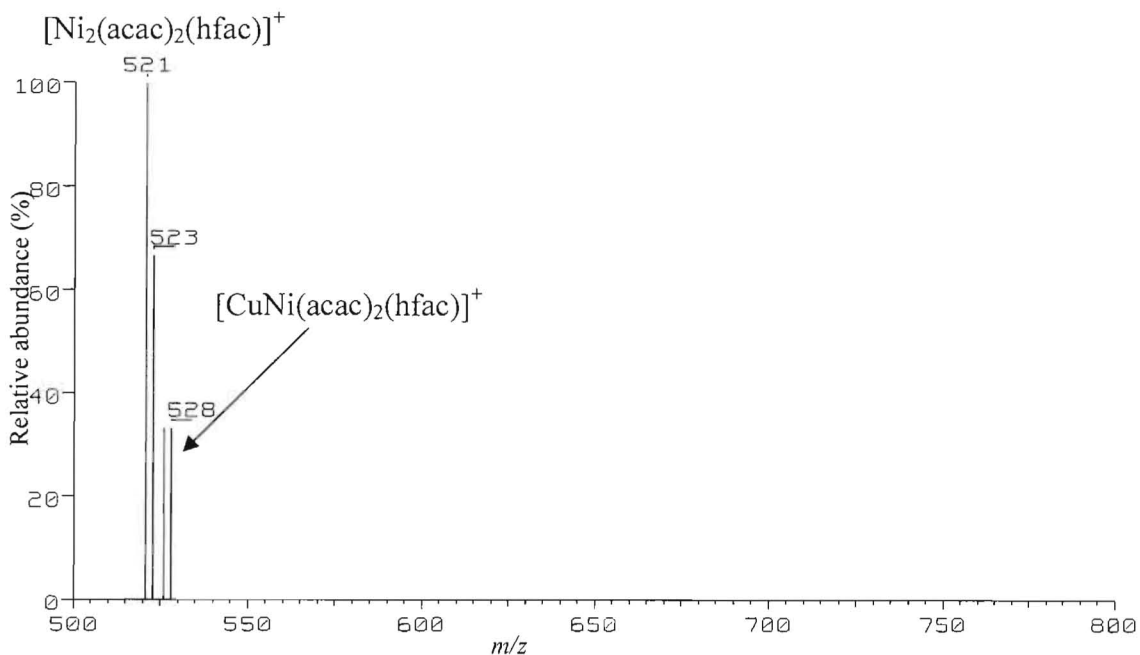
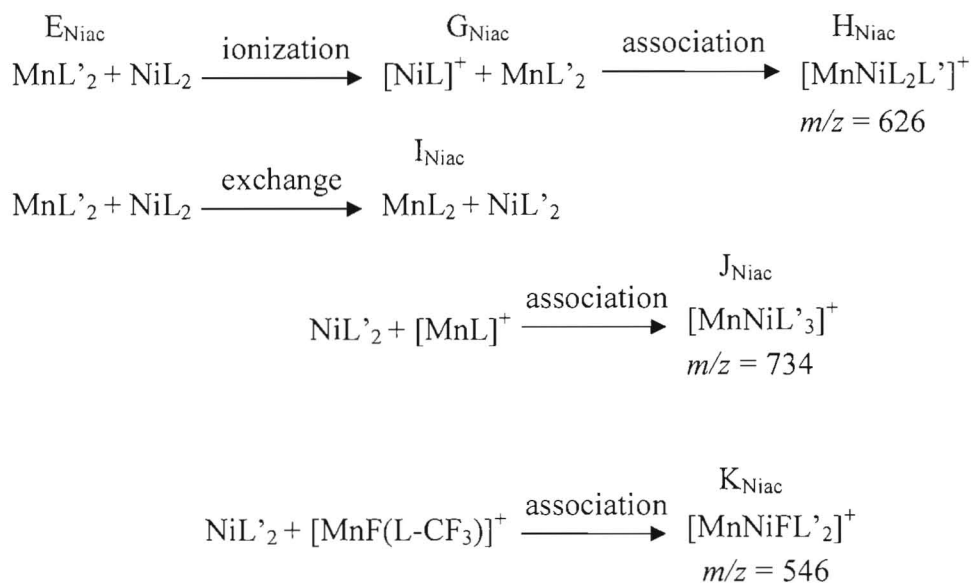


Figure 3.8: The mass spectrum of $Cu(hfac)_2$ mixed with $Ni(acac)_2$ in the upper mass range.

3.3.3.2 Mn(hfac)₂ mixed with Ni(acac)₂

Figure 3.9 shows the full spectrum of the mixture of Mn(hfac)₂ with Ni(acac)₂ where Figure 3.10 shows the upper mass range (500-800 amu). When Ni(acac)₂ mixes with Mn(hfac)₂, the spectra gets much more complicated than just overlaying the individual spectra. The most abundant peak in the spectrum is H₂O from the dissociation of the adduct, Ni(acac)₂·2H₂O. The exchange reaction occurs to such a large extent that the molecular ion of Ni(acac)₂ has completely exchanged its ligands and forms Ni(hfac)₂ at *m/z* 472. Another exchange reaction product seen is that of [Ni(acac)(hfac)]⁺ at *m/z* 364. There are also three mixed-metal ions observed in this spectra: *m/z* 546 ([MnNiF(hfac)₂]⁺), *m/z* 626 ([MnNi(acac)(hfac)₂]⁺), and *m/z* 734 ([MnNi(hfac)₃]⁺). The possible pathways of the formation of each ion are illustrated in Scheme 3.8 where ions J_{Niac} and K_{Niac} must have an exchange reaction occur before association since they have three hfac ligands, and no initial complex has three hfac ligands.



Scheme 3.8: Proposed association reactions to form the three mixed-metal ions where L is acac and L' is hfac.

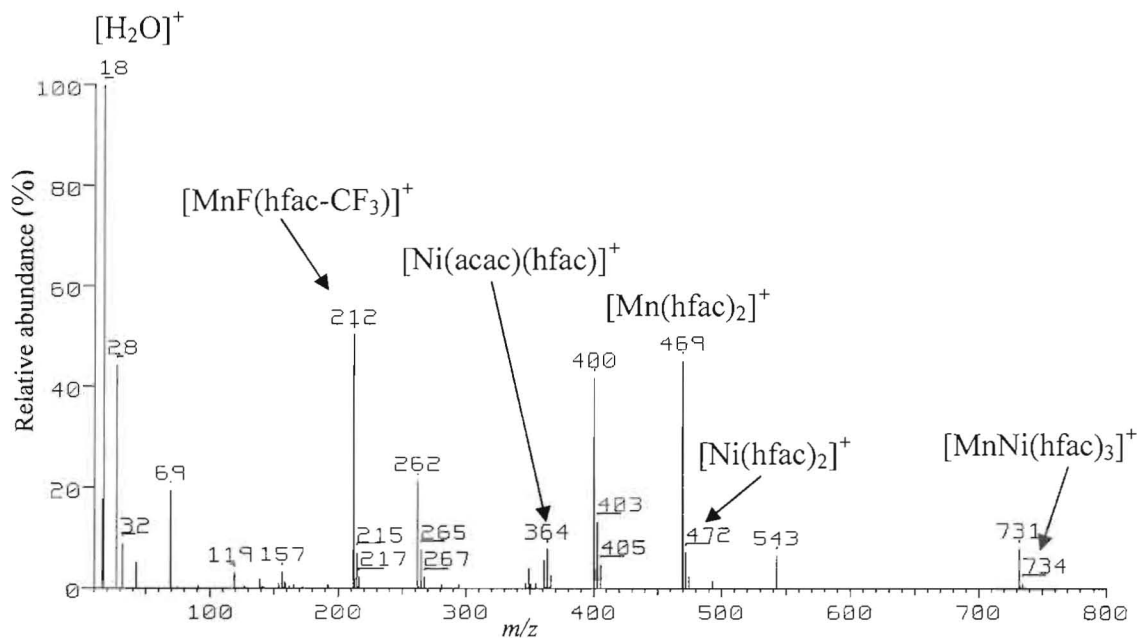


Figure 3.9: The mass spectrum of $\text{Mn}(\text{hfac})_2$ mixed with $\text{Ni}(\text{acac})_2$.

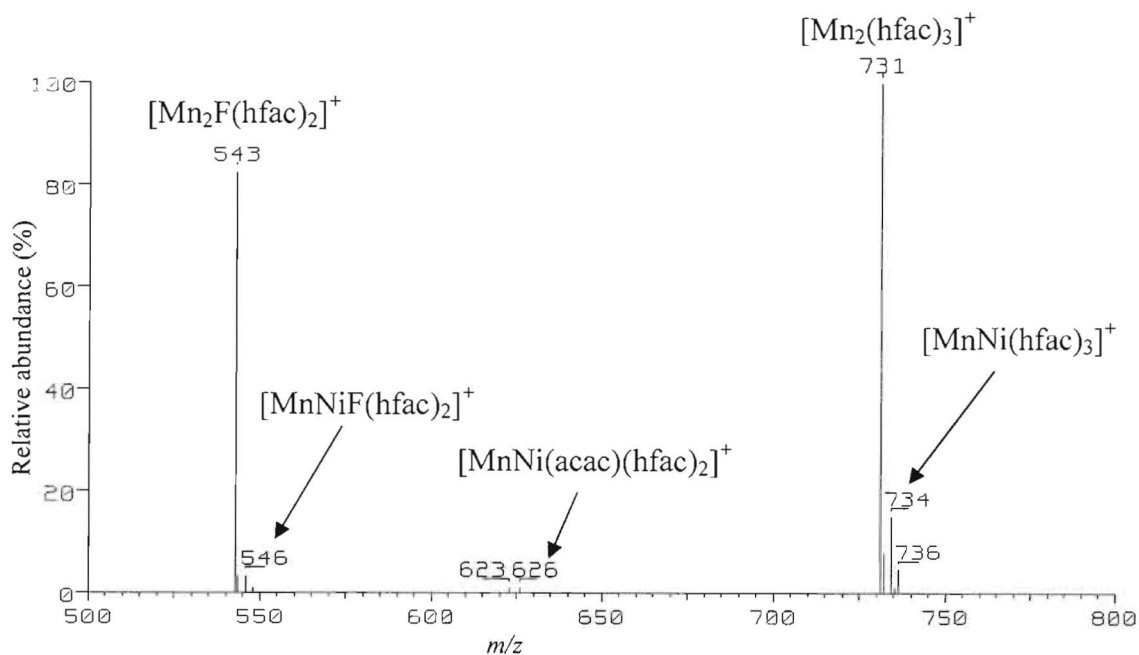


Figure 3.10: The mass spectrum of $\text{Mn}(\text{hfac})_2$ mixed with $\text{Ni}(\text{acac})_2$ in the upper mass range.

3.3.3.3 Mn(hfac)₃ mixed with Ni(acac)₂

The gas phase reaction of Mn(hfac)₃ with Ni(acac)₂, as observed in a mass spectrum, is shown in Figure 3.11. The molecular ion of Ni(acac)₂ at *m/z* 256 and Mn(hfac)₃ at *m/z* 676 are not intense relative to the most abundant ion [Mn(hfac)₂]⁺. The exchange reaction where the peaks at *m/z* 154, 253, 346, and 361 all pertain to the manganese complex obtaining acac ligands and show the extent at which the exchange reaction occurs. There are three relatively weak mixed-metal ion peaks at *m/z* 518, 546, and 734 where the ion with *m/z* 518 is analogous to the copper-nickel mixed-metal complex at *m/z* 526 with manganese associating with the nickel complex forming [MnNi(acac)₂(hfac)]⁺.

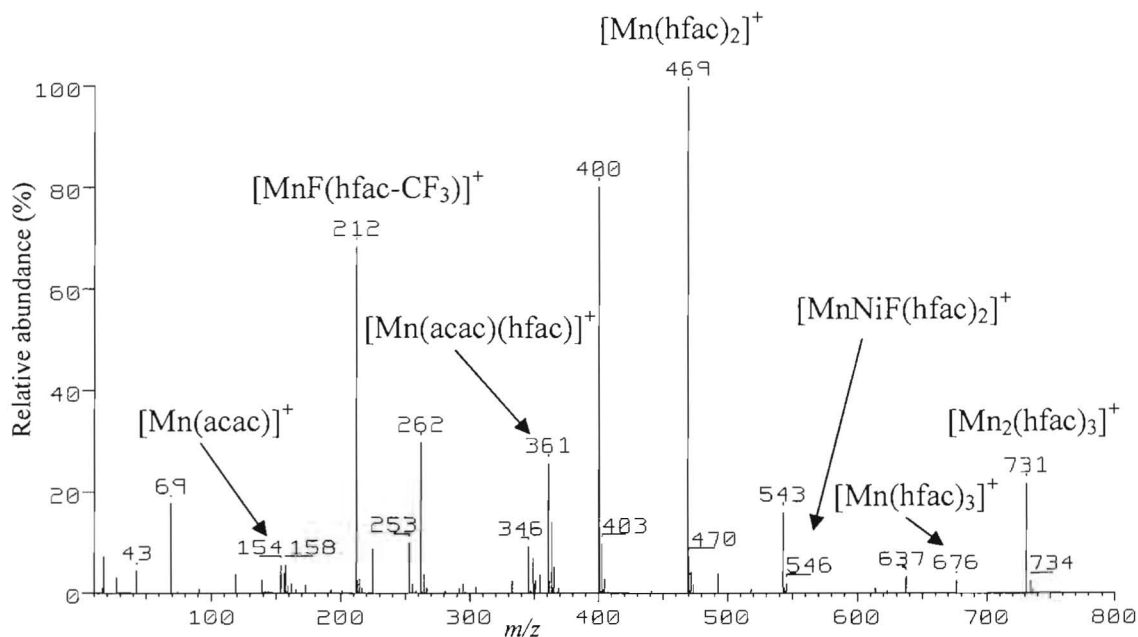


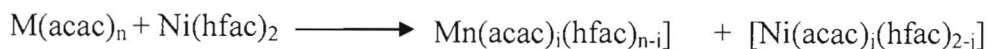
Figure 3.11: The mass spectrum of Mn(hfac)₃ mixed with Ni(acac)₂.

The mixed-metal peaks at *m/z* 734, 546, and 518 are of the arrangement found for metals with oxidation state 2+, MNi(acac)_{*n*}(hfac)_{3-*n*}, however Mn(hfac)₃ is initially in an

oxidation state of 3+. As described earlier in Scheme 2.6, manganese can either decompose to an oxidation state of 2+ before ionization ($C_{Ni(ac)}$) or dissociate and change oxidation state ($E_{Ni(ac)}$). The molecular ion of $Mn(hfac)_3$, $E_{Ni(ac)}$, is still observed which gives evidence for the dissociation pathway. The increased presence of $Mn_2(hfac)_3$ at m/z 731, however, supports decomposition before ionization since it signifies an association reaction between two $Mn(hfac)_2$ molecules. If $Mn(hfac)_2$ is reacting, then additional $hfac$ ligands are necessary for the formation of mixed-metal complex, $[MnNi(hfac)_3]$. The $Ni(acac)_2$ could undergo an exchange reaction as presented, in Scheme 3.8, to make the third $hfac$ ligand available for the appropriate association reaction.

3.3.4 $Ni(hfac)_2$ series

The full list of complexes in Table 1.1 were mixed with $Ni(hfac)_2$. The metal acetylacetonate complexes showed ligand exchange, with two metal centers, copper and manganese showing consistent mixed-metal complexes common to the $Ni(acac)_2$ reactivity series (section 3.3.3). $Cu(acac)_2$ and the four manganese complexes, $Mn(acac)_2$, $Mn(acac)_3$, $Mn(hfac)_2$, and $Mn(hfac)_3$ display the ability to form mixed-metal complexes with $Ni(hfac)_2$. All reactions identified formed the arrangement of $MM'L_nL'_{3-n}$ which maintains the +2 oxidation state as the highest mass mixed-metal complex.



Scheme 3.9: General ligand exchange reaction between $M(acac)_n$ ($n = 1-3$) and $Ni(acac)_2$ where i and j are from 0 to 3.

3.3.4.1 *Cu(acac)₂ mixed with Ni(hfac)₂*

The reaction of $\text{Cu}(\text{acac})_2$ with $\text{Ni}(\text{hfac})_2$ is observed in Figure 3.12. The most abundant peak is the loss of CH_3 from $\text{Ni}(\text{hfac})_2$. The molecular ion of $\text{Cu}(\text{acac})_2$ has a relative abundance around 32%. The combined spectra has many exchange reaction products and some association reaction products. Some significant exchange reaction products are the ions at m/z 349, 364, and 477 corresponding to $[\text{Ni}(\text{acac}-\text{CH}_3)(\text{hfac})]^+$, $[\text{Ni}(\text{acac})(\text{hfac})]^+$, and $[\text{Cu}(\text{hfac})_2]^+$. The ion at m/z 526 is attributed to the formation of $[\text{CuNi}(\text{acac})_2(\text{hfac})]^+$ from the association of $\text{Cu}(\text{acac})_2$ with $[\text{Ni}(\text{hfac})]^+$. This reaction is similar to the reaction analyzed in section 3.3.3.1 when $\text{Cu}(\text{hfac})_2$ was mixed with $\text{Ni}(\text{acac})_2$. The mixed-metal ion, $[\text{CuNi}(\text{acac})_2(\text{hfac})]^+$, has two related mixed-metal products at m/z 319 and 427. These ions may form from the dissociation of the intense mixed-metal product, $[\text{CuNi}(\text{acac})_2(\text{hfac})]^+$, where the ion loses either an hfac ligand or an acac ligand forming either $[\text{CuNi}(\text{acac})_2]^+$ (319) or $[\text{CuNi}(\text{acac})(\text{hfac})]^+$ (427).

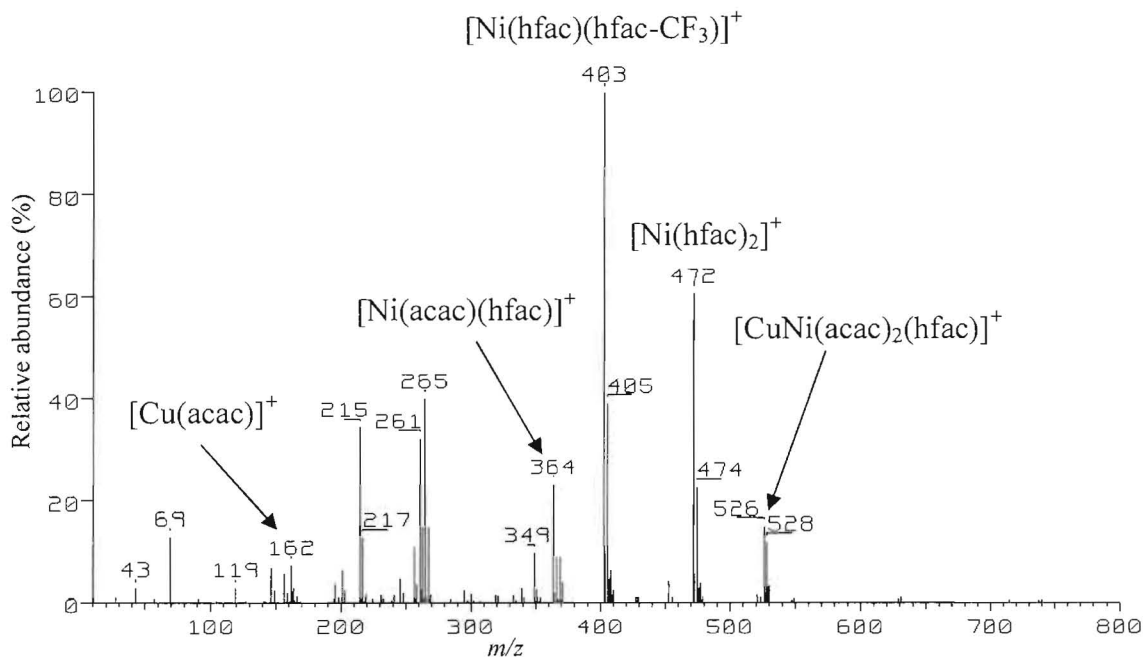
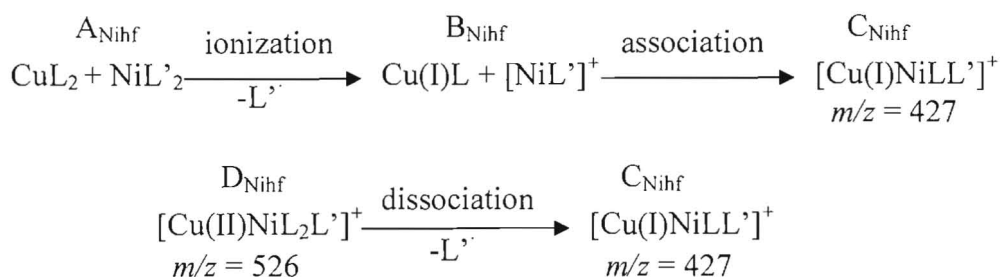


Figure 3.12: Mass spectrum of Cu(acac)₂ mixed with Ni(hfac)₂.

Two possibilities exist in the formation of these complexes, [CuNi(acac)₂]⁺ (319) and [CuNi(acac)(hfac)]⁺ (427). These complexes may form after each complex dissociates, where either [Cu(I)]⁺/[Cu(I)(hfac)] fragments associate with Ni(acac)₂/[Ni(acac)]⁺, or the complex [CuNi(acac)(hfac)]⁺ forms and then dissociates into these two product ions, as illustrated in Scheme 3.10. In either case, the oxidation state of copper is most likely 1+ in the complex ions at *m/z* 319 and 427.



Scheme 3.10: Possible reaction pathways to form the mixed-metal ion C_{Ni_hf} where L is acac and L' is hfac. The upper pathway describes the association reaction, and the lower pathway describes the dissociation from a previous association product.

3.3.4.2 Mn(acac)₂ mixed with Ni(hfac)₂

In Figures 3.13 and 3.14, the mass spectrum of the gas phase mixture of Mn(acac)₂ with Ni(hfac)₂ is given. The spectra is dominated by the dissociation pattern of Ni(hfac)₂. Small exchange reactions are detected but unseen with similar relative intensities to the Mn(acac)₂ peaks at less than 10% relative abundance. There is only one mixed-metal complex consistently found with this mixture occurring at *m/z* 734. The [NiMn(hfac)₃]⁺ (734) ion has a relative intensity of 0.9% and is analogous to [Ni₂(hfac)₃]⁺ observed at *m/z* 737. The mixed-metal ion most likely occurred after an

exchange reaction since neither complex has three hexafluoroacetylacetonate ligands already coordinated to it.

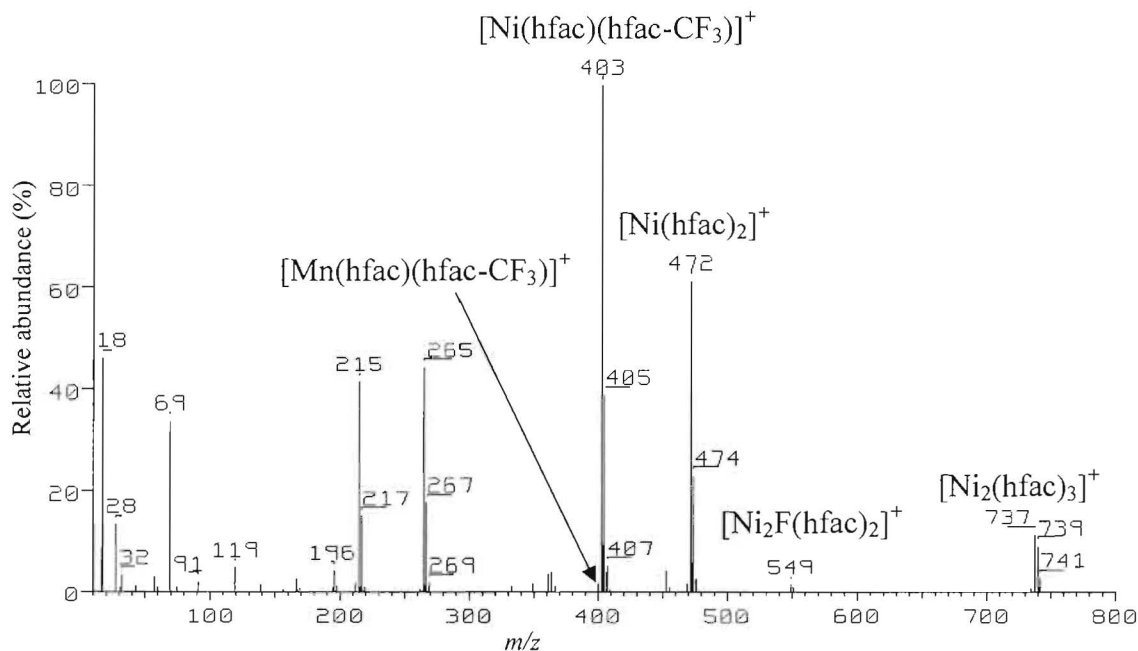


Figure 3.13: The mass spectrum of $\text{Mn}(\text{acac})_2$ mixed with $\text{Ni}(\text{hfac})_2$.

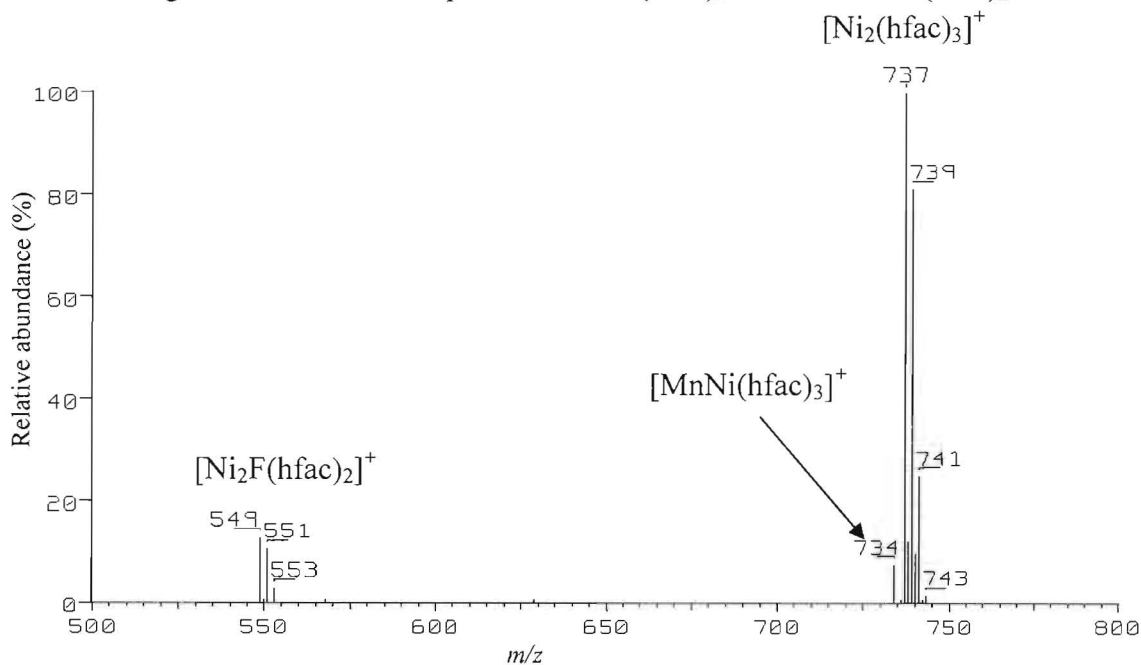


Figure 3.14: The mass spectrum of $\text{Mn}(\text{acac})_2$ mixed with $\text{Ni}(\text{hfac})_2$ in the upper mass range.

3.3.4.3 $Mn(acac)_3$ mixed with $Ni(hfac)_2$

The mixture of $Mn(acac)_3$ with $Ni(hfac)_2$ is depicted in Figures 3.15 and 3.16. The most abundant peak remains the loss of a fluorinated methyl radical from the molecular ion of $Ni(hfac)_2$ at m/z 403, $[Ni(hfac)(hfac-CF_3)]^+$. The $[Mn(acac)_2]^+$ ion has a considerable intensity suggesting that $Mn(acac)_3$ has a relatively high concentration in the gas phase mixture between $Mn(acac)_3$ and $Ni(hfac)_2$. The exchange reactions and mixed-metal ion products are similar to those occurring in the last mixture of $Mn(acac)_2$ with $Ni(hfac)_2$. Unique peaks at m/z 568 and 629 show exchange reactions forming $[Mn(acac)(hfac)_2]^+$ and $[Ni_2(acac)(hfac)_2]^+$, which were not found for the previous reaction. The mixed-metal ion, $[NiMn(hfac)_3]^+$, seems to have formed after an exchange reaction as suggested in the previous mixture of the $Mn(acac)_2$ with $Ni(hfac)_2$ since neither complex has three of the hexafluoroacetylacetonate coordinated to its metal.

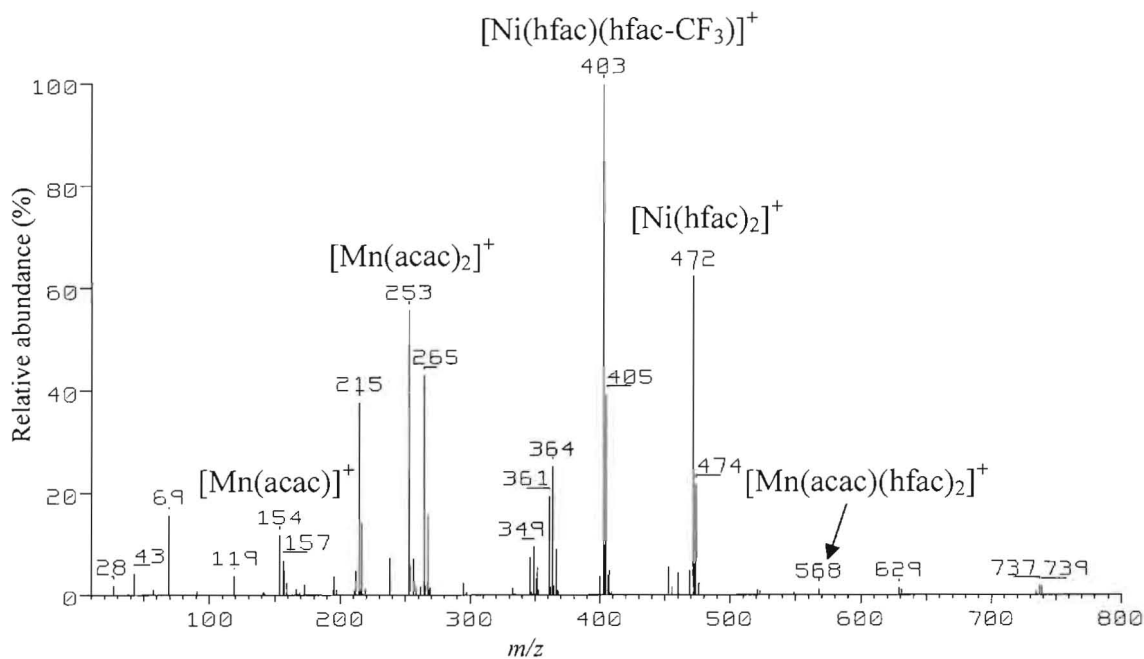


Figure 3.15: The mass spectrum of $Mn(acac)_3$ mixed with $Ni(hfac)_2$.

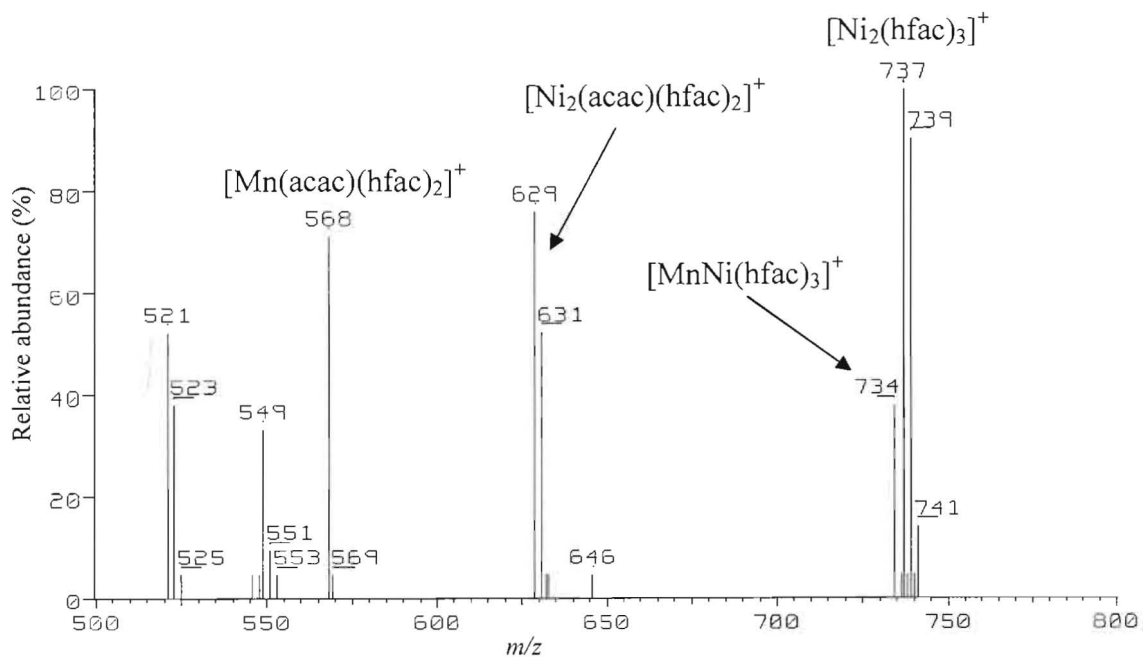
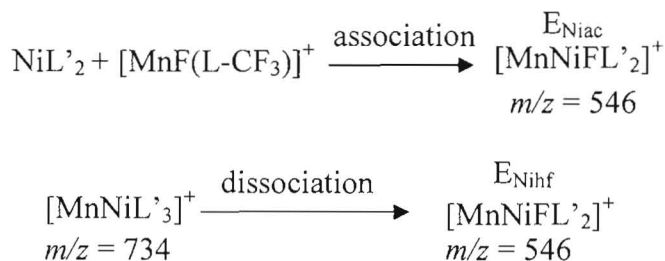


Figure 3.16: The mass spectrum of Mn(acac)₃ mixed with Ni(hfac)₂ in the upper mass range.

3.3.4.4 Mn(hfac)₂ mixed with Ni(hfac)₂

The mass spectrum of the gas phase mixture of Mn(hfac)₂ with Ni(hfac)₂ is presented in Figure 3.17. It shows the Ni(hfac)₂ peaks remain in high relative abundance compared to the Mn(hfac)₂ peaks. It is unknown whether the exchange reactions occur since they have the same ligand and would be mass degenerate. Two mixed-metal ions were found at *m/z* 546 and 734 where the 734 peak of the form [MnNi(hfac)₃]⁺. The 546 peak is indicative of fluorine migration to a metal whether this happens before or after the association reaction is unknown.



Scheme 3.11: Two possible reactions yielding ion E_{Nihf} where the upper pathway describes the association reaction needed, and the lower pathway describes the dissociation of a larger association product.

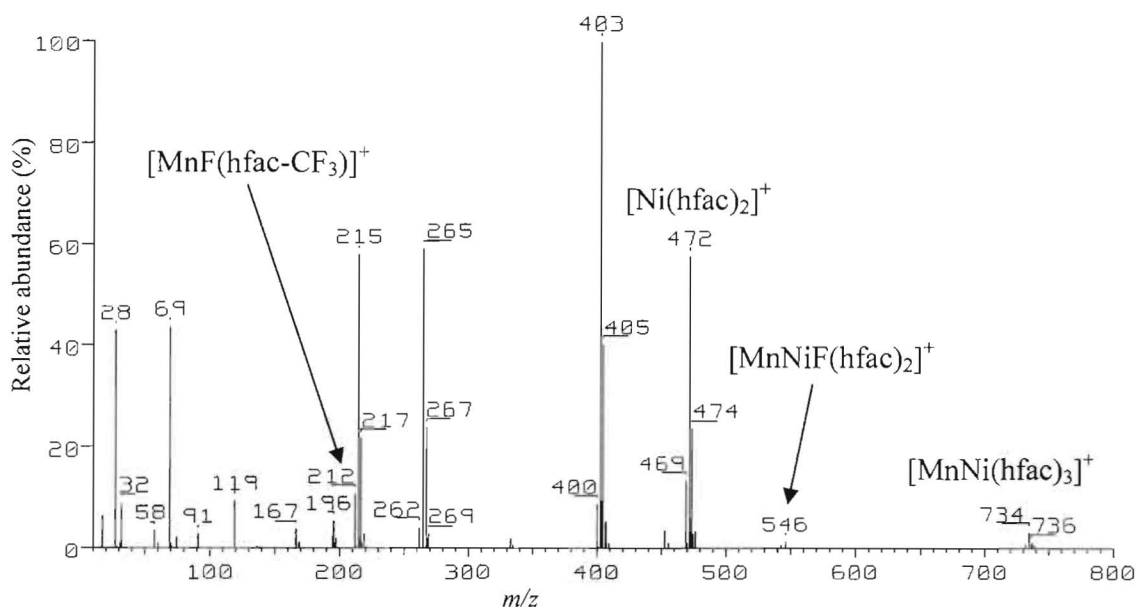


Figure 3.17: The mass spectrum of $\text{Mn}(\text{hfac})_2$ mixed with $\text{Ni}(\text{hfac})_2$.

3.3.4.5 $\text{Mn}(\text{hfac})_3$ mixed with $\text{Ni}(\text{hfac})_2$

The final gas phase reaction observed to incorporate two different metals is when $\text{Mn}(\text{hfac})_3$ mixed with $\text{Ni}(\text{hfac})_2$ where the mass spectrum of the reaction is given in Figures 3.18 and 3.19. The manganese complex ions are slightly higher in relative abundance than the nickel complex ions. The molecular ion of $\text{Mn}(\text{hfac})_3$ is easily seen at m/z 676 along with the most abundant peak at m/z 469. The exchange reactions are mass

degenerate since the same ligand is used. The same mixed-metal complexes are found at m/z 546 and 734 where these peaks increase in relative abundance as the molecular ion decreases in abundance. This is expected since the three plus oxidation state does not form the 734 or 546 complex ions as discussed in section 2.5.1. The decomposition of $\text{Mn}(\text{hfac})_3$ to $\text{Mn}(\text{hfac})_2$ is confirmed by the increase in the 731 peak, and does increase the relative abundance of the mixed-metal ions slightly.

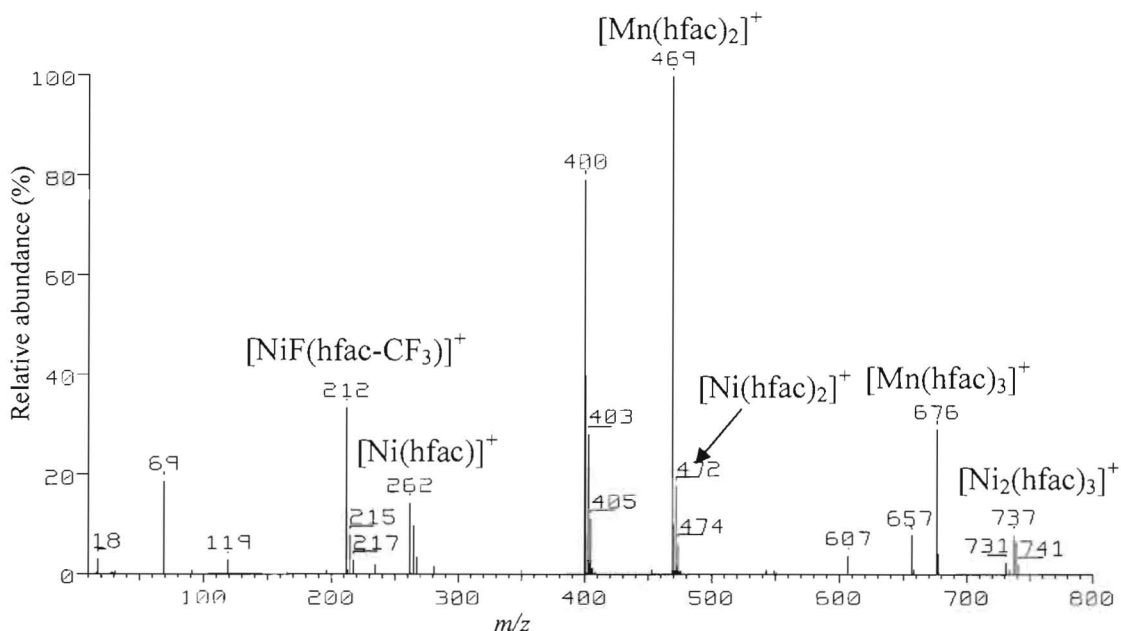


Figure 3.18: The mass spectrum of $\text{Mn}(\text{hfac})_3$ mixed with $\text{Ni}(\text{hfac})_2$.

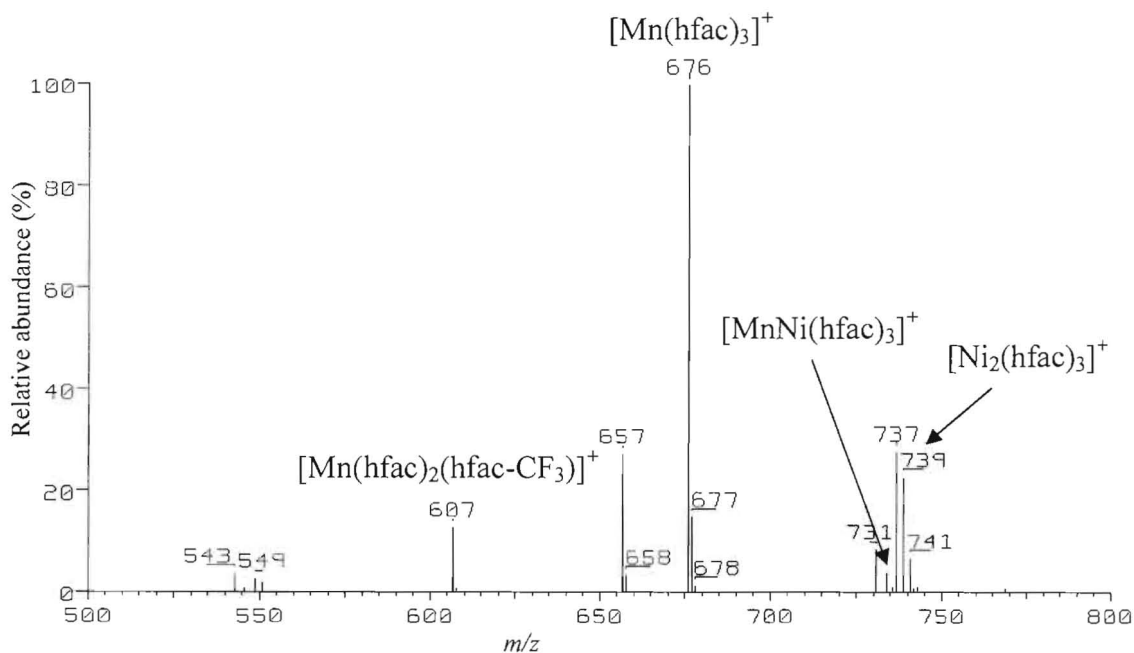


Figure 3.19: The mass spectrum of Mn(hfac)₃ mixed with Ni(hfac)₂ in the upper mass range.

3.4 Conclusions

New mixed-metal complexes were detected by double focusing mass spectrometry along with many exchange reactions common to the mixtures. In most cases, with the low source pressure conditions, no mixed-metal association reactions were observed.

All the mixtures attempted with aluminum tris(hexafluoroacetylacetonate) detected no mixed-metal association products. However, aluminum tris(acetylacetonate) formed mixed-metal complexes with the 3d transition metals from manganese to nickel having the same final ligand arrangement. The difference between Al(hfac)₃ and Al(acac)₃ demonstrates the dramatic effect that the ligand has on the gas phase association reactivity for aluminum. The difference may lie in the complexes ability to stabilize the 3+ oxidation state where Al(hfac)₃ predominately utilizes fluorine migration

to stabilize the molecule, so that reduction of oxidation state does not occur. In $\text{Al}(\text{acac})_3$, the dominant $[\text{Al}(\text{acac})_2]^+$ ion does not seem to readily dissociate further giving **no** other preferred dissociation pathway. The association reactions detected gave ions of the form $[\text{MAl}(\text{acac})_3(\text{hfac})]^+$ and for Co and Mn, $[\text{MAl}(\text{acac})_3(\text{hfac})_2]^+$.

The gas phase mixed-metal association reactions observed for $\text{Ni}(\text{acac})_2$ and $\text{Ni}(\text{hfac})_2$ included reactions only involving manganese, copper, and aluminum, excluding the other 9 metal centers. The ions detected, except for those with Al which is noted above, have the general form $[\text{MNiL}^*_2]^+$ or $[\text{MNiL}^*_3]^+$ with L^* being either acac, hfac, or a mixture of both.

References

1. Kuo, C. K.; Jiang, S.; Sahayam, A. C. *J. Anal. At. Spectrom.* **2007**, *22*, 636–641.
2. Liu, W.; Cai, H.; Li, H. *J. Chromatogr. B* **2007**, *850*, 450-411.
3. Shirke, A.G.; Cavicchi, R. E.; Semancik, S.; Jackson, R. H.; Frederick, B. G.; Wheeler, M. C. *J. Vac. Sci. Technol. A* **2007**, *25(3)*, 514-526.
4. Barker, J.; Davis, R.; Frearson, M. J. In *Mass Spectrometry*; Ando, D. J.; 2nd ed.; Analytical Chemistry by Open Learning; John Wiley & Sons: New York City, NY, 2000; 2.
5. Miller, J. M.; Ross, J.; Rustenburg, J.; Wilson, G. L. *Anal. Chem.* **1973**, *45(3)*, 627-629.
6. Duta, A.; Manolache, S.; Nanu, M.; Goossens, A.; Schoonman, J. *Thin Solid Films* **2006**, *511*, 195-198.
7. Si, R.; Zhang, Y.; Zhou, H.; Sun, L.; Yan, C. *Chem. Mater.* **2007**, *19*, 18-27.
8. Pournaghi-Ahar, M.H.; Ramazani, M.R. *Electroanalysis* 2002, *14(17)*, 1203-1208.
9. Mehrotra, R.C.; Bohra, R.; Gaur, D.P. In *Metal β -Diketonates and Allied Derivatives*; Academic Press Inc. NY, NY 1978; 1-194.
10. Sasaki, S.; Itagaki, Y.; Kurokawa, T.; Nakanishi, K.; Kasahara, A.; *Bulletin Chem. Soc. of Japan* **1967**, *40(1)*, 76-80.
11. Bauer, E.; Muller, H.P.; Sievers, R.E. *Anal. Chem.* 1971, *43*, 2012.
12. Belcher, R.; Blessel, K.; Cardwell, T.; Pravica, M. Stephen, W.I.; Uden, P.C. *J. Inorg. Nucl. Chem.* **1973**, *35*, 1127.
13. Bancroft, G.M.; Reichert, C.; Westmore, J.B.; Gesser, H.D. *Inorg. Chem.* **1969**, *8(3)*, 474-480.

14. Clobes, A.L.; Morris, M.L.; Koob, R.D. *Org. Mass Spec.* **1971**, *5*, 633-649.
15. Rubesch, M.; Clobes, A.L.; Morris, M.L.; Koob, R.D. *Org. Mass Spec.* **1971**, *5*, 237-248.
16. MacDonald, C.G.; Shannon, J.S. *Aust. J. Chem.* **1966**, *19*, 1545-1566.
17. Bancroft, G.M.; Reichert, C.; Westmore, J.B. *Inorg. Chem.* **1968**, *7(5)*, 870-874.
18. Reichert, C.; Westmore, J.B. *Inorg. Chem.* **1969**, *8(4)*, 1012-1014.
19. Curtis, J.M.; Derrick, P.J.; Schnell, A.; Constantin, E.; Gallagher, R.T.; Chapman, J.R. *Inorganica Chimica Acta* **1992**, *201*, 197-201.
20. Morris, M.L.; Koob, R.D. *Inorg. Chem.* **1981**, *20*, 2737-2738.
21. Bryant, J.R.; Taves, J.E.; Mayer, J.M. *Inorg. Chem.* **2002**, *41*, 2769-2776.
22. Bouwman, E.; Caulton, K.G.; Christou, G.; Folting, K.; Gasser, C.; Hendrickson, D.N.; Huffman, J.C.; Lobkovsky, E.B.; Martin, J.D.; Michel, P.; Tsai, H.; Xue, Z. *Inorg. Chem.* **1993**, *32*, 3463-3470.
23. Ast, T.; Kralj, B.; Kramer, V.; Zigon, D. *Internat. J. Mass Spec. and Ion Proc.* **1988**, *86*, 329-339.
24. Schildcrout, S.M. *J. Phys. Chem.* **1976**, *80(26)*, 2834-2838.
25. Majer, J.R.; Perry, R. *Chem. Comm.* **1969**, 454-455.
26. Schildcrout, S.M. *Inorg. Chem.* **1980**, *19*, 224-227.

Appendix: Crystal data and structure refinements.

A.1: Crystal Data and Structure Refinement for $\text{Mn}(\text{hfac})_3$.

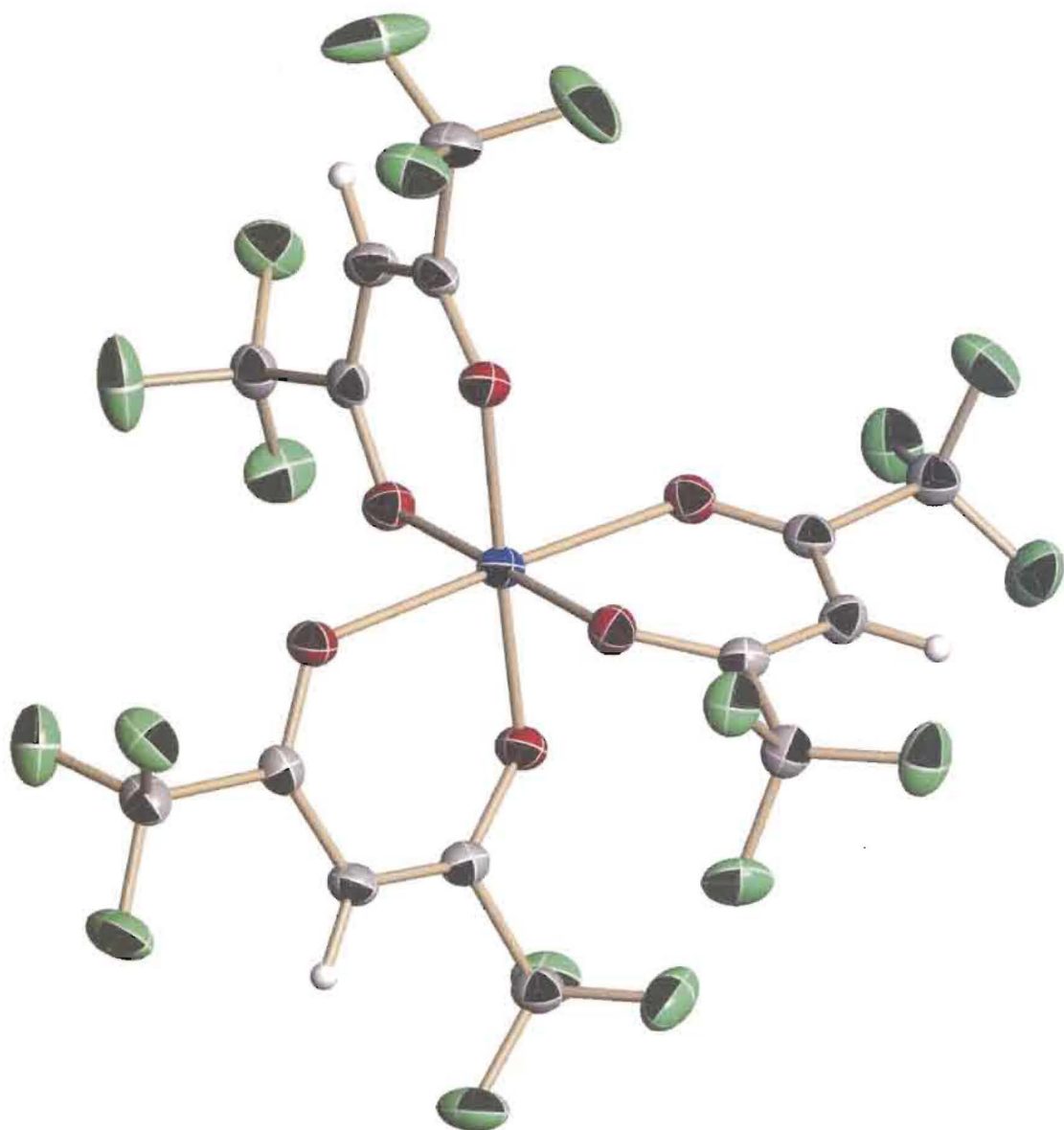


Figure A.1 : The crystal structure of manganese tris(acetylacetonate).

Table A.1: Crystal data and structure refinement of Mn(hfac)₃.

Empirical formula: C₁₅ H₃ F₁₈ Mn O₆

Formula weight: 676.11

Temperature: 100(2) K

Wavelength: 0.71073 Å

Crystal system: Monoclinic

Space group: P2₁/n

Unit cell dimensions:

a = 8.8808(15) Å, α = 90°

b = 12.956(2) Å, β = 91.403(3)°

c = 18.763(3) Å, γ = 90°

Volume, Z: 2158.2(7) Å³, 4

Density (calculated): 2.081 g/m³

Absorption coefficient: 0.800 mm⁻¹

F(000): 1312

Crystal size: 0.43 × 0.30 × 0.14

Crystal shape, colour: block, purple

θ range for data collection: 1.91 to 28.28°

Limiting indices: -11 ≤ h ≤ 11, -17 ≤ k ≤ 17, -25 ≤ l ≤ 24

Reflections collected: 21553

Independent reflections: 5334 (R(int) = 0.0372)

Completeness to θ = 28.28°: 99.8 %

Absorption correction: multi-scan

Max. and min. transmission: 0.894 and 0.756

Refinement method: Full-matrix least-squares on F²

Data / restraints / parameters: 5334 / 0 / 361

Goodness-of-fit on F²: 1.021

Final R indices [I > 2σ(I)]: R1 = 0.0421, wR2 = 0.0971

R indices (all data): 0.0555, wR2 = 0.1058

Largest diff. peak and hole: 0.538 and -0.461 e × Å⁻³

Refinement of F^2 against ALL reflections. The weighted R-factor wR and goodness of fit are based on F^2 , conventional R-factors R are based on F , with F set to zero for negative F^2 . The threshold expression of $F^2 > 2\sigma(F^2)$ is used only for calculating R-factors

Treatment of hydrogen atoms:

All hydrogen atoms were placed in calculated positions and were refined with an isotropic displacement parameter 1.2 times that of the adjacent carbon atom.

Table A.2: Atomic coordinates [$\times 10^4$] and equivalent isotropic displacement parameters [$\text{\AA}^2 \times 10^3$] for Mn(hfac)₃. U(eq) is defined as one third of the trace of the orthogonalized U_{ij} tensor.

	x	y	z	U(eq)
C(1)	907(3)	4306(2)	3560(1)	27(1)
C(2)	2519(2)	4511(2)	3304(1)	23(1)
C(3)	3716(2)	4372(2)	3811(1)	23(1)
C(4)	5197(2)	4396(2)	3621(1)	21(1)
C(5)	6430(3)	4265(2)	4195(1)	25(1)
C(6)	5587(3)	7796(2)	3359(1)	25(1)
C(7)	5915(2)	6988(2)	2789(1)	21(1)
C(8)	7310(2)	6966(2)	2488(1)	23(1)
C(9)	7647(2)	6248(2)	1952(1)	21(1)
C(10)	9147(3)	6361(2)	1566(1)	26(1)
C(11)	2478(3)	5956(2)	261(1)	26(1)
C(12)	3150(2)	5239(2)	838(1)	22(1)
C(13)	3167(2)	4181(2)	707(1)	25(1)
C(14)	3976(2)	3526(2)	1159(1)	23(1)
C(15)	4076(3)	2371(2)	985(1)	29(1)
F(1)	-116(2)	4772(1)	3146(1)	40(1)
F(2)	636(2)	3295(1)	3542(1)	42(1)
F(3)	724(2)	4639(1)	4221(1)	41(1)
F(4)	5898(2)	3925(1)	4810(1)	37(1)
F(5)	7488(2)	3610(1)	3986(1)	31(1)
F(6)	7096(2)	5176(1)	4320(1)	36(1)
F(7)	5373(2)	7334(1)	3987(1)	43(1)
F(8)	4336(2)	8320(1)	3193(1)	33(1)
F(9)	6700(2)	8471(1)	3449(1)	36(1)
F(10)	10037(2)	7084(1)	1849(1)	43(1)
F(11)	9915(2)	5480(1)	1561(1)	34(1)
F(12)	8868(2)	6620(1)	884(1)	41(1)
F(13)	2032(2)	6844(1)	528(1)	39(1)
F(14)	3532(2)	6153(2)	-214(1)	49(1)
F(15)	1310(2)	5530(1)	-82(1)	39(1)

F(16)	5472(2)	2035(1)	1047(1)	37(1)
F(17)	3591(2)	2161(1)	329(1)	61(1)
F(18)	3256(2)	1831(1)	1434(1)	58(1)
Mn(1)	4744(1)	5104(1)	2186(1)	20(1)
O(1)	2637(2)	4742(1)	2664(1)	25(1)
O(2)	5750(2)	4522(1)	2999(1)	23(1)
O(3)	4769(2)	6408(1)	2660(1)	24(1)
O(4)	6841(2)	5526(1)	1727(1)	24(1)
O(5)	3709(2)	5711(1)	1370(1)	25(1)
O(6)	4701(2)	3766(1)	1725(1)	23(1)

All esds (except the esd in the dihedral angle between two l.s. planes) are estimated using the full covariance matrix. The cell esds are taken into account individually in the estimation of esds in distances, angles and torsion angles; correlations between esds in cell parameters are only used when they are defined by crystal symmetry. An approximate (isotropic) treatment of cell esds is used for estimating esds involving l.s. planes.

Table A.3. Bond lengths [\AA] and angles [deg] for Mn(hfac)₃.

C(1)-F(1)	1.325(3)	C(11)-F(13)	1.320(3)
C(1)-F(3)	1.328(3)	C(11)-F(15)	1.327(3)
C(1)-F(2)	1.332(3)	C(11)-F(14)	1.332(3)
C(1)-C(2)	1.545(3)	C(11)-C(12)	1.536(3)
C(2)-O(1)	1.244(3)	C(12)-O(5)	1.263(3)
C(2)-C(3)	1.421(3)	C(12)-C(13)	1.392(3)
C(3)-C(4)	1.372(3)	C(13)-C(14)	1.387(3)
C(3)-H(3)	0.9500	C(13)-H(13)	0.9500
C(4)-O(2)	1.287(3)	C(14)-O(6)	1.268(3)
C(4)-C(5)	1.527(3)	C(14)-C(15)	1.535(3)
C(5)-F(4)	1.332(3)	C(15)-F(16)	1.316(3)
C(5)-F(5)	1.332(3)	C(15)-F(17)	1.323(3)
C(5)-F(6)	1.339(3)	C(15)-F(18)	1.326(3)
C(6)-F(9)	1.328(3)	Mn(1)-O(2)	1.9049(16)
C(6)-F(8)	1.333(3)	Mn(1)-O(3)	1.9103(16)
C(6)-F(7)	1.339(3)	Mn(1)-O(5)	1.9333(16)
C(6)-C(7)	1.530(3)	Mn(1)-O(6)	1.9365(16)
C(7)-O(3)	1.283(3)	Mn(1)-O(4)	2.1413(16)
C(7)-C(8)	1.373(3)	Mn(1)-O(1)	2.1475(16)
C(8)-C(9)	1.408(3)		
C(8)-H(8)	0.9500	F(1)-C(1)-F(3)	107.6(2)
C(9)-O(4)	1.245(3)	F(1)-C(1)-F(2)	108.2(2)
C(9)-C(10)	1.539(3)	F(3)-C(1)-F(2)	108.5(2)
C(10)-F(10)	1.327(3)	F(1)-C(1)-C(2)	111.5(2)
C(10)-F(11)	1.330(3)	F(3)-C(1)-C(2)	111.74(19)
C(10)-F(12)	1.341(3)	F(2)-C(1)-C(2)	109.22(19)

O(1)-C(2)-C(3)	126.7(2)	C(14)-C(13)-H(13)	119.9
O(1)-C(2)-C(1)	116.2(2)	C(12)-C(13)-H(13)	119.9
C(3)-C(2)-C(1)	117.0(2)	O(6)-C(14)-C(13)	127.3(2)
C(4)-C(3)-C(2)	122.0(2)	O(6)-C(14)-C(15)	112.7(2)
C(4)-C(3)-H(3)	119.0	C(13)-C(14)-C(15)	119.9(2)
C(2)-C(3)-H(3)	119.0	F(16)-C(15)-F(17)	107.4(2)
O(2)-C(4)-C(3)	129.0(2)	F(16)-C(15)-F(18)	107.5(2)
O(2)-C(4)-C(5)	111.74(18)	F(17)-C(15)-F(18)	108.1(2)
C(3)-C(4)-C(5)	119.3(2)	F(16)-C(15)-C(14)	111.28(19)
F(4)-C(5)-F(5)	108.19(19)	F(17)-C(15)-C(14)	112.3(2)
F(4)-C(5)-F(6)	107.64(19)	F(18)-C(15)-C(14)	110.1(2)
F(5)-C(5)-F(6)	107.61(19)	O(2)-Mn(1)-O(3)	88.68(7)
F(4)-C(5)-C(4)	112.61(18)	O(2)-Mn(1)-O(5)	179.08(7)
F(5)-C(5)-C(4)	111.24(19)	O(3)-Mn(1)-O(5)	90.50(7)
F(6)-C(5)-C(4)	109.37(19)	O(2)-Mn(1)-O(6)	90.41(7)
F(9)-C(6)-F(8)	107.90(19)	O(3)-Mn(1)-O(6)	178.62(7)
F(9)-C(6)-F(7)	107.71(19)	O(5)-Mn(1)-O(6)	90.40(7)
F(8)-C(6)-F(7)	107.28(19)	O(2)-Mn(1)-O(4)	91.57(7)
F(9)-C(6)-C(7)	112.72(19)	O(3)-Mn(1)-O(4)	87.77(6)
F(8)-C(6)-C(7)	110.94(18)	O(5)-Mn(1)-O(4)	88.82(7)
F(7)-C(6)-C(7)	110.09(19)	O(6)-Mn(1)-O(4)	93.29(6)
O(3)-C(7)-C(8)	129.1(2)	O(2)-Mn(1)-O(1)	88.58(6)
O(3)-C(7)-C(6)	111.60(19)	O(3)-Mn(1)-O(1)	89.90(7)
C(8)-C(7)-C(6)	119.3(2)	O(5)-Mn(1)-O(1)	91.00(7)
C(7)-C(8)-C(9)	121.1(2)	O(6)-Mn(1)-O(1)	89.04(6)
C(7)-C(8)-H(8)	119.4	O(4)-Mn(1)-O(1)	177.67(6)
C(9)-C(8)-H(8)	119.4	C(2)-O(1)-Mn(1)	123.40(14)
O(4)-C(9)-C(8)	127.5(2)	C(4)-O(2)-Mn(1)	126.46(14)
O(4)-C(9)-C(10)	114.11(19)	C(7)-O(3)-Mn(1)	127.25(14)
C(8)-C(9)-C(10)	118.4(2)	C(9)-O(4)-Mn(1)	123.63(14)
F(10)-C(10)-F(11)	108.0(2)	C(12)-O(5)-Mn(1)	126.83(15)
F(10)-C(10)-F(12)	107.4(2)	C(14)-O(6)-Mn(1)	126.72(15)
F(11)-C(10)-F(12)	106.88(19)		
F(10)-C(10)-C(9)	113.12(19)		
F(11)-C(10)-C(9)	111.82(19)		
F(12)-C(10)-C(9)	109.38(19)		
F(13)-C(11)-F(15)	107.96(19)		
F(13)-C(11)-F(14)	108.0(2)		
F(15)-C(11)-F(14)	108.0(2)		
F(13)-C(11)-C(12)	112.04(19)		
F(15)-C(11)-C(12)	112.03(19)		
F(14)-C(11)-C(12)	108.64(18)		
O(5)-C(12)-C(13)	127.6(2)		
O(5)-C(12)-C(11)	113.7(2)		
C(13)-C(12)-C(11)	118.5(2)		
C(14)-C(13)-C(12)	120.2(2)		

Table A.4. Anisotropic displacement parameters [$\text{\AA}^2 \times 10^3$] for $\text{Mn}(\text{hfac})_3$. The anisotropic displacement factor exponent takes the form: $-2 \pi^2 [(h a^*)^2 U_{11} + \dots + 2 h k a^* b^* U_{12}]$

	U11	U22	U33	U23	U13	U12
C(1)	21(1)	29(1)	32(1)	-2(1)	2(1)	0(1)
C(2)	21(1)	20(1)	27(1)	-4(1)	1(1)	-1(1)
C(3)	21(1)	26(1)	22(1)	-1(1)	1(1)	1(1)
C(4)	21(1)	20(1)	23(1)	-2(1)	-3(1)	0(1)
C(5)	22(1)	29(1)	24(1)	1(1)	0(1)	2(1)
C(6)	26(1)	22(1)	28(1)	-3(1)	1(1)	0(1)
C(7)	24(1)	18(1)	21(1)	1(1)	-3(1)	2(1)
C(8)	21(1)	21(1)	26(1)	-3(1)	0(1)	-3(1)
C(9)	20(1)	21(1)	24(1)	3(1)	1(1)	1(1)
C(10)	25(1)	21(1)	32(1)	-2(1)	6(1)	1(1)
C(11)	20(1)	32(1)	26(1)	4(1)	2(1)	-2(1)
C(12)	15(1)	27(1)	23(1)	1(1)	3(1)	-2(1)
C(13)	22(1)	28(1)	25(1)	-4(1)	-3(1)	-4(1)
C(14)	18(1)	23(1)	27(1)	-2(1)	3(1)	-5(1)
C(15)	25(1)	25(1)	37(1)	-7(1)	-2(1)	-3(1)
F(1)	21(1)	54(1)	45(1)	10(1)	-1(1)	5(1)
F(2)	29(1)	32(1)	67(1)	-1(1)	10(1)	-8(1)
F(3)	26(1)	63(1)	34(1)	-10(1)	7(1)	-3(1)
F(4)	29(1)	58(1)	24(1)	8(1)	-1(1)	7(1)
F(5)	23(1)	37(1)	33(1)	4(1)	0(1)	7(1)
F(6)	34(1)	37(1)	38(1)	-8(1)	-13(1)	-5(1)
F(7)	69(1)	35(1)	25(1)	-2(1)	7(1)	3(1)
F(8)	27(1)	26(1)	46(1)	-10(1)	1(1)	6(1)
F(9)	29(1)	31(1)	49(1)	-18(1)	1(1)	-6(1)
F(10)	32(1)	37(1)	60(1)	-19(1)	17(1)	-15(1)
F(11)	24(1)	25(1)	54(1)	3(1)	7(1)	5(1)
F(12)	37(1)	52(1)	35(1)	13(1)	13(1)	8(1)
F(13)	45(1)	30(1)	42(1)	3(1)	-8(1)	10(1)
F(14)	29(1)	73(1)	45(1)	31(1)	12(1)	8(1)
F(15)	33(1)	42(1)	40(1)	7(1)	-16(1)	-5(1)
F(16)	28(1)	28(1)	54(1)	-9(1)	0(1)	3(1)
F(17)	85(1)	37(1)	59(1)	-23(1)	-40(1)	13(1)
F(18)	55(1)	25(1)	97(2)	0(1)	36(1)	-9(1)
Mn(1)	21(1)	19(1)	21(1)	-1(1)	-1(1)	-2(1)
O(1)	21(1)	27(1)	26(1)	1(1)	-3(1)	-3(1)
O(2)	20(1)	28(1)	23(1)	0(1)	1(1)	-1(1)
O(3)	21(1)	24(1)	27(1)	-5(1)	1(1)	-3(1)
O(4)	24(1)	22(1)	26(1)	-4(1)	3(1)	-2(1)
O(5)	25(1)	24(1)	25(1)	0(1)	-2(1)	0(1)
O(6)	23(1)	21(1)	24(1)	-1(1)	-2(1)	-1(1)

Table A.5. Hydrogen coordinates ($\times 10^4$) and isotropic displacement parameters ($\text{\AA}^2 \times 10^3$) for $\text{Mn}(\text{hfac})_3$.

	x	y	z	U(eq)
H(3)	3484	4259	4296	28
H(8)	8059	7444	2645	27
H(13)	2624	3907	307	30

Table A.6. Torsion angles [deg] for $\text{Mn}(\text{hfac})_3$.

F(1)-C(1)-C(2)-O(1)	-23.7(3)
F(3)-C(1)-C(2)-O(1)	-144.1(2)
F(2)-C(1)-C(2)-O(1)	95.9(2)
F(1)-C(1)-C(2)-C(3)	159.0(2)
F(3)-C(1)-C(2)-C(3)	38.6(3)
F(2)-C(1)-C(2)-C(3)	-81.4(3)
O(1)-C(2)-C(3)-C(4)	-5.9(4)
C(1)-C(2)-C(3)-C(4)	171.1(2)
C(2)-C(3)-C(4)-O(2)	-1.1(4)
C(2)-C(3)-C(4)-C(5)	178.7(2)
O(2)-C(4)-C(5)-F(4)	-167.06(19)
C(3)-C(4)-C(5)-F(4)	13.1(3)
O(2)-C(4)-C(5)-F(5)	-45.4(3)
C(3)-C(4)-C(5)-F(5)	134.8(2)
O(2)-C(4)-C(5)-F(6)	73.3(2)
C(3)-C(4)-C(5)-F(6)	-106.5(2)
F(9)-C(6)-C(7)-O(3)	-173.46(19)
F(8)-C(6)-C(7)-O(3)	-52.3(3)
F(7)-C(6)-C(7)-O(3)	66.3(2)
F(9)-C(6)-C(7)-C(8)	6.3(3)
F(8)-C(6)-C(7)-C(8)	127.4(2)
F(7)-C(6)-C(7)-C(8)	-114.0(2)
O(3)-C(7)-C(8)-C(9)	0.9(4)
C(6)-C(7)-C(8)-C(9)	-178.8(2)
C(7)-C(8)-C(9)-O(4)	-5.9(4)
C(7)-C(8)-C(9)-C(10)	171.6(2)

O(4)-C(9)-C(10)-F(10)	-175.3(2)
C(8)-C(9)-C(10)-F(10)	6.9(3)
O(4)-C(9)-C(10)-F(11)	-53.1(3)
C(8)-C(9)-C(10)-F(11)	129.0(2)
O(4)-C(9)-C(10)-F(12)	65.1(3)
C(8)-C(9)-C(10)-F(12)	-112.8(2)
F(13)-C(11)-C(12)-O(5)	-26.7(3)
F(15)-C(11)-C(12)-O(5)	-148.2(2)
F(14)-C(11)-C(12)-O(5)	92.5(2)
F(13)-C(11)-C(12)-C(13)	157.2(2)
F(15)-C(11)-C(12)-C(13)	35.7(3)
F(14)-C(11)-C(12)-C(13)	-83.6(3)
O(5)-C(12)-C(13)-C(14)	-5.9(4)
C(11)-C(12)-C(13)-C(14)	169.6(2)
C(12)-C(13)-C(14)-O(6)	3.1(4)
C(12)-C(13)-C(14)-C(15)	-176.0(2)
O(6)-C(14)-C(15)-F(16)	-46.5(3)
C(13)-C(14)-C(15)-F(16)	132.7(2)
O(6)-C(14)-C(15)-F(17)	-166.9(2)
C(13)-C(14)-C(15)-F(17)	12.2(3)
O(6)-C(14)-C(15)-F(18)	72.6(3)
C(13)-C(14)-C(15)-F(18)	-108.3(3)
C(3)-C(2)-O(1)-Mn(1)	-4.8(3)
C(1)-C(2)-O(1)-Mn(1)	178.22(14)
O(2)-Mn(1)-O(1)-C(2)	15.05(18)
O(3)-Mn(1)-O(1)-C(2)	-73.64(18)
O(5)-Mn(1)-O(1)-C(2)	-164.13(18)
O(6)-Mn(1)-O(1)-C(2)	105.48(18)
C(3)-C(4)-O(2)-Mn(1)	19.4(3)
C(5)-C(4)-O(2)-Mn(1)	-160.34(15)
O(3)-Mn(1)-O(2)-C(4)	68.38(18)
O(6)-Mn(1)-O(2)-C(4)	-110.59(18)
O(4)-Mn(1)-O(2)-C(4)	156.11(18)
O(1)-Mn(1)-O(2)-C(4)	-21.56(18)
C(8)-C(7)-O(3)-Mn(1)	17.2(3)
C(6)-C(7)-O(3)-Mn(1)	-163.14(14)
O(2)-Mn(1)-O(3)-C(7)	70.94(18)
O(5)-Mn(1)-O(3)-C(7)	-109.48(18)
O(4)-Mn(1)-O(3)-C(7)	-20.69(18)
O(1)-Mn(1)-O(3)-C(7)	159.52(18)
C(8)-C(9)-O(4)-Mn(1)	-6.0(3)
C(10)-C(9)-O(4)-Mn(1)	176.42(14)
O(2)-Mn(1)-O(4)-C(9)	-72.93(18)
O(3)-Mn(1)-O(4)-C(9)	15.69(18)
O(5)-Mn(1)-O(4)-C(9)	106.23(18)
O(6)-Mn(1)-O(4)-C(9)	-163.43(17)

C(13)-C(12)-O(5)-Mn(1)	-1.2(3)
C(11)-C(12)-O(5)-Mn(1)	-176.87(13)
O(3)-Mn(1)-O(5)-C(12)	-171.60(18)
O(6)-Mn(1)-O(5)-C(12)	7.36(18)
O(4)-Mn(1)-O(5)-C(12)	100.64(18)
O(1)-Mn(1)-O(5)-C(12)	-81.69(18)
C(13)-C(14)-O(6)-Mn(1)	6.5(3)
C(15)-C(14)-O(6)-Mn(1)	-174.42(14)
O(2)-Mn(1)-O(6)-C(14)	169.72(18)
O(5)-Mn(1)-O(6)-C(14)	-9.84(18)
O(4)-Mn(1)-O(6)-C(14)	-98.68(18)
O(1)-Mn(1)-O(6)-C(14)	81.15(18)

A.2: Crystal data and structure refinement for $\text{Al}(\text{hfac})_3$

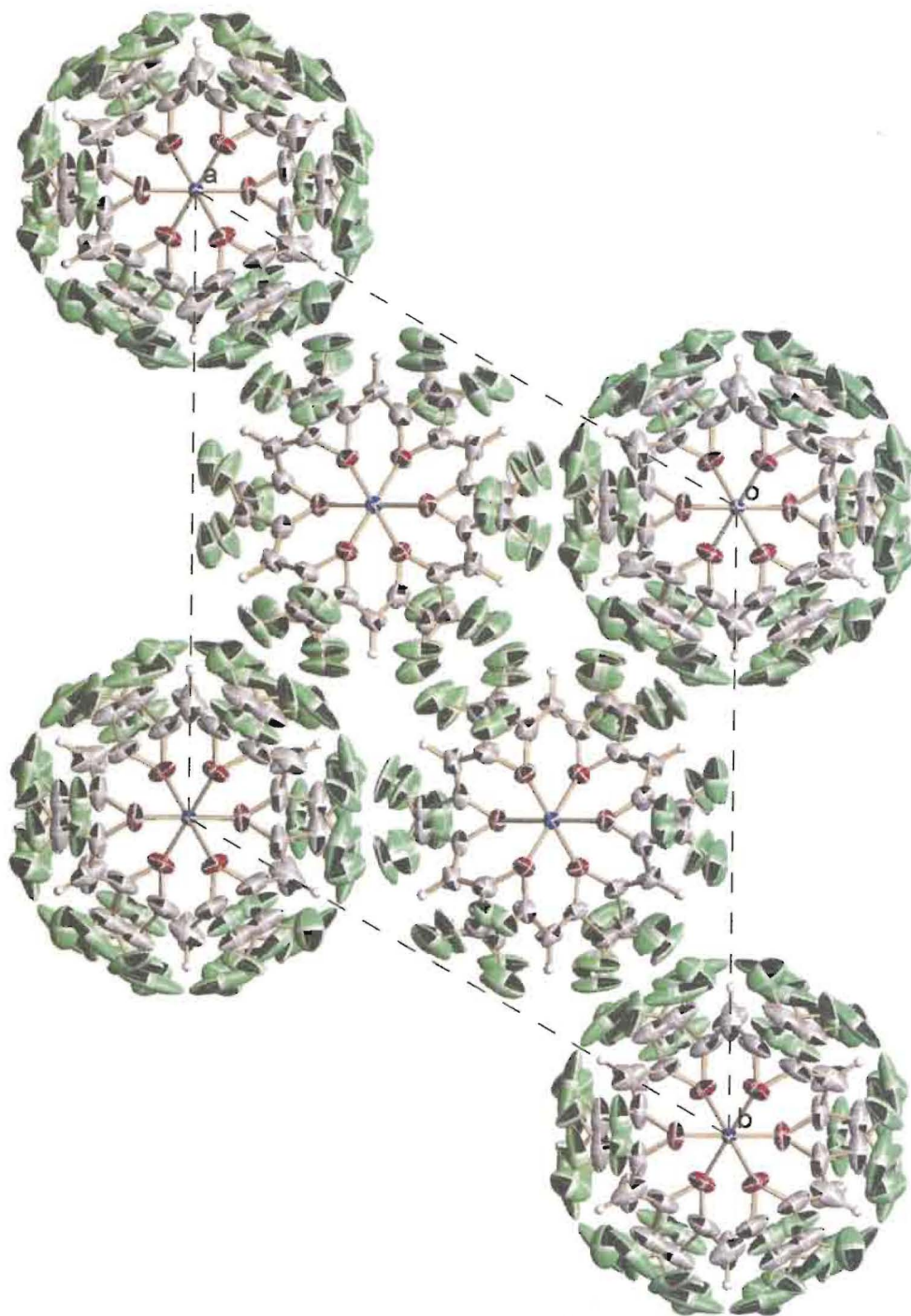


Figure A.2: The crystal structure of aluminum tris(hexafluoroacetylacetonate).

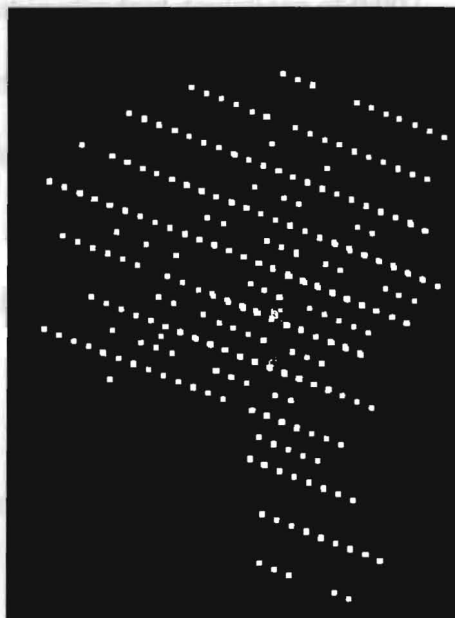
Table A.7: Crystal data and structure refinement for Al(hfac)₃

Empirical formula: C₁₅ H₃ Al F₁₈ O₆
 Formula weight: 648.15
 Temperature: 100(2) K
 Wavelength: 0.71073 Å
 Crystal system: Trigonal
 Space group: P-3c1
 Unit cell dimensions:
 a = 17.7635(11) Å, α = 90°
 b = 17.7635(11) Å, β = 90°
 c = 12.1501(15) Å, γ = 120°
 Volume, Z: 3320.2(5) Å³, 6
 Density (calculated): 1.945 Mg/m³
 Absorption coefficient: 0.276 mm⁻¹
 F(000): 1896
 Crystal size: 0.55 × 0.13 × 0.13 mm
 Crystal shape, colour: needle, colourless
 θ range for data collection: 1.32 to 28.28°
 Limiting indices: -23 ≤ h ≤ 23, 23 ≤ k ≤ 21, 15 ≤ l ≤ 16
 Reflections collected: 22893
 Independent reflections: 2751 (R(int) = 0.0355)
 Completeness to θ = 28.28°: 100.0 %
 Absorption correction: multi-scan
 Max. and min. transmission: 0.965 and 0.755
 Refinement method: Full-matrix least-squares on F²
 Data / restraints / parameters: 2751 / 625 / 288
 Goodness-of-fit on F²: 1.041
 Final R indices [I > 2σ(I)]: R1 = 0.0721, wR2 = 0.1889
 R indices (all data): R1 = 0.0871, wR2 = 0.2014
 Largest diff. peak and hole: 0.563 and -0.540 e × Å⁻³

Refinement of F² against ALL reflections. The weighted R-factor wR and goodness of fit are based on F², conventional R-factors R are based on F, with F set to zero for negative F². The threshold expression of F² > 2σ(F²) is used only for calculating R-factors

Comments:

The compound is merohedrally twinned. Application of the twin matrix $-1\ 0\ 0\ 0\ -1\ 0\ 0\ 0\ 1$ resulted in a refined twinning ratio of 0.437(3) to 0.563(3). The structure also exhibits disorder of the hexafluoro-acac ligands and also pseudosymmetry, and both phenomena are linked to each other. The ligands of both crystallographically independent molecules are disordered over two positions with only the Al and O atoms taking not part in the disorder. The remainder of the each ligand is mirror imaged by planes cutting through the Al-O bonds, thus forming two sets of equivalent hfac ligands. The refined occupancy rates are



0.732(4) to 0.268(4) for the first set of ligands, 0.647(3) to 0.353(7) for the second. With a 1:1 the disorder the structure could also have been described in an alternative unit cell with half the volume and c-axis in the space group P-3m1 (with the above mentioned mirror planes then being crystallographic mirror planes). With a large part of the molecules packing under observation of the symmetry of the smaller unit cell the diffraction pattern actually resembles this and the diffraction spots of every second layer perpendicular to the c^* axis has a significantly lowered intensity (see RLATT plot to the right).

Due to the significant overlap of the atoms in the disordered moieties a range of restraints was applied. All equivalent C-C, C-F and C-O bond distances and C...C and C...F 1,3 distances were restrained to be identical within standard deviations of 0.02.

Equivalent carbon atoms in the major and minor moieties were restrained to have identical anisotropic displacement parameters. Fluorine atoms were restrained to be isotropic within a standard deviation of 0.03, and carbon atom C5 and C5b (which nearly overlap completely) were restrained to be isotropic within standard deviations of 0.007. Additional disorder is evident for the ligands around Al2, but attempts to refine this disorder in a meaningful way failed and were omitted in the final model. To avoid extremes for the anisotropic displacement parameters of C6, C7, C6b and C7b these were restrained to be isotropic within standard deviations of 0.007.

Treatment of hydrogen atoms:

All hydrogen atoms were placed in calculated positions and were refined with an isotropic displacement parameter 1.2 times that of the adjacent carbon atom.

Table A.8. Atomic coordinates [$\times 10^4$] and equivalent isotropic displacement parameters [$\text{\AA}^2 \times 10^3$] for Al(hfac)₃. U(eq) is defined as one third of the trace of the orthogonalized U_{ij} tensor.

	x	y	z	U(eq)
Al(1)	6667	3333	248(2)	29(1)
Al(2)	10000	10000	2500	29(1)
O(1)	7661(2)	3833(2)	-654(3)	36(1)
O(2)	7155(2)	2829(2)	1141(3)	35(1)
C(1)	9051(5)	4368(4)	-1343(5)	43(2)
C(2)	8348(3)	3815(4)	-509(4)	35(1)
C(3)	8514(3)	3357(4)	279(4)	35(1)
C(4)	7880(4)	2879(4)	1061(4)	34(1)
C(5)	8026(5)	2324(5)	1869(6)	46(2)
F(1)	8760(5)	4259(5)	-2354(5)	48(2)
F(2)	9389(5)	5197(4)	-1087(5)	89(2)
F(3)	9696(3)	4197(5)	-1333(5)	89(2)
F(4)	7796(6)	2401(6)	2885(4)	50(2)
F(5)	7554(5)	1489(3)	1621(5)	87(2)
F(6)	8839(4)	2502(5)	1913(5)	88(2)

C(1B)	5664(9)	973(10)	-1377(11)	43(2)
C(2B)	6232(8)	1670(8)	-557(10)	35(1)
C(3B)	6678(8)	1511(10)	238(10)	35(1)
C(4B)	7142(9)	2132(9)	1002(10)	34(1)
C(5B)	7704(10)	1986(11)	1837(12)	46(2)
F(1B)	5831(13)	327(10)	-1387(15)	95(7)
F(2B)	4834(8)	644(10)	-1130(14)	105(8)
F(3B)	5780(14)	1281(15)	-2389(11)	67(8)
F(4B)	7572(17)	2160(16)	2842(12)	88(11)
F(5B)	7534(14)	1172(10)	1831(15)	108(7)
F(6B)	8535(9)	2489(12)	1595(14)	107(8)
O(3)	9021(2)	9508(2)	1598(3)	44(1)
C(6)	7639(8)	8605(9)	837(9)	67(3)
C(7)	8329(7)	8809(9)	1711(8)	49(2)
C(8)	8179(15)	8179(15)	2500	64(3)
F(7)	7166(11)	8966(12)	1003(12)	109(7)
F(8)	8005(9)	8859(7)	-151(8)	41(3)
F(9)	7109(10)	7757(7)	820(11)	102(5)
C(6B)	7631(5)	9075(7)	838(6)	67(3)
C(7B)	8342(4)	9567(5)	1696(5)	49(2)
C(8B)	8163(7)	10000	2500	64(3)
F(7B)	7243(5)	8256(6)	1033(5)	142(6)
F(8B)	7985(5)	9207(7)	-173(5)	97(4)
F(9B)	7055(5)	9342(9)	819(7)	158(6)

All esds (except the esd in the dihedral angle between two l.s. planes) are estimated using the full covariance matrix. The cell esds are taken into account individually in the estimation of esds in distances, angles and torsion angles; correlations between esds in cell parameters are only used when they are defined by crystal symmetry. An approximate (isotropic) treatment of cell esds is used for estimating esds involving l.s. planes.

Table A.9. Bond lengths [\AA] and angles [deg] for $\text{Al}(\text{hfac})_3$.

Al(1)-O(2)	1.874(3)	Al(2)-O(3)#7	1.862(3)
Al(1)-O(2)#1	1.874(3)	O(1)-C(2)	1.249(6)
Al(1)-O(2)#2	1.874(3)	O(1)-C(2B)#2	1.251(14)
Al(1)-O(1)#1	1.881(3)	O(2)-C(4B)	1.239(13)
Al(1)-O(1)#2	1.881(3)	O(2)-C(4)	1.250(6)
Al(1)-O(1)	1.881(3)	C(1)-F(1)	1.310(8)
Al(2)-O(3)#3	1.862(3)	C(1)-F(2)	1.319(9)
Al(2)-O(3)#4	1.862(3)	C(1)-F(3)	1.325(8)
Al(2)-O(3)	1.862(3)	C(1)-C(2)	1.524(7)
Al(2)-O(3)#5	1.862(3)	C(2)-C(3)	1.381(7)
Al(2)-O(3)#6	1.862(3)	C(3)-C(4)	1.391(7)

C(3)-H(3)	0.9500	O(2)#2-Al(1)-O(1)	89.96(13)
C(4)-C(5)	1.503(8)	O(1)#1-Al(1)-O(1)	89.49(15)
C(5)-F(6)	1.316(8)	O(1)#2-Al(1)-O(1)	89.50(15)
C(5)-F(5)	1.323(9)	O(3)#3-Al(2)-O(3)#4	179.7(3)
C(5)-F(4)	1.328(8)	O(3)#3-Al(2)-O(3)	88.90(14)
C(1B)-F(3B)	1.319(13)	O(3)#4-Al(2)-O(3)	91.30(19)
C(1B)-F(1B)	1.320(13)	O(3)#3-Al(2)-O(3)#5	88.90(14)
C(1B)-F(2B)	1.321(12)	O(3)#4-Al(2)-O(3)#5	90.9(2)
C(1B)-C(2B)	1.514(13)	O(3)-Al(2)-O(3)#5	88.90(14)
C(2B)-O(1)#1	1.251(14)	O(3)#3-Al(2)-O(3)#6	91.30(19)
C(2B)-C(3B)	1.365(12)	O(3)#4-Al(2)-O(3)#6	88.90(14)
C(3B)-C(4B)	1.360(13)	O(3)-Al(2)-O(3)#6	90.9(2)
C(3B)-H(3B)	0.9500	O(3)#5-Al(2)-O(3)#6	179.7(2)
C(4B)-C(5B)	1.532(13)	O(3)#3-Al(2)-O(3)#7	90.9(2)
C(5B)-F(4B)	1.310(13)	O(3)#4-Al(2)-O(3)#7	88.90(14)
C(5B)-F(5B)	1.321(13)	O(3)-Al(2)-O(3)#7	179.7(2)
C(5B)-F(6B)	1.322(13)	O(3)#5-Al(2)-O(3)#7	91.30(19)
O(3)-C(7)	1.243(13)	O(3)#6-Al(2)-O(3)#7	88.90(14)
O(3)-C(7B)	1.268(7)	C(2)-O(1)-C(2B)#2	65.0(6)
C(6)-F(7)	1.302(12)	C(2)-O(1)-Al(1)	127.2(3)
C(6)-F(9)	1.318(13)	C(2B)#2-O(1)-Al(1)	128.0(5)
C(6)-F(8)	1.332(12)	C(4B)-O(2)-C(4)	64.1(7)
C(6)-C(7)	1.522(12)	C(4B)-O(2)-Al(1)	128.1(6)
C(7)-C(8)	1.395(13)	C(4)-O(2)-Al(1)	128.8(3)
C(8)-C(7)#6	1.395(13)	F(1)-C(1)-F(2)	108.2(6)
C(8)-H(8)	0.9500	F(1)-C(1)-F(3)	107.2(7)
C(6B)-F(7B)	1.283(11)	F(2)-C(1)-F(3)	107.0(7)
C(6B)-F(9B)	1.326(11)	F(1)-C(1)-C(2)	113.1(6)
C(6B)-F(8B)	1.346(8)	F(2)-C(1)-C(2)	109.4(6)
C(6B)-C(7B)	1.531(9)	F(3)-C(1)-C(2)	111.7(5)
C(7B)-C(8B)	1.375(8)	O(1)-C(2)-C(3)	127.7(5)
C(8B)-C(7B)#4	1.375(8)	O(1)-C(2)-C(1)	112.8(5)
C(8B)-H(8B)	0.9500	C(3)-C(2)-C(1)	119.5(5)
		C(2)-C(3)-C(4)	119.1(5)
O(2)-Al(1)-O(2)#1	89.79(15)	C(2)-C(3)-H(3)	120.5
O(2)-Al(1)-O(2)#2	89.79(15)	C(4)-C(3)-H(3)	120.5
O(2)#1-Al(1)-O(2)#2	89.79(15)	O(2)-C(4)-C(3)	126.0(4)
O(2)-Al(1)-O(1)#1	89.96(13)	O(2)-C(4)-C(5)	114.3(5)
O(2)#1-Al(1)-O(1)#1	90.76(12)	C(3)-C(4)-C(5)	119.6(5)
O(2)#2-Al(1)-O(1)#1	179.39(14)	F(6)-C(5)-F(5)	106.4(7)
O(2)-Al(1)-O(1)#2	179.39(14)	F(6)-C(5)-F(4)	107.1(7)
O(2)#1-Al(1)-O(1)#2	89.95(13)	F(5)-C(5)-F(4)	105.8(7)
O(2)#2-Al(1)-O(1)#2	90.76(12)	F(6)-C(5)-C(4)	113.4(6)
O(1)#1-Al(1)-O(1)#2	89.49(15)	F(5)-C(5)-C(4)	111.5(6)
O(2)-Al(1)-O(1)	90.76(12)	F(4)-C(5)-C(4)	112.2(6)
O(2)#1-Al(1)-O(1)	179.39(14)	F(3B)-C(1B)-F(1B)	107.1(12)

F(3B)-C(1B)-F(2B)	107.7(12)	C(7B)#4-C(8B)-H(8B)	120.7
F(1B)-C(1B)-F(2B)	107.6(12)		
F(3B)-C(1B)-C(2B)	111.9(12)		
F(1B)-C(1B)-C(2B)	111.7(10)		
F(2B)-C(1B)-C(2B)	110.6(11)		
O(1)#1-C(2B)-C(3B)	126.7(10)		
O(1)#1-C(2B)-C(1B)	112.2(10)		
C(3B)-C(2B)-C(1B)	120.9(11)		
C(4B)-C(3B)-C(2B)	119.6(12)		
C(4B)-C(3B)-H(3B)	120.2		
C(2B)-C(3B)-H(3B)	120.2		
O(2)-C(4B)-C(3B)	127.2(10)		
O(2)-C(4B)-C(5B)	113.0(10)		
C(3B)-C(4B)-C(5B)	119.8(11)		
F(4B)-C(5B)-F(5B)	107.0(13)		
F(4B)-C(5B)-F(6B)	108.6(12)		
F(5B)-C(5B)-F(6B)	107.8(13)		
F(4B)-C(5B)-C(4B)	111.7(12)		
F(5B)-C(5B)-C(4B)	111.7(10)		
F(6B)-C(5B)-C(4B)	109.9(11)		
C(7)-O(3)-C(7B)	64.2(7)		
C(7)-O(3)-Al(2)	129.0(5)		
C(7B)-O(3)-Al(2)	127.6(3)		
F(7)-C(6)-F(9)	107.3(12)		
F(7)-C(6)-F(8)	107.4(10)		
F(9)-C(6)-F(8)	108.8(11)		
F(7)-C(6)-C(7)	114.5(11)		
F(9)-C(6)-C(7)	108.2(10)		
F(8)-C(6)-C(7)	110.5(10)		
O(3)-C(7)-C(8)	125.0(13)		
O(3)-C(7)-C(6)	116.0(10)		
C(8)-C(7)-C(6)	118.7(11)		
C(7)-C(8)-C(7)#6	120.4(19)		
C(7)-C(8)-H(8)	119.8		
C(7)#6-C(8)-H(8)	119.8		
F(7B)-C(6B)-F(9B)	109.6(8)		
F(7B)-C(6B)-F(8B)	107.8(9)		
F(9B)-C(6B)-F(8B)	107.4(8)		
F(7B)-C(6B)-C(7B)	110.1(7)		
F(9B)-C(6B)-C(7B)	111.8(8)		
F(8B)-C(6B)-C(7B)	110.0(6)		
O(3)-C(7B)-C(8B)	127.5(7)		
O(3)-C(7B)-C(6B)	115.9(6)		
C(8B)-C(7B)-C(6B)	116.6(7)		
C(7B)-C(8B)-C(7B)#4	118.6(10)		
C(7B)-C(8B)-H(8B)	120.7		

Symmetry transformations used to generate equivalent atoms:
 #1 -x+y+1,-x+1,z #2 -y+1,x-y,z #3 -y+2,x-y+1,z
 #4 x-y+1,-y+2,-z+1/2 #5 -x+y+1,-x+2,z #6 y,x,-z+1/2
 #7 -x+2,-x+y+1,-z+1/2

Table A.10: Anisotropic displacement parameters [$\text{\AA}^2 \times 10^3$] for Al(hfac)3. The anisotropic displacement factor exponent takes the form: $-2 \pi^2 [(h a^*)^2 U_{11} + \dots + 2 h k a^* b^* U_{12}]$

	U11	U22	U33	U23	U13	U12
Al(1)	26(1)	26(1)	36(1)	0	0	13(1)
Al(2)	20(1)	20(1)	46(2)	0	0	10(1)
O(1)	28(1)	40(2)	38(2)	5(1)	3(1)	14(1)
O(2)	42(2)	36(2)	36(1)	4(1)	3(1)	25(1)
C(1)	35(3)	52(4)	35(3)	13(3)	6(3)	18(3)
C(2)	31(3)	44(3)	22(2)	0(2)	-1(2)	13(2)
C(3)	32(2)	61(3)	24(2)	-1(2)	0(2)	32(2)
C(4)	50(3)	47(3)	21(2)	-1(2)	2(2)	36(3)
C(5)	57(5)	62(5)	43(3)	2(3)	0(3)	46(4)
F(1)	42(3)	70(4)	26(2)	9(2)	3(2)	24(3)
F(2)	72(4)	71(4)	50(4)	5(3)	12(3)	-19(3)
F(3)	39(3)	176(6)	50(3)	49(3)	23(2)	51(3)
F(4)	73(4)	74(3)	25(3)	16(2)	10(2)	55(3)
F(5)	172(6)	51(3)	69(4)	7(3)	-3(4)	79(4)
F(6)	91(4)	176(6)	57(3)	49(4)	23(3)	112(5)
C(1B)	35(3)	52(4)	35(3)	13(3)	6(3)	18(3)
C(2B)	31(3)	44(3)	22(2)	0(2)	-1(2)	13(2)
C(3B)	32(2)	61(3)	24(2)	-1(2)	0(2)	32(2)
C(4B)	50(3)	47(3)	21(2)	-1(2)	2(2)	36(3)
C(5B)	57(5)	62(5)	43(3)	2(3)	0(3)	46(4)
F(1B)	146(16)	57(10)	53(10)	-4(8)	-22(10)	30(10)
F(2B)	82(12)	60(11)	77(12)	-35(9)	-11(9)	-37(9)
F(3B)	84(16)	48(9)	38(9)	1(7)	-10(8)	9(9)
F(4B)	112(19)	140(20)	51(12)	4(11)	-4(10)	95(18)
F(5B)	220(20)	93(13)	79(11)	3(10)	-23(12)	130(15)
F(6B)	119(15)	185(19)	60(11)	8(10)	-43(10)	108(14)
O(3)	23(1)	61(2)	39(2)	-17(2)	0(1)	15(2)
C(6)	29(3)	116(7)	20(3)	-6(4)	-1(2)	9(4)
C(7)	24(2)	84(4)	28(3)	-12(3)	-2(2)	19(3)
C(8)	110(9)	110(9)	20(4)	0(3)	0(3)	91(11)
F(7)	120(13)	170(14)	107(13)	47(10)	64(10)	124(12)
F(8)	41(5)	56(5)	26(5)	9(4)	7(3)	25(4)

F(9)	145(14)	80(9)	65(9)	15(7)	19(9)	44(10)
C(6B)	29(3)	116(7)	20(3)	-6(4)	-1(2)	9(4)
C(7B)	24(2)	84(4)	28(3)	-12(3)	-2(2)	19(3)
C(8B)	110(9)	110(9)	20(4)	0(3)	0(3)	91(11)
F(7B)	55(4)	190(11)	36(3)	-33(5)	12(3)	-47(6)
F(8B)	32(3)	172(9)	21(3)	-21(4)	-2(2)	2(5)
F(9B)	49(4)	361(17)	55(4)	-11(8)	-10(3)	96(7)

Table A.11. Hydrogen coordinates ($\times 10^4$) and isotropic displacement parameters ($\text{\AA}^2 \times 10^3$) for Al(hfac)₃.

	x	y	z	U(eq)
H(3)	9055	3368	287	42
H(3B)	6663	969	257	42
H(8)	7644	7644	2500	77
H(8B)	7628	10000	2500	77

Table A.12. Torsion angles [deg] for Al(hfac)₃.

O(2)-Al(1)-O(1)-C(2)	-4.9(4)
O(2)#2-Al(1)-O(1)-C(2)	84.9(4)
O(1)#1-Al(1)-O(1)-C(2)	-94.9(5)
O(1)#2-Al(1)-O(1)-C(2)	175.6(4)
O(2)-Al(1)-O(1)-C(2B)#2	-90.4(8)
O(2)#2-Al(1)-O(1)-C(2B)#2	-0.6(8)
O(1)#1-Al(1)-O(1)-C(2B)#2	179.7(8)
O(1)#2-Al(1)-O(1)-C(2B)#2	90.2(9)
O(2)#1-Al(1)-O(2)-C(4B)	95.6(9)
O(2)#2-Al(1)-O(2)-C(4B)	-174.6(9)
O(1)#1-Al(1)-O(2)-C(4B)	4.8(9)
O(1)-Al(1)-O(2)-C(4B)	-84.7(9)
O(2)#1-Al(1)-O(2)-C(4)	-179.0(4)
O(2)#2-Al(1)-O(2)-C(4)	-89.2(5)
O(1)#1-Al(1)-O(2)-C(4)	90.2(4)
O(1)-Al(1)-O(2)-C(4)	0.7(4)
C(2B)#2-O(1)-C(2)-C(3)	126.9(9)

Al(1)-O(1)-C(2)-C(3)	7.0(8)
C(2B)#2-O(1)-C(2)-C(1)	-54.1(7)
Al(1)-O(1)-C(2)-C(1)	-174.0(4)
F(1)-C(1)-C(2)-O(1)	-45.2(8)
F(2)-C(1)-C(2)-O(1)	75.5(7)
F(3)-C(1)-C(2)-O(1)	-166.3(6)
F(1)-C(1)-C(2)-C(3)	133.9(7)
F(2)-C(1)-C(2)-C(3)	-105.5(8)
F(3)-C(1)-C(2)-C(3)	12.8(9)
O(1)-C(2)-C(3)-C(4)	-3.4(9)
C(1)-C(2)-C(3)-C(4)	177.7(5)
C(4B)-O(2)-C(4)-C(3)	121.3(9)
Al(1)-O(2)-C(4)-C(3)	1.9(8)
C(4B)-O(2)-C(4)-C(5)	-55.5(8)
Al(1)-O(2)-C(4)-C(5)	-174.9(4)
C(2)-C(3)-C(4)-O(2)	-1.3(9)
C(2)-C(3)-C(4)-C(5)	175.4(6)
O(2)-C(4)-C(5)-F(6)	-168.2(6)
C(3)-C(4)-C(5)-F(6)	14.8(9)
O(2)-C(4)-C(5)-F(5)	71.8(7)
C(3)-C(4)-C(5)-F(5)	-105.3(7)
O(2)-C(4)-C(5)-F(4)	-46.7(9)
C(3)-C(4)-C(5)-F(4)	136.3(7)
F(3B)-C(1B)-C(2B)-O(1)#1	50.0(16)
F(1B)-C(1B)-C(2B)-O(1)#1	170.2(13)
F(2B)-C(1B)-C(2B)-O(1)#1	-70.0(15)
F(3B)-C(1B)-C(2B)-C(3B)	-135.4(15)
F(1B)-C(1B)-C(2B)-C(3B)	-15.3(18)
F(2B)-C(1B)-C(2B)-C(3B)	104.6(16)
O(1)#1-C(2B)-C(3B)-C(4B)	-3(2)
C(1B)-C(2B)-C(3B)-C(4B)	-176.3(13)
C(4)-O(2)-C(4B)-C(3B)	-129.3(17)
Al(1)-O(2)-C(4B)-C(3B)	-9(2)
C(4)-O(2)-C(4B)-C(5B)	52.9(9)
Al(1)-O(2)-C(4B)-C(5B)	173.2(7)
C(2B)-C(3B)-C(4B)-O(2)	7(2)
C(2B)-C(3B)-C(4B)-C(5B)	-175.0(13)
O(2)-C(4B)-C(5B)-F(4B)	46.3(17)
C(3B)-C(4B)-C(5B)-F(4B)	-131.8(17)
O(2)-C(4B)-C(5B)-F(5B)	166.0(14)
C(3B)-C(4B)-C(5B)-F(5B)	-12.0(19)
O(2)-C(4B)-C(5B)-F(6B)	-74.4(16)
C(3B)-C(4B)-C(5B)-F(6B)	107.6(17)
O(3)#3-Al(2)-O(3)-C(7)	95.4(9)
O(3)#4-Al(2)-O(3)-C(7)	-84.8(8)
O(3)#5-Al(2)-O(3)-C(7)	-175.6(9)

O(3)#6-Al(2)-O(3)-C(7)	4.1(8)
O(3)#3-Al(2)-O(3)-C(7B)	-179.4(6)
O(3)#4-Al(2)-O(3)-C(7B)	0.4(5)
O(3)#5-Al(2)-O(3)-C(7B)	-90.4(6)
O(3)#6-Al(2)-O(3)-C(7B)	89.4(6)
C(7B)-O(3)-C(7)-C(8)	-127.1(13)
Al(2)-O(3)-C(7)-C(8)	-8.4(16)
C(7B)-O(3)-C(7)-C(6)	59.5(10)
Al(2)-O(3)-C(7)-C(6)	178.2(7)
F(7)-C(6)-C(7)-O(3)	-83.3(15)
F(9)-C(6)-C(7)-O(3)	157.1(12)
F(8)-C(6)-C(7)-O(3)	38.1(15)
F(7)-C(6)-C(7)-C(8)	102.9(14)
F(9)-C(6)-C(7)-C(8)	-16.7(14)
F(8)-C(6)-C(7)-C(8)	-135.7(11)
O(3)-C(7)-C(8)-C(7)#6	4.3(8)
C(6)-C(7)-C(8)-C(7)#6	177.5(12)
C(7)-O(3)-C(7B)-C(8B)	119.7(10)
Al(2)-O(3)-C(7B)-C(8B)	-0.9(11)
C(7)-O(3)-C(7B)-C(6B)	-58.1(8)
Al(2)-O(3)-C(7B)-C(6B)	-178.8(5)
F(7B)-C(6B)-C(7B)-O(3)	74.0(9)
F(9B)-C(6B)-C(7B)-O(3)	-163.9(8)
F(8B)-C(6B)-C(7B)-O(3)	-44.7(11)
F(7B)-C(6B)-C(7B)-C(8B)	-104.1(9)
F(9B)-C(6B)-C(7B)-C(8B)	18.0(10)
F(8B)-C(6B)-C(7B)-C(8B)	137.2(8)
O(3)-C(7B)-C(8B)-C(7B)#4	0.5(6)
C(6B)-C(7B)-C(8B)-C(7B)#4	178.4(8)

Symmetry transformations used to generate equivalent atoms:

#1 $-x+y+1, -x+1, z$ #2 $-y+1, x-y, z$ #3 $-y+2, x-y+1, z$
#4 $x-y+1, -y+2, -z+1/2$ #5 $-x+y+1, -x+2, z$ #6 $y, x, -z+1/2$
#7 $-x+2, -x+y+1, -z+1/2$